Optimal Scaling in Ductile Fracture

Thesis by

Landry Fokoua Djodom

In Partial Fulfillment of the Requirements

for the Degree of

Doctor of Philosophy

California Institute of Technology

Pasadena, California

2014

(Submitted October 16, 2013)

To my family.

Acknowledgments

I would like to express my profound gratitude and appreciation to Professor Michael Ortiz for his supervision and guidance throughout my stay at Caltech. I am deeply grateful for his support, his motivation and his patience. He has provided me with a multidisciplinary research experience from which I have learned a lot and his constant encouragement for innovative and challenging ideas has contributed to an exciting PhD work.

I would like to specially acknowledge Professor Sergio Conti from the Hausdorff Research Institute of Mathematics, University of Bonn (Germany), for his collaboration throughout this thesis work. I gratefully acknowledge support provided by the Hausdorff Trimester Program "mathematical challenges of materials science and condensed matter physics: From quantum mechanics through statistical mechanics to nonlinear PDEs", Hausdorff Research Institute for Mathematics (HIM), University of Bonn, Germany.

I also gratefully acknowledge the support of the Department of Energy National Nuclear Security Administration through Caltech's ASC/PSAAP Center for the Predictive Modeling and Simulation of High Energy Density Dynamic Response of Materials.

I am particularly thankful to Professor Ravichandran, Professor Bhattacharya and Professor Weinberg for serving on my thesis committee. I would like to thank Professor Andrade and Professor Kochmann for serving on my candidacy exam and for their useful suggestions and comments. I am grateful to Professor Ravichandran for providing insights about my work, for supporting me throughout my stay at GALCIT, and for being a good resource for career aspirations. I thank Professor Weinberg for her feedback, help and useful discussions on my research.

During summer 2011, I had the opportunity to spend ten weeks at the Lawrence Livermore

National Laboratory. Very warms thanks are addressed to Sylvie Aubry, Tom Arsenlis and Jaime Marian for welcoming me to the lab and exposing me to the exciting field of dislocation dynamics and computational material science.

I owe special gratitude to Lydia who has always been available for me, I deeply appreciate her attention and her care which have made my life enjoyable in the office. She has been and will remain a life mentor to me. Special thanks also go to Marta for her availability and help with computer issues. I would also like to acknowledge Cheryl Gause, Dimity Nelson, and Christine Ramirez who have facilitated my insertion into the GALCIT community. I thank the members of my lab group with whom I have had several instructive discussions: Jonathan, Panos, Stephanie, Anie, Gwen, Brandon, Sarah, Jeff, Cindy.

My life at Caltech and in the Los Angeles area wouldn't have been pleasant without the presence of my friends. I owe a sincere acknowledgement to Stephanie, Adam, Ignacio, Jen, Sid, Jomela, Xin, Philipp, Jocelyn, Adrian, Juan, Vicki, Andy, Kristen, Ryan, Cheikh, Gloria, Eleni. I would like to specially acknowledge Terry with whom I have shared many exciting adventures at Caltech and who will remain a close friend. I am deeply grateful to Namiko who has provided me with her presence and attention, and whose friendship will remain precious. I am also thankful to my friends from Santa Barbara, especially Maxime and Kai. Special thanks also to Professor Frédéric Gibou for his support and encouragement since my research internship at the University of California, Santa Barbara. I would like to express my very deep gratitude to Alan and his family who have welcomed me in their lives and I cherish the time that I have spent with them in Pasadena.

I am profoundly indebted to Cabral and Ange-Thérèse who I have known during my undergraduate studies in France, and even before, and with whom I have shared a deep friendship over several years. Their continued presence and support have always been invaluable.

I thank the Caltech Graduate Student Council which has provided me with the unique opportunity to contribute to the campus life. I am thankful to all the students I collaborated with and I particularly thank Felicia Hunt who has strongly contributed to the success of our events.

Finally, but not least, I profoundly thank my family who has always been on my side, and to

whom I simply owe everything.

Abstract

This work is concerned with the derivation of optimal scaling laws, in the sense of matching lower and upper bounds on the energy, for a solid undergoing ductile fracture. The specific problem considered concerns a material sample in the form of an infinite slab of finite thickness subjected to prescribed opening displacements on its two surfaces. The solid is assumed to obey deformation-theory of plasticity and, in order to further simplify the analysis, we assume isotropic rigid-plastic deformations with zero plastic spin. When hardening exponents are given values consistent with observation, the energy is found to exhibit sublinear growth. We regularize the energy through the addition of nonlocal energy terms of the strain-gradient plasticity type. This nonlocal regularization has the effect of introducing an intrinsic length scale into the energy. We also put forth a physical argument that identifies the intrinsic length and suggests a linear growth of the nonlocal energy. Under these assumptions, ductile fracture emerges as the net result of two competing effects: whereas the sublinear growth of the local energy promotes localization of deformation to failure planes, the nonlocal regularization stabilizes this process, thus resulting in an orderly progression towards failure and a well-defined specific fracture energy. The optimal scaling laws derived here show that ductile fracture results from localization of deformations to *void sheets*, and that it requires a well-defined energy per unit fracture area. In particular, fractal modes of fracture are ruled out under the assumptions of the analysis. The optimal scaling laws additionally show that ductile fracture is cohesive in nature, i.e., it obeys a well-defined relation between tractions and opening displacements. Finally, the scaling laws supply a link between micromechanical properties and macroscopic fracture properties. In particular, they reveal the relative roles that surface energy and microplasticity play as contributors to the specific fracture energy of the material. Next, we present

an experimental assessment of the optimal scaling laws. We show that when the specific fracture energy is renormalized in a manner suggested by the optimal scaling laws, the data falls within the bounds predicted by the analysis and, moreover, they ostensibly collapse—with allowances made for experimental scatter—on a master curve dependent on the hardening exponent, but otherwise material independent.

Contents

List of Figures

List of Tables

Chapter 1

Introduction

1.1 General overview

1.1.1 Experimental observations

Ductile fracture is a fundamental failure mode of metals that results from a concatenation of microscopic mechanisms of deformation including void nucleation, growth, coalescence and, ultimately, localization into fracture planes, cf. Figure 1.1, cf. also [31], [127] and references therein. In structural materials, the voids nucleate mainly at inclusions and second phase particles, by decohesion of the particle-matrix interface or by particle cracking (Goods and Brown 1979 [44], Puttick 1959 [94]), and subsequent void growth is driven by the plastic flow around the surrounding matrix. Unlike brittle materials, ductile materials undergo extensive plastic deformation before reaching the final stage of fracture. Tensile experiments on rounds bars often reveal that the failure is preceded by an important flow localization process characteristic of *necking*. Indeed, it is a common observation that necking comes with a substantial reduction in the cross sectional area, and further plastic deformation requires less applied stress. As a consequence, typical engineering stress-strain curves go through a maximum, sometimes identified as the Ultimate Tensile Strength (UTS) or *onset of necking*, a process which is followed by a geometrical softening until final separation of the specimen. As a result, the total work of fracture is ostensibly much larger in ductile materials than brittle materials, the excess being attributed to the plastic dissipation.

The evidence that void growth and coalescence represents the major failure mechanism in most

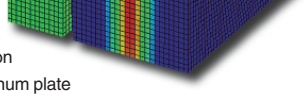

In this simulation of a gas-gun experiment, (a) is the initial configuration of aluminum striking a copper target, and (b) shows formation of spall. The green area on the left is the aluminum plate that strikes a 5-millimeter-thick cylindrical disk target. The target's two spall rings can be seen on the disk. The formation of voids (red) is seen in the center of the disk.

material, which closes the voids created by the original shock. Under these conditions, the damaged material could jet out from pores, continue deforming, have localized heating, and even melt.

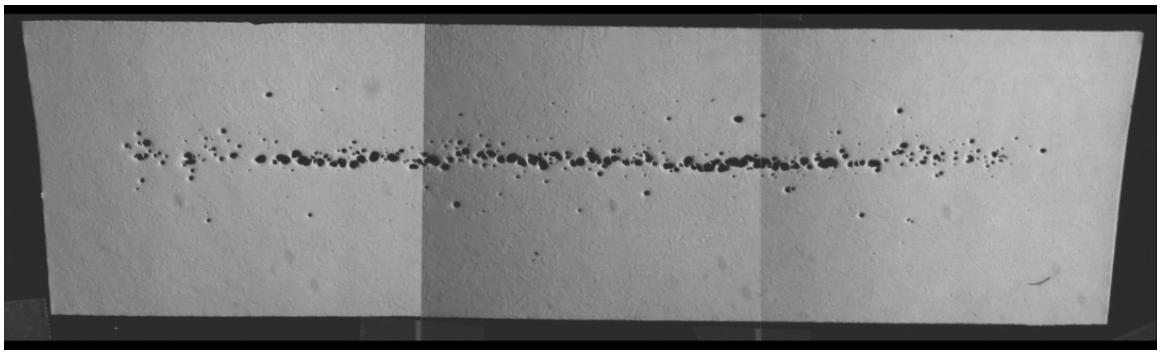

This photomicrograph of a copper disk used in a gas-gun experiment shows the formation of voids in the spall layer.

Figure 1.1: Photomicrograph of a copper disk tested in a gas-gun experiment showing the formation of voids and their coalescence into a fracture plane [49].

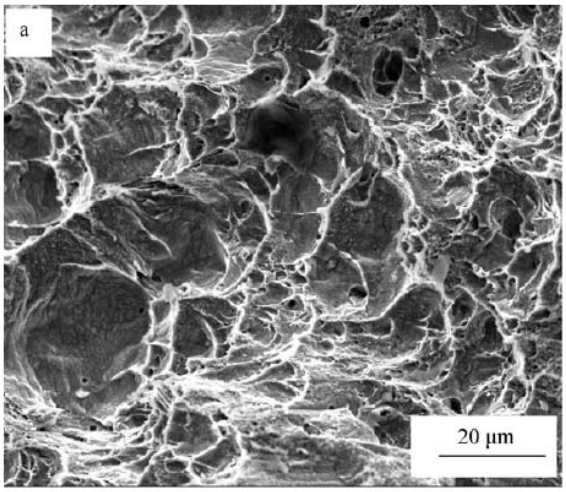

Figure 1.2: Fracture surface in SA333 steel at room temperature and strain rate $3 \times 10^{-3} s^{-1}$. Taken from Kamat et al [60]

structural materials comes from *fractography* studies using Transmission Electron Microscopy. These studies reveal that the fracture surfaces contain spherical dimples, which represent microvoids, cf. Figure 1.2. This is in stark contrast to the sharp specular cracks that result from brittle fracture.

Ductile fracture is of particular importance for industrial applications (oil and gas pipelines, nuclear powerplants, etc.) and the determination of fracture properties of ductile materials has been the focus of numerous investigations. In particular, a certain number of testing standards have been put forth, that, in turn, provide the basis for experimental design of materials. Among these testing standards, two require specific attention: *J-testing* and *Impact testing*.

1.1.2 *J*-integral testing

J-testing, which has been widely used in fracture mechanics, expresses the fracture criterion as a critical value of the J-integral. The standard J_{Ic} Test Method, E 813, has been issued by ASTM for determining the plane strain value of J at initiation of crack growth, namely J_{Ic}. The value of J_{Ic} obtained by this method may be used to characterize the toughness of materials at the onset of crack extension. The method originates from the observation of Begley and Landes [11] that J can be experimentally determined by the energy released rate according to the relation

$$J = -\frac{1}{B}(\frac{\partial U}{\partial a})_{\Delta} \tag{1.1.1}$$

where U is the strain energy and B is the thickness of the specimen. For a given value of Δ, one can use multiple specimens with different crack lengths a to compute the load-displacement curve. The area under this curve therefore represents the total strain energy, which can then be plotted as a function of the crack length. The value of J is retrieved from taking the negative slope of the strain energy versus crack length curve. The procedure could be repeated for different values of Δ to obtain a curve J versus Δ. Evidently, this method requires the use of multiple specimens and therefore has been improved in order to estimate J from a single measure load-displacement curve, as proposed by Rice et al [99]. More specifically, the standard J_{Ic} testing procedure, which uses a three point bend specimen and a compact specimen, requires the measurement of applied load and load-point displacement to obtain the total work done on the specimen. The load versus displacement is recorded automatically by an X-Y recorder and the extensions of the crack length are measured after breaking up the specimen upon deforming the specimen to desired values. The values of J are plotted against the crack growth to obtain an R-resistance curve which is fitted through a linear regression line. The critical J_{Ic} is then determined by the intersection between this line and the blunting line defined by

$$J = 2\sigma_y \Delta a_p \tag{1.1.2}$$

where σ_y represents the yield stress and Δa_p the physical crack extension. The use of the blunting line in equation (1.1.2) refers to the crack growth due to crack-tip blunting. It bears noting that this testing procedure additionally assumes specific validity conditions on the geometry of the specimen, as explained in the comprehensive study of fracture mechanics presented in Kanninen and Popelar [61]. Further details about the procedure have been skipped in this overview, but the reader can find a more extensive review of the method in [61]. This standard testing approach has found important applications in the characterization of a wide range of ductile engineering materials.

1.1.3 Impact testing

Impact testing measures the energy required to break a material sample. On the contrary of J-testing, the fracture energy obtained cannot be formally put into an equation. The most standard impact test is the Charpy V notch impact test which consists of a specimen containing a $2mm$ deep notch with radius $0.25mm$. The specimen, treated at a desired temperature, is placed into a holder and then struck with a hammer. The hammer is mounted at the end of a pendulum which is adjusted so that its kinetic energy is $240ft - lb$ when it hits the specimen. Upon breaking of the bar, the hammer reaches a final height, and the difference between the initial height and the final height translates into the energy absorbed by the material sample during the breaking. This energy is measured as the fracture energy of the material. This method has been extensively used to characterize fracture properties of materials at diverse temperatures and it has been observed that the specific fracture energy increases as a function of the temperature, which in turn, suggests that different fracture mechanisms occur at low temperatures and high temperatures. Figure 1.3 shows a typical Charpy curve obtained from a French $A508(16MND5)$ steel broken at various temperatures and strain rates. This picture illustrates a complex dependence of the fracture energy on temperature and reveals that at high temperatures, $A508$ steels fail by microvoid coalescence, characteristic of ductile failure whereas at low temperatures, they undergo cleavage fracture. This leads to the existence of a transition temperature at which the material behavior goes from brittle to ductile, and such temperature often receives the name of Ductile to Brittle Transition Temperature

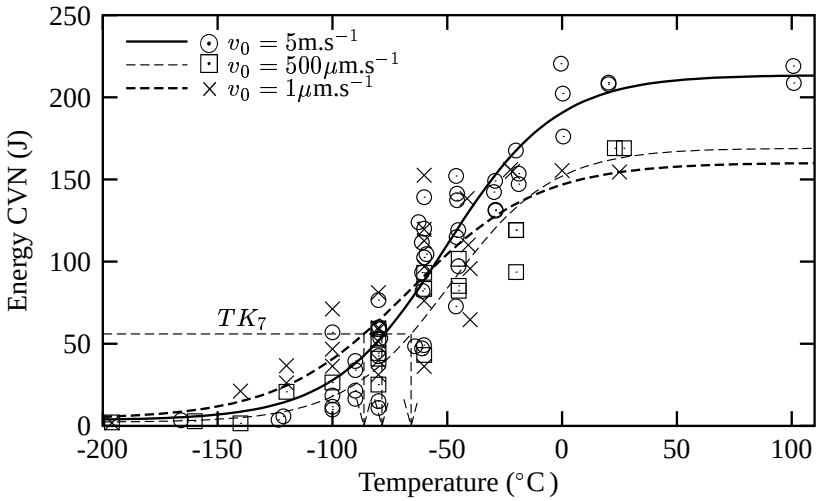

Fig. 4. Charpy V–notch (CVN) fracture toughness transition curves of 16MND5 (A508) for T-L Charpy specimens tested at different loading rates.

Figure 1.5: Temperature dependence of the fracture energy of an $A508$ steel. Taken from [112]

(DBTT). In general, the temperature and strain rate dependence of fracture properties of materials has been the subject of scientific investigation, see for instance Kamat et al [60], Tvergaard and Needleman [128], Shin et al [106], Shetty et al [105], Armstrong and Walley [3], Wang et al [130], and references therein.

1.1.4 Surface energies

We summarize here two major mechanisms responsible for the surface energies in ductile fracture: the coalescence of cavities by internal necking and the cleavage crack growth in presence of plastic deformation.

In Thomason 1970 [120], an estimate of the surface energy for the coalescence of cavities was derived. The results suggested that internal microscopic necking of ligaments between cavities contributes to the total surface energy and that the corresponding surface energy is a function of the mean-free-path between cavities or second phase particles. The model used a coalescence criterion derived in Thomason 1968 [119] to compute the plastic work per unit area of subsequent fracture surface during *necking down*, i.e. when the the cross sectional area of the ligaments is further reduced after a uniform extension. The theoretical values of the coalescence energy obtained were

found to be about an order of magnitude less than experimental estimates of the total surface energy for ductile crack propagation. In reality, experimental measurements include a contribution from pre-coalescence straining ahead of the advancing crack which strongly depends on the extent of the plastic zone ahead of the crack.

Plastic dissipation around a crack tip supplies a considerable contribution to the fracture energy in ductile materials. The surface energy associated with crack growth is related to the microscopic mechanisms of cleavage in the presence of plastic flow. A wealth of experimental evidence exhibited the phenomenon of crack propagation in the presence of pre-existing dislocations. For example, it was found in Lipkin et al, [71] that a sharp crack can propagate along a gold-sapphire interface, nevertheless the gold deforms plastically, indicating the motion of vast quantities of dislocations and the measured fracture energy was found to be orders of magnitude larger than the surface energy. When fracture occurs by atomic separation, the length scale of the fracture process is typically smaller than the dislocation spacing or the elastic cell size within the dislocation structure, which is the length scale of the plastic deformation. Thus, in a small region near the tip, the stress fields are more like those at a linear elastic crack tip singularity. Because of the large disparity between relevant length scales involved in plastic flow processes around cracks in metals and metal-ceramic interfaces [110], Suo et al, [110] have proposed the use of a long dislocation free strip of elastic material inside which the crack propagates. These lengths typically consist of the Burgers vector, $b \sim 10^{-10}m$ which is relevant for fracture by atomic separation; the nominal dislocation spacing, around $10^{-7} - 10^{-6}m$, characteristic of plastic flow; and the overall plastic zone size. A similar approach using an elastic strip was further used by Beltz et al, [12] to develop a self-consistent model for cleavage. Basically, the idea is to postulate that the crack tip does not emit any dislocation and there exists a core elastic region (i.e. free of dislocations) near the tip surrounded by the plastic zone. Using finite element calculations, it was found that, in order for a steady-state crack growth to occur, the applied energy release rate must generally be several orders of magnitude larger than Griffith energy at the crack tip (i.e. inside the elastic strip). This result is well in agreement with experimental observations, e.g. Tetelman [116], which suggest that the fracture energy is expected to be up to 4 orders of magnitude

larger than surface energies.

1.2 Previous work on ductile fracture

The first micromechanical studies of ductile fracture go back to the pioneer works of McClintock 1968 [77] and Rice and Tracey 1969 [98] who studied the growth of a single void in an infinite elastic-plastic solid, and showed that fracture by void coalescence is promoted by a high level of stress triaxiality. This was confirmed by numerous triaxial tension test experiments on tensile specimens (Hanckok and Mackenzie 1976 [48], Hancock and Brown 1983 [47]). Gurson 1977 [45] developed the most widely known porous ductile material model based on averaging techniques. His void growth model was given in terms of a macroscopic yield condition as a function of one microstructural parameter, namely the void volume fraction. A number of extension models have been attempted in order to account for void nucleation (Chu and Needleman 1980 [16]), void shape effects (Gologanu, Leblond and Devaux [37], [39], [41], [43]), strain hardening effects (Leblond et al 1995 [70]), kinematic hardening (Mear and Hutchinson 1985 [79]). Also, computational models have been put forth to investigate the void growth and coalescence mechanism. Such micromechanical models, sometimes referred to as *cell model studies*, have been the focus of numerous authors such Tvergaard [121], [124], [126],[125], Hutchinson and Tvergaard 1987 [58], Needleman and Tvergaard 1984 [88]. Coalescence models also include the studies of Gologanu [38], [40], [42] or Thomason [119], [117], [118]. During the deformation of ductile solids, it is observed that a smooth deformation can develop into a highly concentrated deformation pattern, which corresponds to the localization of the plastic flow into shear bands. Analysis of the bifurcation into shear bands has been the subject of the works of Hill 1962 [52], Rice 1977 [96], and Rudnicki and Rice 1975 [100]. A wealth of computational description of plastic localization is contained in the works of Tvergaard [121], [124], [126],[125]. Those treatments, which complement the initial void model of Gurson, mainly revealed the presence of voids as main catalysts of localization and derived critical coalescence conditions.

Recently, efforts have been made to relate macroscopic properties to the structure and material behavior at the microscale. For instance, Pardoen and Hutchinson 2002 [93] developed relations

between fracture toughness and microstructural details for ductile materials based on a generalized Gurson model that accounts for both growth and coalescence. The microstructural parameters were the initial porosity, the void shape and spacing, as well as the void spacing anisotropy. In the works of Tvergaard ([126],[122], [123],[89]) and Nielsen and Tvergaard [89], an emphasis has been on the interaction between voids with two size length scales, the smaller size voids appearing as defects in the ligaments, i.e. spacing between primary voids.

1.3 Motivation

So far, the existing experimental data at best provide partial coverage of ductile fracture properties over a limited range of temperatures, strain rates and other relevant operating conditions, and may be entirely lacking under off-normal or extreme conditions and for new materials. The existing micromechanical models, which strongly rely on conventional plasticity theories, partially explain the complex dependence of the fracture properties on temperature and strain rate. Moreover, models that accurately quantify surface energies and rigorously predict their contribution to the total work of fracture are still almost non existent. Finally, the classical models (mostly empirical or computational) rely strongly on heuristics and intuition and often do not lend themselves to a mathematically rigorous analysis of ductile fracture. The goal of this thesis is to present a rigorous mathematically tractable model that unifies plasticity, surface energy and fracture. An emphasis will be put on the complex relationship between macroscopic quantities and microscopic properties, along with their temperature dependence, within a multiscale framework. In this way, the present work describes ductile fracture as a multiscale phenomenon, and therefore falls naturally within a multiscale hierarchy.

The multiplicity of length scales involved in ductile fracture strongly suggests the use of methods of multiscale analysis from the calculus of variations. Indeed, despite the irreversible and path-dependent character of plasticity, under monotonic and proportional loading conditions plasticity problems may be recast as energy minimization problems by recourse to deformation-theory of plasticity (e. g., [75] and references therein). Throughout this work, we therefore assume deformation

theory of plasticity and by *effective energy* we specifically mean a deformation-theoretical energy that jointly accounts for both free energy and plastic dissipation.

Two main features render the resulting ductile-fracture problem non-standard and lend it mathematical interest, namely, *sublinear energy growth* and *strain-gradient hardening*. The physical basis underlying these fundamental properties may be understood as follows. For large material samples undergoing slowly-varying deformations in their interior, the effective energy of metals is observed to ostensibly exhibit conventional volume scaling, i.e., it scales with the volume of the sample when all lengths, including displacements, are scaled uniformly. Energies that possess volume scaling are referred to as *local*, since they can be written as the integral of an energy density which depends on the local deformation gradient. Such local energies can be characterized by means of conventional constitutive testing, such as uniaxial tension tests, tension-torsion tests, and other similar means. However, when observed through constitutive tests on large samples, the local limit of the effective energy of metals is invariably found to exhibit *sublinear growth* at large deformations (cf. section 2.1.1). Such sublinear growth is a reflection of the work hardening characteristics of large metallic specimens and gives rise to well-known geometric instabilities such as the necking of bars, sheet necking, and others (cf., e. g., [76]). From the viewpoint of the calculus of variations, energies with sublinear growth relax to zero for every deformation and thus fail to supply useful information regarding the fracture properties of metals. Physically, the relaxation process corresponds to the concentration of deformation to small volumes such as shear bands. The deformation is then proportional to $1/\delta$ in a volume of size $\delta \to 0$, and since the energy density has sublinear growth its contribution to the total energy is negligible in the limit. Similar instabilities are present in many local problems characterized by nonconvex energy densities.

In metals undergoing ductile fracture this inherently unstable behavior is held in check by a second fundamental property of metals, namely, the *strain-gradient hardening* [27, 30, 28, 29]. This property of metals has been extensively investigated and demonstrated by means of torsion tests in wires [30], nanoindentation [90, 132, 54], and by other means. Specifically, for fixed local deformation, the effective energy density of metals is observed to be an increasing function of the local strain

gradient, or the second deformation gradient. This property results in deviations from volume scaling, i.e., in *nonlocal behavior* and *size dependency*, in sufficiently small material samples. Under these conditions, we show in the present work that ductile fracture emerges as the net result of two competing effects: whereas the sublinear growth of the energy in the large-body limit promotes localization of deformation in large samples to failure planes, the size-dependence of metal plasticity stabilizes this process of localization in its advanced stages, thus resulting in an orderly progression towards failure and a well-defined specific fracture energy.

1.4 Outline of the thesis

The plan of the thesis is as follows:

The last section of this introductory chapter is devoted to some mathematical preliminaries. We present basic concepts from topology and functional analysis, and define notations that will be used throughout the thesis.

In Chapter 2, we show that homogenization fails for ductile fracture. More precisely, we show explicitly, by means of a simple construction, later referred to as a *necking construction*, that the sublinear growth of the energy density is responsible for the localization of deformations. The strain energy then relaxes to zero, which evidently provides no useful information on fracture properties. This motivates the addition of a stabilizing non-local component to the strain energy density that accounts for size effects using strain gradient plasticity. As a consequence, a characteristic length scale is introduced, in the same spirit of previous strain gradient plasticity models in the literature, which will briefly be discussed as well in this chapter. We present a simple deformation theory of plasticity model that accounts for both local and non-local effects.

The aim of Chapter 3 is to present a rigorous analysis of some qualitative properties of ductile fracture. The key strategy consists of the derivation of *optimal scaling laws*—as opposed to searching for exact minimizers—for energies exhibiting both sublinear growth in the local limit and strain-gradient hardening. The main result is that optimal scaling is achieved by a void sheet construction and the fracture energy obeys a well- defined relationship with respect to other material parameters,

namely the imposed displacement, the length scale and the hardening exponent.

Physical interpretation and experimental validation are the core of Chapter 4. On the one hand, we derive a physical explanation of the optimal scaling laws of Chapter 3. On the other hand, we assess the validity of the scaling relations based on experimental data. We show that the test data collapse remarkably within the bounds predicted by the analysis.

We present our concluding remarks and future directions as part of Chapter 5. We particularly evoke some aspects of the numerical implementation using finite elements.

1.5 Mathematical Preliminaries

We present some basic concepts of functional analysis and topologies associated with function spaces. Throughout this work, the notation "D" will be used to denote the gradient. We start with the definition of the classical *Lebesgue* spaces L^p.

Definition 1.5.1 *(Lebesgue spaces)*

(i) Let $\Omega \subset \mathbb{R}^n$ be an open set and $1 \leq p \leq \infty$. For $u : \Omega \to \mathbb{R}$, we set:

$$\|u\|_{L^p} := (\int_\Omega |u|^p dx)^{1/p} \ if \ 1 \leq p < \infty$$

$$\|u\|_{L^\infty} := inf\{C \in [0,\infty] : |u(x)| \leq C \ for \ a.e. \ x \in \Omega\}$$

We say that $u \in L^p(\Omega)$ if $\|u\|_{L^p(\Omega)} < \infty$. The set $L^p(\Omega)$ is a Banach space and $\|.\|_{L^p}$ is a norm on that space.

(ii) Let $u_n, u \in L^p(\Omega)$. We say that $u_n \to u$ strongly in L^p if $\|u_n - u\|_{L^p} \to 0$ as $n \to \infty$.

As illustrated in Definition 1.5.1, the definition of the Lebesgue space does not involve first or higher order derivatives. Derivatives are accounted for by extending the concept of norm L^p to u and its derivatives, which gives rise to Sobolev spaces.

Definition 1.5.2 *(Sobolev spaces) Let $\Omega \subset \mathbb{R}^n$ be an open set and $1 \leq p \leq \infty$. We define the Sobolev space $W^{1,p}(\Omega)$ by the set of functions $u : \Omega \to \mathbb{R}, u \in L^p(\Omega)$, whose weak partial derivatives*

$\frac{\partial u}{\partial x_i} \in L^p(\Omega)$ *for every* $i = 1, .., n$. *We endow this space with the following norm*

$$\|u\|_{W^{1,p}} := (\|u\|_{L^p}^p + \|Du\|_{L^p}^p)^{1/p} \ if \ 1 \leq p < \infty$$

$$\|u\|_{W^{1,\infty}} := max\{\|u\|_{L^\infty}, \|Du\|_{L^\infty}\} \ if \ p = \infty$$

Strong connections between Lebesgue spaces, Sobolev spaces and their topologies are reflected through the Sobolev embedding theorem and Sobolev inequalities, whose statements and complete proof can be found in [26]. Here we simply recall the classical Sobolev inequalities, also referred to as Poincaré inequalities.

Theorem 1.5.1 *Let* $\Omega \subset R^n$ *be a bounded open set with a Lipschitz boundary.*

(i) Case 1. If $1 \leq p < n$, *then* $W^{1,p}(\Omega) \subset L^q(\Omega)$ *for every* $q \in [1, p*]$, *where* $p*$ *is the Sobolev exponent defined by*

$$\frac{1}{p*} = \frac{1}{p} - \frac{1}{n}, \ i.e. \ p* = \frac{np}{n-p} \tag{1.5.1}$$

More precisely, for every $q \in [1, p*]$ *there exists* $c = c(\Omega, p, q)$ *such that*

$$\|u\|_{L^q} \leq c\|u\|_{W^{1,p}} \tag{1.5.2}$$

(ii) Case 2. If $p = n$, *then* $W^{1,n}(\Omega) \subset L^q(\Omega)$ *for every* $q \in [1, \infty)$. *More precisely, for every* $q \in [1, \infty)$ *there exists* $c = c(\Omega, p, q)$ *such that*

$$\|u\|_{L^q} \leq c\|u\|_{W^{1,n}} \tag{1.5.3}$$

For more details concerning Sobolev spaces, we refer to Adams [1], Brezis [13], Dacorogna [21], Dacorogna-Marcellini [22], Ekeland-Temam [25], Evans [26], Gilbarg and Trudinger [35], Giusti [36], Kufner-John-Fucik [65], Ladyzhenshaya-Uraltseva [69] or Morrey [84].

We finish this section with a brief overview of functions of bounded variation. Functions of bounded variations (BV functions) have an important application for problems in the calculus of

variations. This class of functions has been the natural tool to study problems characterized by free discontinuities, for example image segmentation theory or fracture mechanics. BV functions have two main characteristics: they are functions with a measure distributional derivative or function which are L^1 limits of of bounded sequences in $W^{1,1}$. In what follows, we present some of the basic definitions and results, taken from the book of Ambrosio, Fusco and Pallara [2]. We refer the reader to this book for a thorough description of BV spaces.

Definition 1.5.3 *Let $u \in L^1(\Omega)$; we say that u is a function of bounded variation in Ω if the distributional derivative of u is representable by a finite Radon measure in Ω, i.e. if*

$$\int_\Omega u \ \frac{\partial \phi}{\partial x_i} dx = -\int_\Omega \phi \ dD_i u \ \forall \phi \in C_c^\infty(\Omega), \ i = 1, ..., N \tag{1.5.4}$$

for some $\mathbb{R}^N$-valued measure $Du = (D_1 u, ..., D_N u)$ in Ω. The vector space of all functions of bounded variation in Ω is denoted by $BV(\Omega)$

An equivalent representation of the formulae in 1.5.3 is:

$$\int_\Omega u \ div\phi dx = -\sum_{i=1}^N \int_\Omega \phi_i \ dD_i u \ \forall \ \phi \in [C_c^1(\Omega)]^N \tag{1.5.5}$$

An important observation is that the Sobolev space $W^{1,1}(\Omega)$ is contained in $BV(\Omega)$, because its directional derivative is absolutely continuous with the standard Lebesgue measure of $\mathbb{R}^N$, with a Radon-Nikodym derivative corresponding to the (approximate) gradient of u, see [2]. An advantage of BV spaces is that, unlike Sobolev spaces, they include characteristic functions of sufficient regular sets, and more generally piecewise smooth functions. Now, we proceed to the definition of the variation of BV functions, which provides an equivalent characterization of BV spaces.

Definition 1.5.4 *(i) Let $u \in [L^1_{loc}(\Omega)]^m$ (locally integrable). The variation $V(u, \Omega)$ is defined by*

$$V(u, \Omega) := sup\{\sum_{i=1}^N \int_\Omega u^\alpha div\phi^\alpha dx : \phi \in [C_c^1(\Omega)]^{n \times N}, \|\phi\|_\infty \leq 1\} \tag{1.5.6}$$

For u continuously differentiable, then $V(u, \Omega) = \int_\Omega |Du| dx$.

(ii) Let $u \in [L^1(\Omega)]^m$. Then u belongs to $[BV(\Omega)]^m$ if and only if $V(u,\Omega) < \infty$. In addition, $V(u,\Omega) = |Du|(\Omega)$ for $u \in [BV(\Omega)]^m$, here $|Du|(\Omega)$ represents the total variation of the measure Du.

(iii) The space $[BV(\Omega)]^m$ endowed with the norm

$$\|u\|_{BV} := \int_\Omega |u|dx + |Du|(\Omega) \tag{1.5.7}$$

is a Banach space.

Now we introduce the so-called weak* convergence in $BV(\Omega)$, which is weaker than the norm convergence.

Definition 1.5.5 *(Weak* convergence) Let $u, u_n \in [BV(\Omega)]^m$. We say that (u_n) weakly* converges in $[BV(\Omega)]^m$ to u if (u_n) converges to u in $[L^1(\Omega)]^m$ and (Du_n) weakly* converges to Du in measure in Ω, i.e.*

$$\lim_{n\to\infty} \int_\Omega \phi \; dDu_n = \int_\Omega \phi \; dDu \;\; \forall \;\; \phi \in C_0(\Omega) \tag{1.5.8}$$

A simple criterion for weak* convergence is given by the following proposition (see [2], Proposition 3.13)

Proposition 1.5.1.1 *Let $(u_n) \subset [BV(\Omega)]^m$. Then (u_n) converges weakly* to u in $[BV(\Omega)]^m$ if and only if (u_n) is bounded in $[BV(\Omega)]^m$ and converges to u in $[L^1(\Omega)]^m$.*

The concepts above mentioned are useful for the analysis presented in Chapter 2 and Chapter 3 of this thesis.

Chapter 2

From Necking Instability to Strain Gradient Plasticity

In this chapter, we wish to argue that conventional plasticity models do not suffice to understand ductile fracture, and thus, one has to introduce non-local effects, which naturally suggests the existence of a characteristic length scale. The key point to this observation is that, from the standpoint of the calculus of variations, the energy densities are concave due to their sublinear growth (see section 2.1.1), and thus their corresponding energy functionals relax to zero. We illustrate this concept by means of a simple example, which mainly serves as a motivation for formulating a strain gradient plasticity model. The relaxation is achieved by a localization technique suitable for non-convex problems.

2.1 A localization construction

In conventional theories of plasticity, large material samples exhibit energies that have a volume scaling, i.e. energies scale as the volume of the sample when all lengths, including the displacements, are scaled uniformly. Such energies are referred to as *local* and are appropriate to describe plasticity for *bulk* materials. Local theories derive mostly from conventional constitutive testing, e.g. uniaxial tension experiments, which provide the basis for constitutive laws, which in turn, can be recast in the form of energy functionals by recourse to the deformation theory of plasticity. For large deformations, the energies possess a *sublinear* growth that is a reflection of the work hardening

characteristic of large metallic specimen and gives rise to geometric instabilities such as *necking*. In this section, we present an analytical description of *necking* and how it relates to localization of plastic deformation which usually precedes fracture in ductile materials.

2.1.1 Uniaxial tension test

Let $\Omega \in \mathbb{R}^3$ be a bounded domain undergoing a transformation $u : \Omega \to \mathbb{R}^3$. Within the context of deformation theory of plasticity, the bulk energy density of crystalline materials results from the contribution of both an elastic energy and a plastic stored energy according to the relation:

$$W(F, F_p) = W^e(FF_p^{-1}) + W^p(F_p) \tag{2.1.1}$$

where $F = Du$ and F_p represents the plastic transformation. We have used the the multiplicative decomposition $F = F_e F_p$. The incompressibility of the plastic transformation yields the additional constraint

$$detF_p = 1 \tag{2.1.2}$$

Consider the uniform uniaxial tension (along the x_3 direction) of a rigid-plastic bar for which the deformation gradient is homogeneous and given by $\mathbf{F} = Du = diag(\frac{1}{\sqrt{\lambda}}, \frac{1}{\sqrt{\lambda}}, \lambda)$. We further assume that the material undergoes a fully plastic deformation, in which case $Du = F_p$. The energy density then reads:

$$W(F) = W^p(F) \tag{2.1.3}$$

We have assumed the material to be rigid plastic, i.e W^e vanishes in $SO(3)$. The incompressibility condition further reduces to

$$detF = 1 \tag{2.1.4}$$

For crystalline materials, stress-strain curves exhibit a power-law relationship between the true stress and the engineering strain in the form $\sigma = K(\lambda - 1)^n$ where K is the strength coefficient and n is the hardening exponent, with $0 < n < 1$ for metals. Then the Piola-Kirchhoff stress P, which is

equal to the axial force applied to the rod divided by the undeformed cross-sectional area, is given by:

$$P = \partial_\lambda W = K(\lambda - 1)^n \lambda^{-1} \tag{2.1.5}$$

which for large λ scales as

$$\partial_\lambda W \sim K\lambda^{n-1} \tag{2.1.6}$$

Therefore, in the same range the energy density scales as

$$W \sim \frac{K}{n}\lambda^n \tag{2.1.7}$$

Now let us denote for the rest of the sequel

$$A = \frac{K}{n} \tag{2.1.8}$$

We take the previous assumptions as grounds for defining a bulk energy functional of the form:

$$E_{bulk}(u) = A \int_\Omega (|Du|^n - 3^{n/2}) dx \tag{2.1.9}$$

The term $3^{n/2}$ guarantees that the stored energy is zero when $Du = I$, where I is the identity matrix. A simple dimensional analysis shows that the quantity A is in the unit of a pressure (Pascal) which corresponds to an energy per unit volume. Conformably to (2.1.9), the strain energy density satisfies

$$W(F) \sim |F|^n \tag{2.1.10}$$

with $0 < n < 1$. Because the exponent $n < 1$, the strain energy density W is said to have a *sublinear growth*. For the homogeneous deformation considered in this section, the bulk energy reads:

$$E_{bulk}(\lambda) = A|\Omega|((\lambda^2 + \frac{2}{\lambda})^{n/2} - 3^{n/2}) \tag{2.1.11}$$

where $|\Omega|$ represents the volume of the domain Ω. The Piola stress then reads:

$$P(\lambda) = \frac{\partial W}{\partial \lambda} = An(\lambda - \frac{1}{\lambda^2})(\lambda^2 + \frac{2}{\lambda})^{\frac{n}{2}-1} \tag{2.1.12}$$

Figure 2.1 illustrates the dependence of the force P as function of the elongation for different values of n. It is clear from the plot that for $n \geq 1$, the force increases continually with the elongation, but this behavior is different when $n < 1$, the range for most metals. Indeed, the curve shows an increase of the force versus elongation up to a maximum value, and subsequent elongation requires less applied force. This decrease of the force with respect to the elongation for sufficient large elongations is characteristic of *geometrical softening*, a fundamental property of ductile materials. Such behavior is mainly tied to the sublinear growth of the energy density and confirms the Considère prediction [17] that necking is more likely to occur for materials whose force-elongation curves go through a maximum.

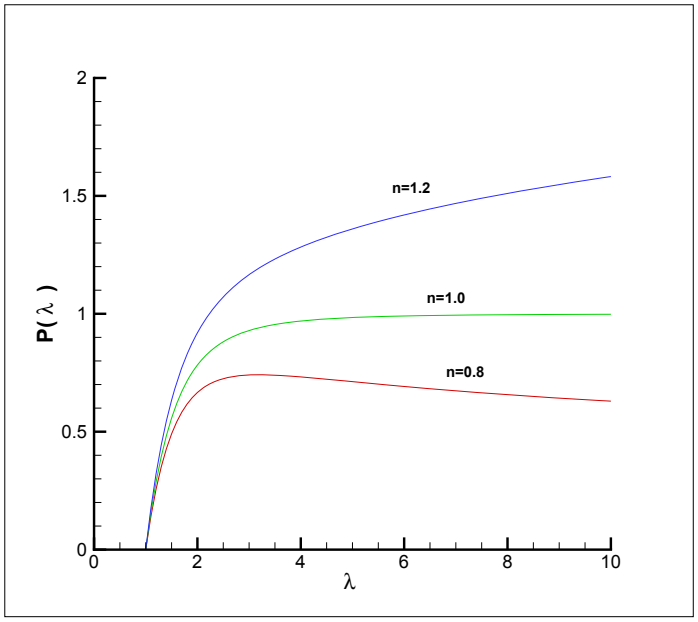

Figure 2.1: Force-elongation curve for different values of n.

2.1.2 Necking construction

In this section, we provide an analytical, but simple characterization of plastic localization, by means of a simple example. We consider here a bar with square cross-sectional area, clamped at its bottom and subject to a prescribed displacement on its top. Within the assumptions of section 2.1.1, we wish to minimize the quantity (2.1.9). More precisely, we consider the minimum problem:

$$inf\{E_{bulk}(u) = A\int_{\Omega}(|Du|^n - 3^{n/2})dx : detDu = 1\} \tag{2.1.13}$$

The infimum value for (2.1.13) is zero and is achieved by a minimizing sequence that exhibits concentration on the mid-plane, as stated in the following proposition:

Proposition 2.1.0.2 *Let* $\Omega = \{(x_1, x_2, x_3), -\frac{a}{2} \leq x_1 \leq \frac{a}{2}, -\frac{a}{2} \leq x_2 \leq \frac{a}{2}, -L \leq x_3 \leq L\}$. *The bar is subject to uniaxial axial tension along the* x_3 *axis and the boundary conditions are expressed as follows:*

$$\begin{cases} u_3(x_1, x_2, -L) = -L \\ u_3(x_1, x_2, L) = L + \delta \end{cases} \tag{2.1.14}$$

Let $\Phi : [-L, L] \to \mathbb{R}$ *continuous and compactly supported on* $[-L, L]$ *defined by:*

$$\Phi(x_3) = \begin{cases} \frac{\delta}{L}(\frac{x_3}{L} + 1), & if\ -L \leq x_3 \leq 0 \\ \frac{\delta}{L}(-\frac{x_3}{L} + 1), & if\ 0 \leq x_3 \leq L \end{cases} \tag{2.1.15}$$

Now consider the following sequence u_n *of deformations:*

$$\begin{cases} u_{1n} = \frac{x_1}{\sqrt{\varphi_n'(x_3)}} \\ u_{2n} = \frac{x_2}{\sqrt{\varphi_n'(x_3)}} \\ u_{3n} = \varphi_n(x_3) \end{cases} \tag{2.1.16}$$

where $\varphi_n : [-L, L] \to \mathbb{R}$ *is a sequence of continuous functions such that*

$$\varphi_n'(x_3) = \lambda_n(x_3) = 1 + n\Phi(nx_3) \tag{2.1.17}$$

Then the following holds:

(i) $\lim_{n\to\infty} E_{bulk}(u_n) = 0$

(ii) u_n *converges weakly* to* u *in* $BV(\Omega, \mathbb{R}^3)$ *where*

$$\begin{cases} u_1 = x_1 \\ u_2 = x_2 \\ u_3 = \varphi(x_3) \end{cases} \tag{2.1.18}$$

with

$$\varphi(x_3) = \begin{cases} x_3, & -L \le x_3 \le 0 \\ x_3 + \delta, & 0 \le x_3 \le L, \end{cases} \tag{2.1.19}$$

proof 2.1.1 *(i) We prove part (i). In order to avoid confusion of notation, the growth exponent is denoted p instead of n which will be used to label any given sequence. Denoting* $\varphi_n'(x_3) = \lambda_n(x_3)$*, the deformation gradient is given by :*

$$Du_n = \begin{pmatrix} \lambda_n^{-1/2}(x_3) & 0 & -\frac{1}{2}\lambda_n^{-3/2}(x_3)\lambda_n'(x_3)x_1 \\ 0 & \lambda_n^{-1/2}(x_3) & -\frac{1}{2}\lambda_n^{-3/2}(x_3)\lambda_n'(x_3)x_2 \\ 0 & 0 & \lambda_n(x_3) \end{pmatrix}, \tag{2.1.20}$$

The sequence λ_n *such defined is compactly supported in* $[-L/n, L/n]$ *and the resulting sequence of maps exhibits a concentration effect on the plane* $x_3 = 0$*. More precisely, the sequence* λ_n *is defined by:*

$$\lambda_n(x_3) = \begin{cases} 1, & -L \le x_3 \le -L/n \\ 1 + n\frac{\delta}{L}(n\frac{x_3}{L} + 1), & -L/n \le x_3 \le 0 \\ 1 + n\frac{\delta}{L}(-n\frac{x_3}{L} + 1), & 0 \le x_3 \le L/n \\ 1, & L/n \le x_3 \le L, \end{cases} \tag{2.1.21}$$

It follows that the corresponding sequence of maps can be expressed in the following form:

$$\begin{cases} u_1^n = \frac{x_1}{\sqrt{\varphi_n'(x_3)}} \\ u_2^n = \frac{x_2}{\sqrt{\varphi_n'(x_3)}} \\ u_3^n = \varphi_n(x_3) \end{cases} \tag{2.1.22}$$

where

$$\varphi_n(x_3) = \begin{cases} x_3, & -L \le x_3 \le -L/n \\ x_3 + n\frac{\delta}{L}(n\frac{x_3^2}{2L} + x_3) + \frac{\delta}{2}, & -L/n \le x_3 \le 0 \\ x_3 + n\frac{\delta}{L}(-n\frac{x_3^2}{2L} + x_3) + \frac{\delta}{2}, & 0 \le x_3 \le L/n \\ x_3 + \delta, & L/n \le x_3 \le L, \end{cases} \tag{2.1.23}$$

In what follows we wish to compute the following quantity

$$\hat{E} = \lim_{n\to\infty} E_{bulk}(u_n) \tag{2.1.24}$$

A straightforward computation shows that:

$$|Du_n| = [\lambda_n^2 + \frac{2}{\lambda_n} + \frac{x_1^2 + x_2^2}{4}\frac{\lambda_n'^2}{\lambda_n^3}]^{1/2} \tag{2.1.25}$$

The bulk energy is given by:

$$E_{bulk}(u_n) = \int_{-\frac{a}{2}}^{\frac{a}{2}}\int_{-\frac{a}{2}}^{\frac{a}{2}}\int_{-L}^{L}\left([\lambda_n^2 + \frac{2}{\lambda_n} + \frac{x_1^2 + x_2^2}{4}\frac{\lambda_n'^2}{\lambda_n^3}\right]^{p/2} - 3^{p/2})dx_1dx_2dx_3 \tag{2.1.26}$$

We can write that:

$$\begin{aligned} \int_{-L}^{L}(\lambda_n^2 + \frac{2}{\lambda_n} + \frac{r^2}{4}\frac{\lambda_n'^2}{\lambda_n^3})^{p/2}dx_3 = 2\int_{-L}^{-L/n} 3^{p/2}dx_3 \\ + \int_{-L/n}^{0}(\lambda_n^2 + \frac{2}{\lambda_n} + \frac{x_1^2 + x_2^2}{4}\frac{\lambda_n'^2}{\lambda_n^3})^{p/2}dx_3 \\ + \int_{0}^{L/n}(\lambda_n^2 + \frac{2}{\lambda_n} + \frac{x_1^2 + x_2^2}{4}\frac{\lambda_n'^2}{\lambda_n^3})^{p/2}dx_3 \end{aligned}$$

Now let

$$I_1 = \int_{-L/n}^{0} (\lambda_n^2 + \frac{2}{\lambda_n} + \frac{x_1^2 + x_2^2}{4}\frac{\lambda_n'^2}{\lambda_n^3})^{p/2} dx_3 \tag{2.1.27}$$

And similarly let

$$I_2 = \int_{0}^{L/n} (\lambda_n^2 + \frac{2}{\lambda_n} + \frac{x_1^2 + x_2^2}{4}\frac{\lambda_n'^2}{\lambda_n^3})^{p/2} dx_3 \tag{2.1.28}$$

Using the inequality $(a+b)^{p/2} \leq a^{p/2} + b^{p/2}$ *for* $a, b > 0, p/2 < 1$ *we can write:*

$$I_1 \leq \int_{-L/n}^{0} \lambda_n^p dx_3 + 2^{p/2} \int_{-L/n}^{0} \lambda_n^{-p/2} dx_3 + (\frac{x_1^2 + x_2^2}{4})^{p/2} \int_{-L/n}^{0} \frac{|\lambda_n'|^p}{\lambda_n^{3p/2}} dx_3 \tag{2.1.29}$$

By a change of variable $u = \frac{\delta}{L}(n\frac{x_3}{L} + 1)$ *we have the following equalities:*

$$\begin{aligned}
\int_{-L/n}^{0} \lambda_n^p dx_3 &= \int_{-L/n}^{0} (1 + n\frac{\delta}{L}(n\frac{x_3}{L} + 1))^p dx_3 \\
&= \frac{L^2}{n\delta}\frac{1}{n}\int_0^{\frac{\delta}{L}} n(1+nu)^p du \\
&= \frac{L^2}{\delta n^2}[\frac{(1+nu)^{p+1}}{p+1}]_0^{\frac{\delta}{L}} \\
&= \frac{L^2}{\delta(p+1)}\frac{1}{n^2}((1+n\frac{\delta}{L})^{p+1} - 1) \\
&= \frac{L^2}{\delta(p+1)}(\frac{(1+n\frac{\delta}{L})^{p+1}}{n^2} - \frac{1}{n^2}) \to 0 \ as \ n \to \infty \ for \ p < 1.
\end{aligned} \tag{2.1.30}$$

Similarly,

$$\begin{aligned}
\int_{-L/n}^{0} \lambda_n^{-p/2} dx_3 &= \frac{L^2}{n\delta}\frac{1}{n}\int_0^{\frac{\delta}{L}} \frac{n}{(1+nu)^{p/2}} du \\
&= \frac{L}{\delta n^2}\frac{1}{\frac{p}{2}-1}[\frac{-1}{(1+nu)^{\frac{p}{2}-1}}]_0^{\frac{\delta}{L}} \\
&= \frac{L^2}{\delta(\frac{p}{2}-1)}\frac{1}{n^2}(1 - \frac{1}{(1+n\frac{\delta}{L})^{\frac{p}{2}-1}}) \to 0 \ as \ n \to \infty.
\end{aligned} \tag{2.1.31}$$

Finally

$$\begin{aligned}\int_{-L/n}^{0}\frac{|\lambda_n'|^p}{\lambda_n^{3p/2}}dx_3 &= \frac{\delta^p}{L^{2p}}\frac{L^2}{\delta n}\int_0^{\frac{\delta}{L}}\frac{n^{2p}}{(1+nu)^{3p/2}}du \\ &= \frac{\delta^p}{L^{2p}}n^{2(p-1)}\frac{L^2}{\delta(\frac{3p}{2}-1)}[\frac{-1}{(1+nu)^{3p/2-1}}]_0^{\frac{\delta}{L}} \\ &= \frac{\delta^p}{L^{2p}}\frac{L^2}{\delta(\frac{3p}{2}-1)}(n^{2(p-1)}-\frac{n^{2(p-1)}}{(1+n\frac{\delta}{L})^{\frac{3p}{2}-1}}) \\ &\to 0 \text{ as } n\to\infty \text{ when } p<1 \text{ and } p\neq 2/3.\end{aligned} \tag{2.1.32}$$

For $p = 2/3$, the previous calculation resumes to evaluating

$$\begin{aligned}n^{2p-2}\int_0^{\frac{\delta}{L}}\frac{n}{1+nu}dx &= n^{2p-2}[log(1+nu)]_0^{\frac{\delta}{L}} \\ &\to 0 \text{ as } n\to\infty\end{aligned} \tag{2.1.33}$$

It follows that $I_1 \to 0$ as $n \to \infty$. A similar calculation also shows that $I_2 \to 0$. Finally, we have shown that:

$$\lim_{n\to\infty} E_{bulk}(u_n) = 0 \tag{2.1.34}$$

(ii) Now we turn to part (ii). In virtue of proposition 1.5.1.1, it is enough to show that $u_n \to u$ in L^1 and $\int_\Omega |Du_n|dx$ bounded. We have:

$$\begin{aligned}&\int_{-L}^{L}|\varphi_n(x_3)-\varphi(x_3)|dx_3 \\ &= \int_{-L/n}^{0}|n\frac{\delta}{L}(n\frac{x_3^2}{2L}+x_3)+\frac{\delta}{2}|dx_3+\int_0^{L/n}|n\frac{\delta}{L}(-n\frac{x_3^2}{2L}+x_3)-\frac{\delta}{2}|dx_3 \\ &= \frac{\delta}{2}\int_{-L/n}^{0}|\frac{nx_3^2}{L^2}+2n\frac{x_3}{L}+1|dx_3+\frac{\delta}{2}\int_0^{L/n}|-\frac{nx_3^2}{L^2}+2n\frac{x_3}{L}-1|dx_3 \\ &= \frac{\delta}{2}\int_{-L/n}^{0}(n\frac{x_3}{L}+1)^2dx_3+\frac{\delta}{2}\int_0^{L/n}(-n\frac{x_3}{L}+1)^2dx_3 \\ &= \frac{L}{\delta n}\int_0^1 v^2dv \to 0 \text{ as } n\to\infty\end{aligned} \tag{2.1.35}$$

In the last equality, we have used the change of variables $v = \frac{nx}{L}+1$ and $v = -\frac{nx}{L}+1$

respectively. It follows then that:

$$\varphi_n \to \varphi \text{ strongly in } L^1[-L, L]. \tag{2.1.36}$$

Besides, using appropriate change of variable,

$$\begin{aligned} \int_{-L}^{L} |\lambda_n^{-1/2} - 1| dx_3 &= \frac{2L^2}{\delta n} \int_0^{\frac{\delta}{L}} |(1+nv)^{-1/2} - 1| dv \\ &= \frac{2L^2}{\delta n} [v - \frac{2}{n}(1+nv)^{1/2}]_0^{\frac{\delta}{L}} \to 0 \text{ as } n \to \infty \end{aligned} \tag{2.1.37}$$

i.e.

$$\lambda_n^{-1/2} \to 1 \text{ strongly in } L^1[-L, L] \tag{2.1.38}$$

From (2.1.36) *and* (2.1.38) *it follows easily that*

$$\|u_n - u\|_{L^1} \to 0 \text{ as } n \to \infty \tag{2.1.39}$$

i.e.

$$u_n \to u \text{ strongly in } L^1(\Omega, \mathbb{R}^3) \tag{2.1.40}$$

Finally, the boundedness of $\int_\Omega |Du_n| dx$ *comes naturally from the same calculations as in the proof of part (i) with* $p = 1$*, in which case the boundedness of* I_1 *(and thus* I_2*) strictly follows from (2.1.30), (2.1.31), and (2.1.32). This concludes the proof.* □

The construction defined by the sequence u_n can be intuitively understood as follows. We assume the minimizers to belong to a class of deformation mappings of the form given by (2.1.16), which evidently satisfy the conservation of volume constraint and the boundary conditions. The deformation inside the bar is homogeneous everywhere, except in a layer of size ϵ, see Figure 2.3, in which the plastic deformation is concentrated. The size of the layer, which depends on the sequence label n, is chosen such as to decrease to zero when n goes to infinity. At the same time, the cross sectional area inside the layer undergoes a drastic decrease, as the deformation in the x_1 and x_2 directions are

divided by $\sqrt{\lambda_n}$ (see the expressions of u_{1n} and u_{2n} in (2.1.16)). To make things more explicit, the sequence of stretches λ_n is defined by $\lambda_n(x_3) = 1 + n\Phi(nx_3)$, where Φ is compactly supported in $[-L, L]$. In this way, λ_n is supported on the set $[-\frac{L}{n}, \frac{L}{n}]$, i.e. the size ϵ of the layer undergoing large amounts of deformation. The multiplicative factor n contributes to increase the intensity of the deformation in the localized region, thereby decreasing the cross-sectional area, which in the limit becomes restricted to a point. We illustrate this concentration mechanism in Figure 2.3. Intuitively, the construction should converge to a discontinuous map with a crack amplitude at the mid plane equal to the imposed displacement. This discontinuous map u is characteristic of fracture of the material and part (ii) of proposition 2.1.0.2 states that the proposed construction indeed converges to a crack as expected. More importantly, the analytical construction reveals that the infimum energy is equal to zero.

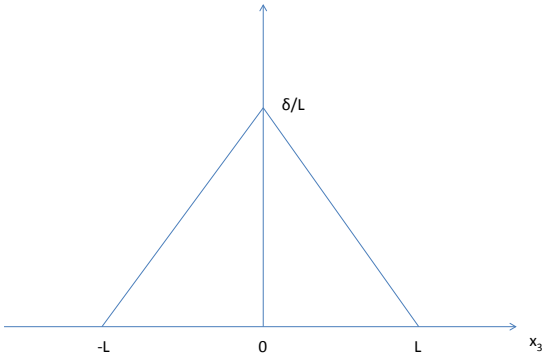

Figure 2.2: Plot of the function Φ used in the localization construction.

In order to glean insight into the choice of the function $\Phi(x_3)$, we reason as follows. We seek to construct a sequence of smooth deformations whose strains $(\lambda_n(x_3) - 1)$ concentrate at the origin. This is achieved by a simple piecewise linear function vanishing exactly at $x_3 = -L$ and $x_3 = L$ as depicted in Figure 2.2. The slope of each linear portion is then determined by making the sequence of strains $(\lambda_n(x_3) - 1)$ localize at the origin and converge to singular measure (dirac delta) with a jump equal to the amplitude δ. Recall that $\lambda_n = \varphi_n^{'}$, therefore if λ_n is proved to converge to a

singular measure, the corresponding limit of φ_n will be discontinuous. More precisely, the limit of φ_n belongs to SBV, the Special function of Bounded Variation, see [2]. To be more precise, let $\phi \in C_0[-L, L]$. It is clear that

$$\int_{-L}^{L} \lambda_n(x_3)\phi(x_3)dx_3 = \int_{-L}^{L} \phi(x_3)dx_3 + \int_{-L/n}^{L/n} n\Phi(nx_3)\phi(x_3)dx_3 \tag{2.1.41}$$

Then

$$\int_{-L/n}^{L/n} n\Phi(nx_3)\phi x_3)dx_3 = \int_{-L}^{L} \Phi(v)\phi(\frac{v}{n})dv \to \int_{-L}^{L} \Phi(v)\phi(0)dv = \int_{-L}^{L} \Phi(v)dv < \delta_0, \phi > . \tag{2.1.42}$$

i.e.

$$\lambda_n \overset{*}{\rightharpoonup} 1\ \mathcal{L}^1 + (\int_{-L}^{L} \Phi(v)dv)\delta_0 \quad weakly\ *\ in\ measure. \tag{2.1.43}$$

Note that $\mathcal{L}^1$ represents the one dimensional Lebesgue measure and δ_0 represents the delta Dirac measure at the origin. Now remark that, due to the discontinuity of $\varphi(x_3)$ see (2.1.19), its derivative is a measure, i.e.

$$D\varphi = 1\ \mathcal{L}^1 + \delta\ \delta_0 \tag{2.1.44}$$

Equating $\int_{-L}^{L} \Phi(v)dv$ and δ identifies the amplitude of the discontinuity at the origin to the imposed displacement δ. This is achieved for $\Phi(0) = \frac{\delta}{L}$, and thus makes the choice of Φ more concise and given by (2.1.15), see Figure 2.2. The convergence of u_n to u follows naturally from this construction. For reasons of simplicity, we have chosen the weak* convergence in BV as the main topology of convergence.

The physical meaning of the results of proposition 2.1.0.2 is thus clear. On the one hand, the optimization problem (2.1.13) is ill-posed, as it relaxes to zero and provides no information about fracture properties. The infimum is obtained by means of a construction that features localization of plastic deformation. This localization of plastic flow is mainly attributed to the sublinear growth of the energy density and characteristic of necking. On the other hand, the necking construction converges to a discontinuous map, see Figure 2.3, which strongly implies fracture at zero cost. This

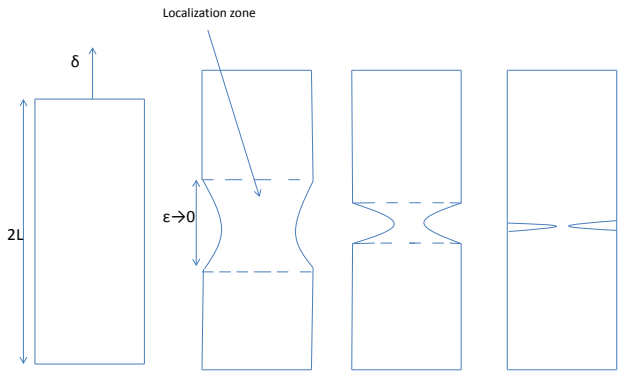

Figure 2.3: Necking construction exhibiting localization on the central plane. The construction converges to fracture

contradiction is often referred to as the *necking instability* . From the viewpoint of the calculus of variations, the instability results from the lack of convexity (or quasi-convexity more precisely) of the integrand in the energy functional, and therefore minimizing sequences have to develop either oscillations or concentrations.

In light of the analysis presented so far, local theories solely are insufficient to describe ductile fracture in metals. Although they can predict localization, necking and explain geometrical softening, they fail to provide useful and complete characterization of ductile materials. However, in metals undergoing ductile fracture, this inherent unstable behavior of large material samples is held in check by a second fundamental property of metals, namely, the *strain gradient hardening*. In section 2.2, we introduce a non-local model which will be the grounds for the explanation of size effects and surface energies, and yield a new multiscale model for ductile fracture.

2.1.3 Some remarks

In concluding this section, we make some additional remarks concerning the type of energy functionals given by (2.1.13). Such a model is analogous to energy minimization problems in finite deformation elasticity. The subject of existence of minimizers in non-linear elasticity has been the

focus of tremendous research in the calculus of variations, starting with the pioneering work of John Ball, [7]. The problem under investigation is the minimization of the elastic energy

$$I(u) = \int_{\Omega} W(Du)dx \tag{2.1.45}$$

for the special class of stored-energy functions W that can be expressed as convex functions of the determinant and all the minors of the deformation gradient, functions which are referred to as *polyconvex*. From a physical point of view, this class of functions satisfy not only the material frame indifference, but also the condition that it takes an infinite amount of energy to compress the material to zero, requirements that are proper to finite elasticity. From a mathematical standpoint, this class of functions facilitates the use of the direct methods in the calculus of variations to prove existence of minimizers. More precisely, the problem reduces to proving the weak continuity of the determinant and other minors of the deformation gradient. Ball was able to show the existence of minimizers when W satisfies suitable growth conditions such as:

(i) $W(F) \geq c|F|^p$, for some $c > 0$ and $p > 3$;

(ii) $W(F) \geq c(|F|^p + |cofF|^q)$, for some $c > 0$, with $p \geq 2$ and $q > p/p - 1$ or;

(iii) $W(F) \geq c(|F|^p + |cofF|^q + |detF|^r)$, for some $c > 0$, $p \geq 2$ and $q \geq p/p - 1$ and $r > 1$.

Many refinements of Ball's results exist in the literature and we refer the reader to Ball and Murat[8], Giaquinta, Modica and Soucek [73], Muller, Tang and Yan [104]. The structure of the energy functional used in (2.1.13) is identical to (2.1.45), but evidently the energy density does not satisfy the growth conditions above stated, which makes the direct methods fail for plasticity problems, especially due to the sublinear growth. Instead, one has to perform a relaxation procedure and this was the core of section 2.1.2.

The extension of Ball's results to finite plasticity has been less studied, i.e. finite elastoplasticity problems of the form

$$E_{bulk}(u, F_p) = \int_{\Omega} [W^e(DuF_p^{-1}) + W^p(F_p)]dx \tag{2.1.46}$$

In previous sections, we had made additional assumptions, such as $Du = F_p$ for the purpose of illustration. The main difficulty here arises from the multiplicative elastic-plastic decomposition $Du = F_e F_p$. This problem was first attempted by Mielke and Muller [82] who showed the existence of minimizers for sufficient mild growth conditions on the energy densities, at the expense of adding a stabilizing energy term that comes from dislocations. The use of the direct methods in this context strongly relied on the *div-curl* lemma, the cornerstone of the theory of compensated compactness, see [86],[87],[114],[113],[115], [24],[103], for the statement and many of its refinements. Without the addition of a dislocation energy, the minimum problem does not admit a solution and minimizing sequences develop microstructures or concentrations and we refer the reader to [102],[46],[74],[80],[81],[91] for more details about relaxation and microstructures.

In the same spirit, we need to formulate a stabilizing energy, which will relate to size effects and non-local plasticity. This is the focus of the next section.

2.2 Strain gradient plasticity

A large body of literature has emerged on non-local theories of plasticity to explain size effects observed in the macroscopic response of materials as a function of microstructural sizes. For instance, a widely known result is the Hall-Petch effect which states that the yield stress is inversely proportional to the square root of the grain size in nanocrystalline materials. Size effects can be attributed to the presence of strain gradients, see [27], [30], [28], [29], which make conventional plasticity models break down for phenomena that involve a characteristic length scale. It is well known that plasticity is driven by the motion of dislocations which multiply and entangle to cause strain hardening, a process in which continued plastic deformation increases the crystal's strength. The storage of dislocations comes from two sources: (1) dislocations accumulate by random trapping to form *statistically stored dislocations*; (2) because of the geometry of the solid or the material inhomogeneity, gradients in the plastic strain result in the formation of *geometrically necessary dislocations* , see [30] and Figure 2.4. Direct evidence for the notion that geometrically necessary dislocations lead to enhanced hardening comes from the compression tests of Russell and Ashby [101], Brown and Stobbs

[14], and other authors. This strain gradient hardening property of metals has also been extensively investigated and demonstrated by means of torsion tests in wires [30], nanoindentation [90], [132], [54], and by other means. In general, strain gradients are inversely proportional to the length scale at which deformation occurs. When the length scale associated with the deformation field is large, strain gradients are very small and hardening is caused by *statistically stored dislocations*. In this case, conventional theories of plasticity apply and there is no internal length scale. On the other hand, when the deformations are small enough, it becomes a necessity to introduce strain gradient effects in the constitutive laws.

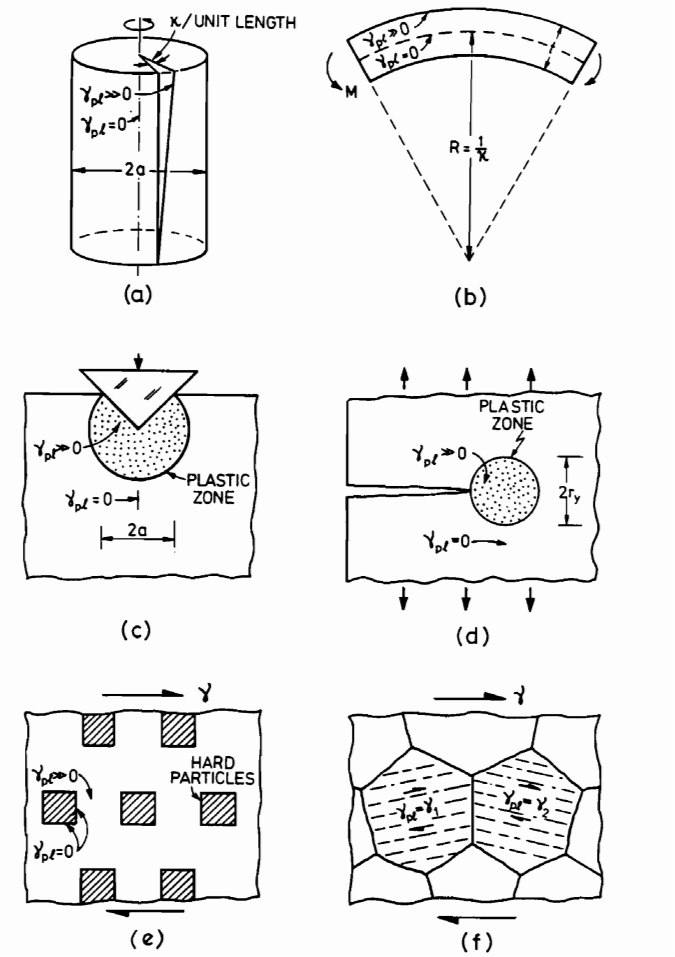

Figure 2.4: Plastic strain gradients are caused by the geometry of deformation(a,b), by local boundary conditions (c,d) or by the microstructure itself (e,f). Source:[30]

2.2.1 Overview of strain gradient phenomena and previous models

Numerous phenomena in plasticity that depend on strain gradients have been presented in [28]. These phenomena include, but are not limited to, torsion of thin wires, grain size effect on polycristalline yield strength, void growth and softening, cavitation instabilities, etc. Torsion experiments Figure 2.5, see [28], [30] revealed a systematic increase of torsional hardening with decreasing wire diameter which implied the existence of a characteristic length scale in the constitutive laws. A candidate for strain gradient plasticity law was proposed by Fleck and Hutchinson in which size effect enters the constitutive law through the postulate that stress depends on strain and strain gradient. The formulation is presented within the context of deformation theory of plasticity, which assumes no important path-dependant behavior and monotone loading. In their approach to develop a strain gradient law, Fleck and Hutchinson [28] postulated that the strain density energy is a function of the *overall effective strain* which is defined by :

$$\mathcal{E} = \sqrt{\epsilon_e^2 + \ell^2 \chi_e^2} \tag{2.2.1}$$

where ϵ_e is the second invariant of strain $\epsilon_e = \sqrt{\frac{2}{3}\epsilon_{ij}\epsilon_{ij}}$, and an analogous definition for the curvature $\chi_e = \sqrt{\frac{2}{3}\chi_{ij}\chi_{ij}}$. The length parameter ℓ is introduced for dimensional consistency. A power-law dependance of the strain energy density w on the effective strain $\mathcal{E}$ has the form

$$w = \frac{n}{n+1}\Sigma_0 (\frac{\mathcal{E}}{\mathcal{E}_0})^{\frac{n+1}{n}} \tag{2.2.2}$$

where Σ_0, $\mathcal{E}_0$ and the strain hardening exponent n are material constants. Then the uniaxial stress σ is related to the uniaxial strain via the relation

$$\sigma = \Sigma_0 (\frac{\mathcal{E}}{\mathcal{E}_0})^{1/n} \tag{2.2.3}$$

Fleck *et al* [28] were able to calibrate and validate their coupled stress version of strain gradient plasticity to the experimental results on copper wires (Figure 2.5) and found that values of ℓ between

$2\mu m$ and $4\mu m$ matched experimental data.

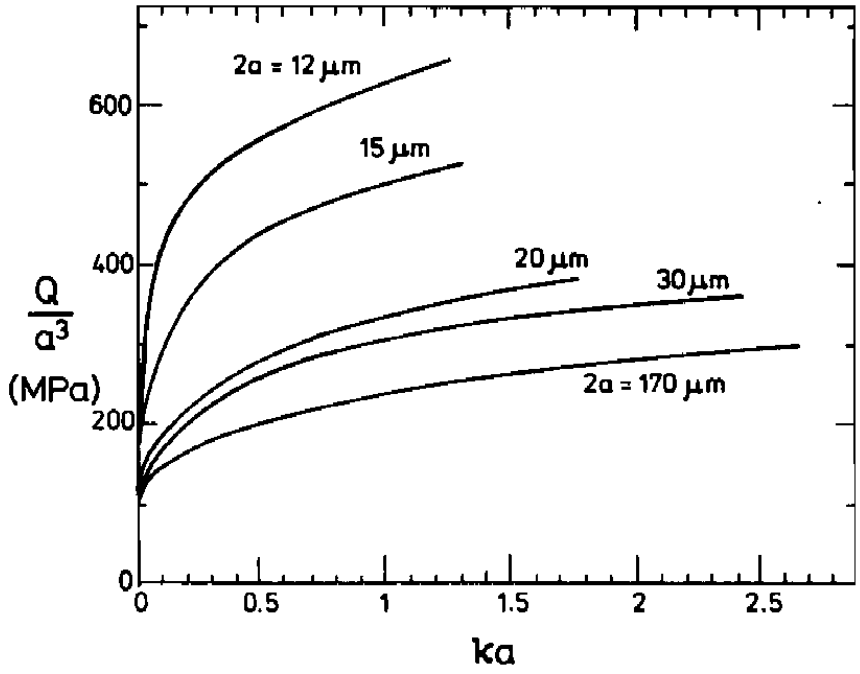

Figure 2.5: Torsional response of copper wires of diameter 2a in the range 12-170 μm. If the constitutive law were independent of strain gradients, the plots of normalized torque Q/a^3 vs κa would all lie on the same curve. Source:[30]

Bassani [9] proposed a strain gradient model based on the postulate that the non-local tangent modulus, which accounts for strain hardening in addition to the conventional strain hardening, can be defined by the relation:

$$E_t = \frac{E}{n}\left(\frac{\epsilon_e^p}{\epsilon_0}\right)^{\frac{1}{n}-1}\left[1 + \frac{\ell^2\alpha^2}{(\epsilon_0 + \kappa\epsilon_p^e)^2}\right]^{1/2} \tag{2.2.4}$$

ϵ_0 represents the yield strain in uniaxial tension, n is the hardening exponent and ϵ_p^e is the effective plastic strain. The material length parameter ℓ has been introduced again for dimensional consistency. The parameter α represents the maximum derivative of the plastic strain, through which non-local effects enter the model and κ is a dimensionless constant. By choosing appropriate values for the parameters appearing in equation 2.2.4, a good agreement was found between the model and the experimental results on copper wires by Fleck *et al* (1994). This approach of strain gradient plasticity has been used in the computational works of Tvergaard and Niordson, see [129], to account

for the presence of a length scale in the interaction between voids.

Nanoindentation experiments, see [90] also exhibit the importance of size effects due to strain gradients. The increase of hardness when the indentation size decreases, especially in the sub-micrometer depth regime, is attributed to large strain gradients inherent in small indentations that lead to the formation of geometrically necessary dislocations. First developed by Stelmashenko *et al* [109], [108], and De Guzman *et al* [23], the model of geometrically necessary dislocations was used by Nix-Gao to describe the depth-dependance of the hardness of crystalline materials. Specifically, they considered the indentation by a rigid cone (see Figure 2.6). Geometrically necessary dislocations develop in order to accommodate the indentation and the permanent shape change at the surface. Denoting θ_0 the angle between the indenter and the surface, a the contact radius, h the depth of the indentation and s the spacing between slip steps at the surface, the contact angle θ_0 can be evaluated by

$$tan\theta_0 = \frac{h}{a} = \frac{b}{s} \tag{2.2.5}$$

If we assume that the dislocations remain inside a half sphere of volume $V = \frac{2}{3}\pi a^3$, it can be shown ([90]) that the density of geometrically dislocations, which is the total length of dislocation loops divided by the volume, becomes

$$\rho_G = \frac{3}{2bh} tan^2\theta_0 \tag{2.2.6}$$

Using the Taylor relation for the shear stress $\tau = \alpha\mu b\sqrt{\rho_G}$ (statistically stored dislocations are negligible in the indentation problem) and the Tabor's factor to convert the flow stress into hardness we have

$$\sigma = \sqrt{3}\tau, \;\; H = 3\sigma \tag{2.2.7}$$

Using the previous relations, the following characteristic form for the depth dependence of the hardness was then derived:

$$\frac{H}{H_0} = \sqrt{1 + \frac{h^*}{h}} \tag{2.2.8}$$

where H is the hardness for a given depth of indentation, h, H_0, is the hardness in the limit of

infinite depth and h^* is a characteristic length that depends on the shape of the indenter, the shear modulus and H_0, see Figure 2.7 for comparison with experimental data from McElhaney et al [78]. Such a model can be used to derive a strain gradient plasticity law. Indeed, a measure of strain gradient in this problem is

$$\chi = \frac{tan\theta_0}{a} \tag{2.2.9}$$

in which case the depth dependence of the hardness can be rewritten as

$$(\frac{\sigma}{\sigma_0})^2 \approx 1 + b(\frac{\mu}{\sigma_0})^2 \tag{2.2.10}$$

where σ and σ_0 represent the flow stress in presence of strain gradient and the flow stress without strain gradient respectively. For power law hardening of the form $\sigma_0 = \sigma_{ref}\epsilon^n$, this can be recast into a new strain gradient plasticity law of the form

$$(\frac{\sigma}{\sigma_0})^2 = \epsilon^{2n} + \ell\chi \tag{2.2.11}$$

with the strain independent length scale ℓ given by

$$\ell = b(\frac{\mu}{\sigma_{ref}})^2 \tag{2.2.12}$$

The length parameter ℓ is a function of the Burger's vector b and other material constants, χ is the effective strain gradient. This model derived by Nix and Gao resembles the phenomenological law of Fleck and Hutchinson, with their length scale interpreted this time in function of material parameters.

2.2.2 Problem formulation

In this work, we propose a new formulation that takes into account strain gradient effects. The idea will be to postulate an additive decomposition of the energy density into two components: a first component depending on the first deformation gradient (as in section 2.1.1), and a second that is

$\chi = \pi na/b$. The average GND density can be obtained from $\rho_G = \chi/V$, where $V = (2/3)\pi a^3$ is the volume of the hemisphere (Nix and Gao, 1998). This gives $\rho_G = (3\tan^2\theta_0)/2bh$, which becomes very large at small indentation depth h (as in nano indentation).

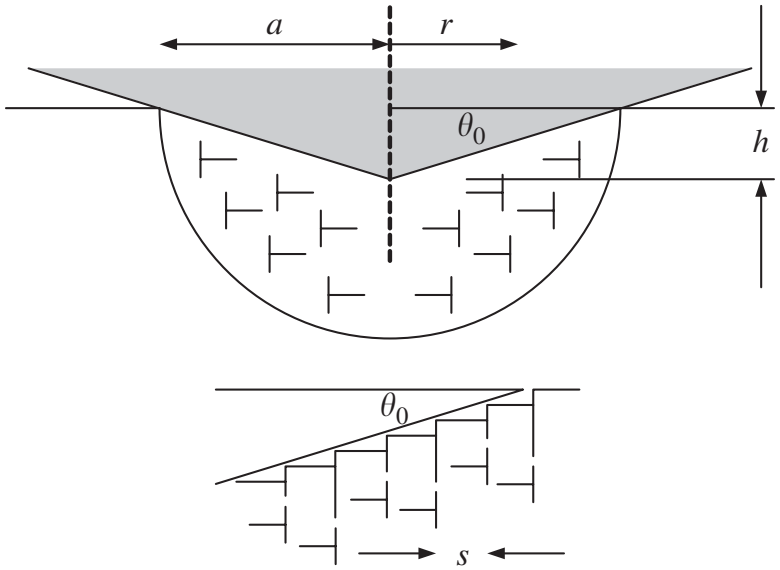

Fig. 3. S o, 1998)

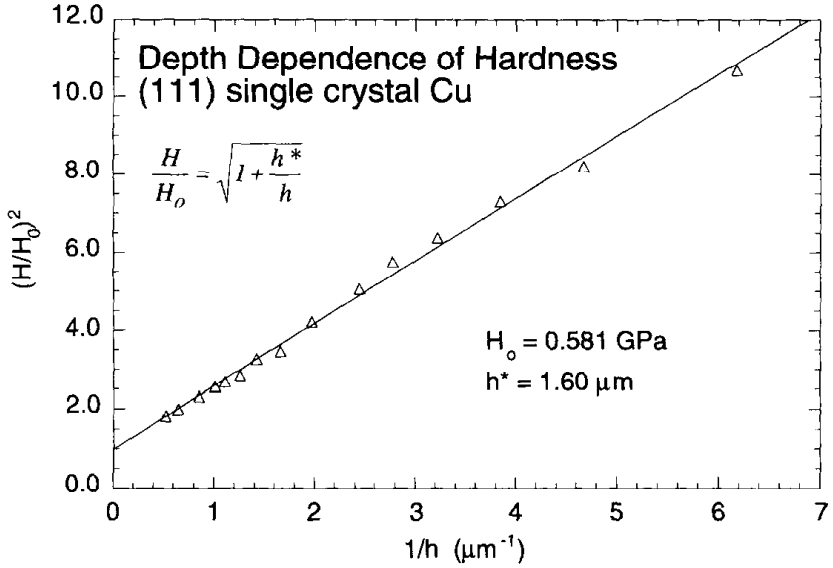

Fig. 3. Depth dependence of the hardness of (111) single crystal copper, taken from Fig. 1, plotted according to eqn (8).

Figure 2.7: Depth dependence of the hardness of (111) single crystal copper. Source:[90]

a regularization term that entails strain gradients. In the following, we provide the mathematical framework that will be the basis for our formulation of strain gradient plasticity within the context of deformation theory.

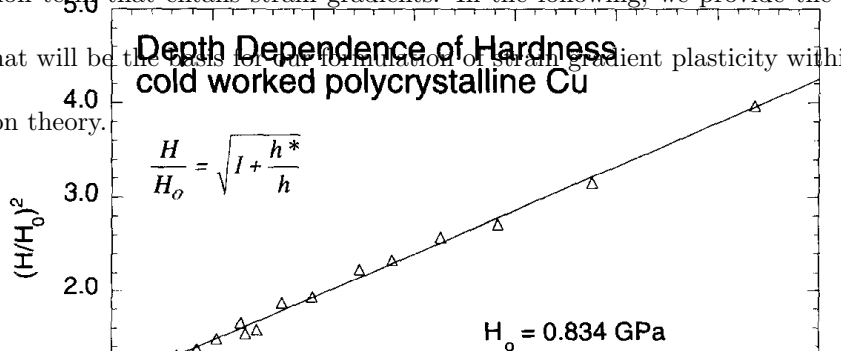

2.2.3 Rate problems and deformation theory

Suppose that the states of the body are defined by elements u of some appropriate configuration space X, to be specified. In order to describe the dissipation and kinetics attendant to plastic deformation, we consider time evolutions of u over a time interval $[0, T]$, or *trajectories*, and assume that the evolution of the system is governed by *rate problem*

$$v(t) \in \operatorname{argmin} G(\cdot, u(t), t), \tag{2.2.13a}$$

$$u(t) = u_0 + \int_0^t v(t')\, dt' \tag{2.2.13b}$$

where $G(v, u, t)$ is a *rate functional*, which we allow to depend explicitly on time in order to account for external forcing, e. g., in the form of prescribed boundary displacements imparted by a rigid loading device. The Euler-Lagrange equations of the rate problem (2.2.13a), when defined, express a balance between dissipative and energetic forces, which in turn results in irreversible and hysteretic behavior for arbitrary loading histories.

The rate problem (2.2.13) can be recast as a minimum problem for *trajectories* by recourse to the corresponding *energy-dissipation functional* [83]

$$\mathsf{F}_\epsilon(\mathsf{u}) = \int_0^T \mathrm{e}^{-t/\epsilon} G(\dot{u}(t), u(t), t)\, dt, \tag{2.2.14}$$

where ϵ is a small parameter and F_ϵ is defined over entire trajectories $\mathsf{u} : [0, T] \to X$ in some appropriate space X of trajectories. As noted in [83], the Euler-Lagrange equations of F_ϵ differ from those of the rate problem (2.2.13) by terms that vanish in the limit of $\epsilon \to 0$, which establishes a formal connection between the differential inclusion problem and the minimizing trajectories of F_ϵ over X. Specifically, we identify the trajectories of interest as the limits of sequences u_ϵ of minimizing trajectories of F_ϵ as $\epsilon \to 0$.

A further simplification, which effectively replaces the evolution problem by a time-wise sequence of minimization problems, is furnished by *deformation theory*, originally developed in the context of

rate-independent plasticity (e. g., [75] and references therein). Thus, suppose that there is a subspace Y of X of trajectories along which the rate functional $G\big(\dot{u}(t), u(t), t\big)$ is a *perfect differential*, i.e., there exists a function $E : X \times [0,T] \to \bar{\mathbb{R}}$, known as the *deformation-theoretical energy*, such that

$$G\big(\dot{u}(t), u(t), t\big) = \frac{d}{dt} E\big(u(t), t\big), \tag{2.2.15}$$

provided that $\mathsf{u} \in \mathsf{Y}$. In particular, $G(v, u, t)$ is homogeneous of degree one in v, denoting rate-independent behavior. Then, when restricted to Y, (2.2.14) specializes to

$$\mathsf{F}_\epsilon(\mathsf{u}) = \int_0^T \mathrm{e}^{-t/\epsilon} \frac{d}{dt} E\big(u(t), t\big)\, dt, \tag{2.2.16}$$

and an integration by parts gives

$$\mathsf{F}_\epsilon(\mathsf{u}) = \int_0^T \frac{1}{\epsilon} \mathrm{e}^{-t/\epsilon} E\big(u(t), t\big)\, dt + \Big[\mathrm{e}^{-t/\epsilon} E\big(u(t), t\big)\Big]_0^T, \tag{2.2.17}$$

on Y. Evidently, (2.2.17) is minimized for any $\epsilon > 0$ if

$$u(t) \in \operatorname{argmin}\{E(\cdot, t)\}, \tag{2.2.18}$$

which corresponds to minimizing the deformation-theoretical energy functional pointwise in time. Evidently, the deformation-theoretical energy functional E combines both energy and dissipation. The advantage of deformation theory is that, when applicable, it reduces the problem to a sequence of classical energy-minimization problems parameterized by time. This reduction, in turn opens the way to the application of methods of the calculus of variations. However, it should be carefully noted that the deformation-theoretical solutions u given by (2.2.18) are solutions of the original problem only if it may be verified *a posteriori* that $\mathsf{u} \in \mathsf{Y}$. Specifically, if u belongs to the interior of Y, then (2.2.14) and (2.2.17) coincide in a neighborhood of u and, therefore, the Euler-Lagrange equation (2.2.13) is satisfied.

2.2.4 Deformation theory of plasticity

Next, we proceed to formulate a simple deformation theory for *isotropic, rigid-plastic, strain-gradient Mises plasticity*. We recall that von Mises theory of plasticity is intended to supply a simple description of the behavior of polycrystalline metals (e. g., [72]). We consider a plastic solid occupying a domain $\Omega \subset \mathbb{R}^d$ and undergoing large deformations described by a deformation mapping $\varphi : \Omega \to \mathbb{R}^d$. The solid is assumed to obey multiplicative elastic-plastic kinematics of the form

$$D\varphi \equiv F = F_{el}F_{pl} \tag{2.2.19}$$

where F_{el} and F_{pl} are the elastic and plastic components of the deformation gradient $D\varphi$, respectively. We assume that plastic deformation is volume preserving, i. e.,

$$\det(F_{pl}) = 1. \tag{2.2.20}$$

We additionally postulate a free-energy functional of the general form

$$E(u,t) = \begin{cases} \int_\Omega A\big(D\varphi F_{pl}^{-1}, \varepsilon_{pl}, D\varepsilon_{pl}\big)\, dx, & \text{if } \varphi|_{\partial\Omega} = g(t), \\ +\infty, & \text{otherwise.} \end{cases} \tag{2.2.21}$$

where $A(F_{el}, \varepsilon_{pl}, D\varepsilon_{pl})$ is the free-energy density, ε_{pl} is an effective (scalar) plastic strain, $g(t)$ is the prescribed value of the deformation mapping over $\partial\Omega$ at time t, and we write $u = \{\varphi, F_{pl}, \varepsilon_{pl}\}$. Throughout this work, we consider isothermal processes and omit the dependence of the free energy on temperature for simplicity of notation. The additional dependence of the free-energy density on the effective plastic strain gradient is intended to introduce and internal lengthscale in the spirit of strain-gradient plasticity theories. We additionally introduce the *Mises kinetic potential*

$$\Psi(\dot{u}) = \begin{cases} 0, & \text{if } \sqrt{3/2}\,|\dot{e}_{pl}| = \dot{\varepsilon}_{pl}, \\ +\infty, & \text{otherwise,} \end{cases} \tag{2.2.22}$$

where

$$e_{pl} = \log U_{pl} \tag{2.2.23}$$

is the logarithmic plastic strain and

$$F_{pl} = R_{pl} U_{pl} \tag{2.2.24}$$

is the polar decomposition of F_{pl}. The kinetic potential (2.2.22) effectively enforces the *von Mises flow rule*, which places non-holonomic constraints on the plastic deformation. The corresponding rate functional now follows as

$$G(v, u, t) = \Psi(v) + \langle DE(u, t), v \rangle, \tag{2.2.25}$$

and the energy-dissipation functional as (2.2.14). Suppose that $e_{pl}(x, t)$ is *proportional and monotonic* in Ω, i. e.,

$$\dot{e}_{pl}(x, t) = \dot{\varepsilon}_{pl}(x, t) m(x), \tag{2.2.26}$$

with

$$\sqrt{3/2}\, |m(x)| = 1, \tag{2.2.27}$$

and $\varepsilon_{pl}(x, t)$ monotonic. Then

$$\int_0^T \mathrm{e}^{-t/\epsilon} \Psi(\dot{u})\, dt = \begin{cases} 0, & \text{if } \sqrt{3/2}\, |e_{pl}(x, t)| = \varepsilon_{pl}(x, t), \\ +\infty, & \text{otherwise.} \end{cases} \tag{2.2.28}$$

For these paths, the energy-dissipation functional reduces to the form (2.2.18), with deformation-theoretical energy $E(u, t)$ given by (2.2.21) with ε_{pl} set to $|e_{pl}|$. In particular, by this restriction the deformation-theoretical energy depends on $u = \{\varphi, F_{pl}\}$ only.

Suppose, in addition, that the solid is rigid-plastic, i. e.,

$$A\big(F_{el}, \varepsilon_{pl}, D\varepsilon_{pl}\big) = W_{el}(F_{el}) + W_{pl}(\varepsilon_{pl}, D\varepsilon_{pl}), \tag{2.2.29}$$

where $W_{pl}(\varepsilon_{pl}, D\varepsilon_{pl})$ is a *stored energy density* and

$$W_{el}(F_{el}) = \begin{cases} 0, & \text{if } F_{el} \in \mathrm{SO}(n) \\ +\infty, & \text{otherwise,} \end{cases} \tag{2.2.30}$$

is the *elastic energy density*. By virtue of this assumption, we can restrict attention to plastic-deformation fields of the form

$$F_{pl} = R_{el}^T D\varphi, \tag{2.2.31}$$

with $R_{el} \in \mathrm{SO}(n)$. Therefore,

$$C_{pl} = D\varphi^T D\varphi, \tag{2.2.32}$$

and

$$U_{pl} = \sqrt{D\varphi^T D\varphi}. \tag{2.2.33}$$

Owing to these identities, the deformation-theoretical energy reduces to the form

$$E(\varphi, t) = \begin{cases} \int_\Omega W(D\varphi, DD\varphi)\, dx, & \text{if } \varphi|_{\partial\Omega} = g(t), \\ +\infty, & \text{otherwise,} \end{cases} \tag{2.2.34}$$

with

$$W(F, DF) = W_{pl}(\varepsilon_{pl}, D\varepsilon_{pl}), \tag{2.2.35}$$

and

$$\varepsilon_{pl} = |\log \sqrt{F^T F}|. \tag{2.2.36}$$

The final form (2.2.34) of the deformation-theoretical energy falls in the class of *non-local* or *generalized continua*, whose energy densities depend on the local deformation gradient and higher-order derivatives thereof. Generalized continua have been extensively treated in the classical literature on continuum mechanics, both as part of the development of the fundamental theory as well as in connection with a broad range of applications [64].

2.2.5 Energy growth properties

A number of model strain-gradient stored energy functions W_{pl} of varying complexity are available in the literature [27, 29, 9, 67, 66, 68]. However, as shown in the sequel, the detailed structure of W_{pl} is inconsequential as regards optimal scaling (see Chapter 3). Instead, conveniently, only the *growth* properties of the effective strain-energy density W play a role, which adds greatly to the generality of the analysis. Therefore, it is important to ascertain the growth properties of general materials, and polycrystalline metals in particular, that are consistent with experimental observations.

In order to glean insight into such properties, we may begin by considering the uniaxial tension test in the *local limit*, i. e., for specimens sufficiently large that non-local effects, including boundary layers, can be neglected. For the reader's convenience, we may repeat some aspects of the derivations of section 2.1.1. Specifically, we may consider a rod deforming in uniform uniaxial tension, so that $F = \mathrm{diag}\{\lambda, 1/\sqrt{\lambda}, 1/\sqrt{\lambda}\}$, with λ denoting the axial stretch ratio, and $DF = 0$. Under monotonic uniaxial tension, polycrystalline metals undergo hardening that is well-described by a power-law relation of the type

$$\sigma = K\epsilon^n \tag{2.2.37}$$

where σ is the axial Cauchy or true stress, $\epsilon = \lambda - 1$ is the engineering strain, n is the hardening exponent and K is a constant. The corresponding first Piola-Kirchhoff stress, which equals the axial force applied to the rod divided by the undeformed cross-sectional area, is given by

$$\partial_\lambda W = \sigma/\lambda = K(\lambda - 1)^n/\lambda, \tag{2.2.38}$$

which for large λ scales as

$$\partial_\lambda W \sim K\lambda^{n-1}. \tag{2.2.39}$$

Therefore, in the same range the energy density scales as

$$W \sim \frac{K}{n}\lambda^n, \tag{2.2.40}$$

i. e., it exhibits power-law behavior with exponent set by the hardening characteristics of the material.

We may take this observed scaling as grounds for assuming an energy growth of the type

$$W(F,0) \sim A|F|^p \tag{2.2.41}$$

for large F, with $p = n$ and $A = \frac{K}{n}$. In view of the experimentally observed values of the hardening exponent, which are in the range $0 < n < 1$ (cf., e. g., [5] for a compilation of strain-hardening exponents for metals), it follows that the local energy has *sublinear growth*, i. e., $p < 1$, see 2.1.1. For definiteness, in the present work we assume a non-local energy growth of the form

$$W(F, DF) \sim A(|F|^p + \ell|DF|), \tag{2.2.42}$$

i.e. there exists $0 < k_L \leq k_U$ such that

$$k_L A(|F|^p + \ell|DF|) \leq W \leq k_U A(|F|^p + \ell|DF|) \tag{2.2.43}$$

where ℓ is an intrinsic or characteristic length. The assumption of linear growth of the deformation-theoretical energy density with respect to the second deformation gradient is indeed consistent with a number of strain-gradient plasticity models (e. g., [29]). In addition, linear growth with respect to the second deformation gradient is characteristic of Γ-limits of microplasticity theories based on dislocation mechanics [91, 92, 4, 33, 34, 32, 19]. That prediction is in turn born out by a wealth of experimental observations of dislocation walls (see section 2.2.6), such as low-angle grain boundaries, which can only occur if the energy exhibits linear growth with respect to the second deformation gradient. In the present model, we therefore assume that the energy functional has the form

$$E(u) \sim A \int_\Omega (|Du|^p - 3^{p/2})dx + \ell A \int_\Omega |DDu|dx \tag{2.2.44}$$

with A as in (2.1.8). The parameter $B = \ell A$ accounts for the surface energy and is in the unit of $Joule/m^2$. We consider surface energies to be entirely captured by strain gradients and thus are mainly tied to non local effects. The link between surface energy and strain gradient follows for instance from the observation that the presence of strain gradients is a reflection of the large disparities between the plastic flow induced by local boundary conditions, e.g. appearance of steep gradients of plastic strain in the plastic zone at the crack tip in an otherwise elastic medium, see Figure 2.4. It is therefore natural to relate the crack propagation and its corresponding surface energy to the gradients of the plastic strain. In general, we will assume in the rest of this work that all surface energy mechanisms enter the model through the constant B.

2.2.6 The intrinsic length ℓ

In the present setting, the intrinsic length ℓ arises and figures explicitly in the growth assumptions on the deformation-theoretical energy density. As we shall see, these growth assumptions in turn play a central role in determining optimal scaling laws for the specific fracture energy. Similar intrinsic length parameters arise in other formulations of strain-gradient plasticity. For each such formulation, the empirical determination of ℓ requires the execution of specially-designed experiments (cf.[30, 10, 90, 132, 54]) or, alternatively, must be related to quantities that are measurable from standard experiments. The experiments considered to date, such as torsion and indentation experiments, are characterized by highly inhomogeneous deformations, which compound the unambiguous identification of the intrinsic length parameter. Next we show that, within the present formulation, the intrinsic length parameter can also be identified from deformation patterns that are uniform on average, such as lamellar structures. The energetics of lamellar structures also supply justification for the assumed linear growth of the non-local energy.

The test deformation under consideration occurs at the single-crystal level and has been discussed by [**?**] as an example of a microstructure, known as *fence* microstructure, generated through the activation of a single slip system. Fence microstructures are indeed observed during the early stages of stage II of hardening in FCC crystals [107, 51]. Because the dislocation walls in fence

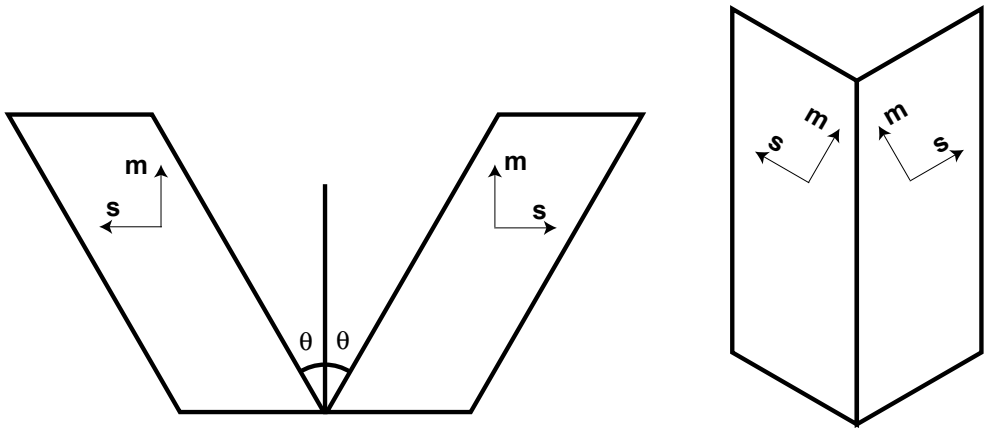

Figure 2.8: Schematic of kink formation (reproduced from [**?**]). a) Slip strains $\gamma^{\pm} = \pm\tan\theta$; b) rotations through $\pm\tan\theta$.

microstructures are normal to the primary slip direction they are sometimes termed *kinks*, and the resulting microstructures *kink bands* [51].

The fence microstructure is a laminate consisting of alternating layers of uniform deformation separated by interfaces in the form of dislocation walls, Figure 2.8. Let $(\boldsymbol{s}, \boldsymbol{m})$ be the slip direction and slip-plane normal defining the active slip system. Choose $\boldsymbol{s}$ as the interface normal, and impart slip strains $\gamma^{\pm} = \pm\tan\theta$ on both sides of the interface, Figure 2.8a, $\theta \in [0, \pi/2)$. Restore compatibility by applying rotations $\boldsymbol{R}^{\pm}$ around the normal axis $s \times m$ through angles $\pm\theta$. Since the planes on both sides of the interface remain unstretched along the $\boldsymbol{s} \times \boldsymbol{m}$ direction and stretch by the same amount in the $\boldsymbol{m}$ direction, the rotated crystals fit compatibly, Figure 2.8b. The resulting deformations are

$$\boldsymbol{F}^{\pm} = \boldsymbol{R}^{\pm}\,(\boldsymbol{I} \pm \tan\theta\, \boldsymbol{s} \otimes \boldsymbol{m}). \tag{2.2.45}$$

A straightforward calculation further gives

$$[\![\boldsymbol{F}]\!] = 2\sin\theta\, \boldsymbol{m} \otimes \boldsymbol{s}, \tag{2.2.46}$$

and

$$\big|[\![\boldsymbol{F}]\!]\big| = 2\sin\theta \tag{2.2.47}$$

Let b be the size of the Burgers vector. Then we have

$$\gamma^{\pm} = \pm\frac{b}{d}, \tag{2.2.48}$$

where d is the distance between slip planes. Thus, the interfaces in the microstructure are *tilt boundaries* consisting of dislocations at distance

$$D = \frac{d}{2\cos\theta} = \frac{b}{2\sin\theta}. \tag{2.2.49}$$

We now identify the non-local part of the deformation-theoretical energy with the interfacial energy. A standard theory of tilt boundary energies [53] consists of assuming a dislocation energy T per unit length of dislocation, resulting in an energy

$$\Gamma = \frac{T}{D} = \frac{2T\sin\theta}{b} \tag{2.2.50}$$

per unit area of interface. Energies of the form (2.2.50) have been successfully taken as a basis for elucidating scaling relations and size effects attendant to dislocation structures in deformed single crystals [**?** 92, 4, 20]. Eliminating θ between (2.2.47) and (2.2.50) we obtain

$$\Gamma = \frac{T}{b}\big|[\![\boldsymbol{F}]\!]\big|, \tag{2.2.51}$$

which shows that the non-local energy of the microstructure has indeed linear growth in $\boldsymbol{F}$, interpreted distributionally, with intrinsic length

$$\ell = \frac{T}{bA}. \tag{2.2.52}$$

If, for definiteness, we use a conventional representation of the dislocation line energy density T of the form (cf., e. g., [55])

$$T = \alpha\mu b^2 \tag{2.2.53}$$

where μ is an elastic shear modulus and α is a coefficient of order unity, then (2.2.52) becomes, explicitly,

$$\ell = \frac{\alpha \mu b}{A}, \tag{2.2.54}$$

which, given α, can be evaluated in terms of fundamental material constants.

Chapter 3

Optimal Scaling Laws in Ductile Fracture by Void Sheet Formation

In Chapter 2, we have formulated a simple strain gradient model which led to define a deformation-theoretical energy functional of the form

$$E(u) \sim A \int_\Omega (|Du|^p - 3^{p/2}) dx + \ell A \int_\Omega |DDu| dx \tag{3.0.1}$$

The goal of this chapter will be to present a rigorous mathematical analysis on the minimization of the energy functional in eq. (3.0.1). The key point is to find rigorous bounds on the minimum energy, as opposed to searching for exact minimizers. This approach is known as *optimal scaling*. In the analysis presented in this chapter, the energy has been normalized by the factor A.

Suppose that an energy functional $E(u, \epsilon_1, \dots, \epsilon_N)$, depending on N small parameters $(\epsilon_1, \dots, \epsilon_N)$, satisfies *matching bounds* of the form

$$C_L \epsilon_1^{\alpha_1} \dots \epsilon_N^{\alpha_N} \leq \inf E(\cdot, \epsilon_1, \dots, \epsilon_N) \leq C_U \epsilon_1^{\alpha_1} \dots \epsilon_N^{\alpha_N}, \tag{3.0.2}$$

where $C_L > 0$ and $C_U > 0$ are constants and the exponents $(\alpha_1, \dots, \alpha_N)$ are identical in both the lower and the upper bounds. Then we say that (3.0.2) defines an *optimal scaling law* for the energy $E(u, \epsilon_1, \dots, \epsilon_N)$ [62, 63, 15]. The methods for establishing the optimal scaling properties of energy functionals are typically somewhat lax as regards the determination of the constants C_L and C_U. By contrast, the exponents $(\alpha_1, \dots, \alpha_N)$ are precise and unambiguous and represent an intrinsic

property of the material.

In this chapter we derive optimal scaling laws for the deformation-theoretical energy functionals discussed in the foregoing under conditions representing ductile rupture across a plane of failure. We specifically consider an infinite slab subjected to prescribed uniform opening displacements on its surfaces and undergoing periodic deformations in the in-plane directions. By an appropriate normalization or, equivalently, by an appropriate choice of units, the in-plane periodic cell can be scaled to unity and the parameters of the energy functional may be reduced to: i) the prescribed opening displacement δ across the failure plane; ii) an intrinsic length parameter ℓ; iii) and the slab thickness H. Under these conditions, we supply an optimal scaling law for the deformation-theoretical energy in the parameters (δ, ℓ, H). In particular, the constants C_L and C_U and the optimal exponents are provided in terms of the local energy density growth exponent p, which, as discussed in Section 2.2.5, in turn coincides with the hardening exponent of the material. Remarkably, the energy is found to be independent of H, indicative of fracture-like behavior and a well-defined specific fracture energy per unit area.

3.0.7 Main result

We consider periodic deformations of a slab of thickness $2H$ occupying the domain $\{|x_3 \leq H\}$ subject to prescribed opening displacements on its surfaces. We identify a periodic unit cell $\Omega = [-L, L]^2 \times (-H, H)$. The deformation of the slab is described by a map $u : \Omega \to \mathbb{R}^3$ such that $u \in W^{1,1}(\Omega; \mathbb{R}^3)$ and $Du \in BV(\Omega; \mathbb{R}^{3\times 3})$ subject to the constraint of volume conservation

$$\det Du = 1, \tag{3.0.3}$$

a. e. in Ω, and to displacement boundary conditions

$$u_3(x_1, x_2, -H) = -H - \delta, \tag{3.0.4a}$$

$$u_3(x_1, x_2, H) = H + \delta, \tag{3.0.4b}$$

for all $(x_1, x_2) \in [-L, L]^2$ and opening displacement δ. In view of the assumed growth (4.2.1) of the energy, it suffices to consider the functional

$$E(u) = \int_\Omega (|Du|^p - 3^{p/2})dx + \ell \int_\Omega |DDu|dx. \tag{3.0.5}$$

However, it bears emphasis that the deformation-theoretical energy need not be of the exact form (3.0.5), but only bounded above and below by it modulo multiplicative constants. The constant $3^{p/2}$ in (3.0.5) is chosen so that the minimum of the energy is zero.

We shall show that the optimal scaling of the energy is achieved by maps in which the deformation is concentrated within a thin layer. In particular, we shall prove (cf. Theorem 3.0.1 and Theorem 3.0.2 below for precise statements) that, for ℓ sufficiently small,

$$\inf E \sim \ell^{\frac{1-p}{2-p}} \delta^{\frac{1}{2-p}}. \tag{3.0.6}$$

The origin of this scaling maybe be heuristically understood as follows. Consider a mapping u reducing to a rigid translation for $|x_3| \geq a$ and $Du = \operatorname{diag}(1, 1, 1+\delta/a)$ over a central layer of width $2a$. Formally inserting u into (3.0.5) gives an energy

$$E \sim \delta^p a^{1-p} + \ell \frac{\delta}{a}, \tag{3.0.7}$$

up to inconsequential multiplicative constants that do not affect scaling. This energy is minimized for

$$a \sim \ell^{\frac{1}{2-p}} \delta^{\frac{1-p}{2-p}}, \tag{3.0.8}$$

whereupon

$$E \sim \ell^{\frac{1-p}{2-p}} \delta^{\frac{1}{2-p}}. \tag{3.0.9}$$

Evidently, the mapping u is not admissible since it violates the volume constraint (3.0.3) in the central layer $|x_3| \leq a$. The subtle point in the proof of the optimal scaling law (3.0.6) is to show

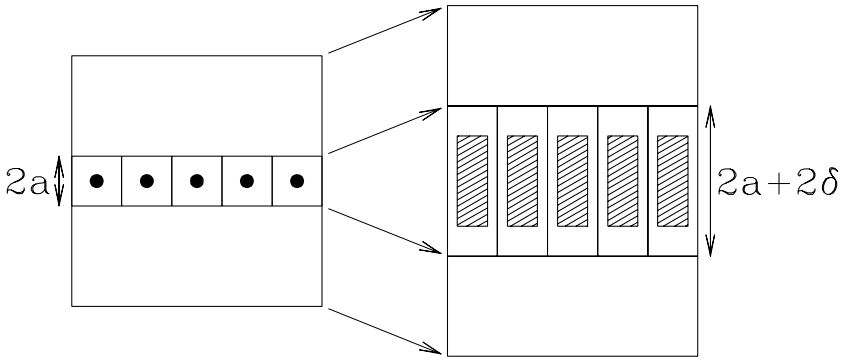

Figure 3.1: Sketch of the deformation mapping u employed in the upper bound. The central layer of thickness $2a$ stretches to a thickness $2a + 2\delta$. A number of voids, shown as dots in the reference configuration on the left and as shaded regions in the deformed configuration on the right, open in order to satisfy the volume constraint.

that the same scaling can also be achieved by a means of volume-preserving map. Evidently, this map cannot be one-dimensional. Instead, it requires the opening of *voids*, or the formation of a *void sheet*, Figure 3.1. This void-sheet construction is related to constructions used in the mathematical literature of cavitation, cf., e.g., [6, 111, 85, 18, 50] and references therein. Here, we provide an explicit piecewise-smooth void-sheet construction in order to illustrate the expected geometry of the failure mechanism as well as to render the estimate of the second gradient term explicit.

In closing this introduction, we additionally remark that the key energetic balance underlying the optimal scaling is indeed one-dimensional and arises, as in the sketch above, from embedding $W^{1,1}$ (or BV) into L^∞ in the normal direction, cf. eq. (3.0.19) below. The naive higher-dimensional approach, which would correspond to estimating from below DDu in L^1 (or $\mathcal{M}$) by Du in $L^{3/2}$ from the classical Poincaré inequalities in Sobolev spaces, would give a different non-optimal exponent.

3.0.8 Lower bound

Theorem 3.0.1 *Let* $\Omega = [-L, L]^2 \times (-H, H)$, $H > 1$, $\ell \in (0, 1)$, $p \in (0, 1)$, *and*

$$E(u) = \int_\Omega (|Du|^p - 3^{p/2})dx + \ell \int_\Omega |DDu|dx\,. \tag{3.0.10}$$

Fix $\delta > 0$. For every map $u : \Omega \to \mathbb{R}^3$ such that

$$u_3(x_1, x_2, -H) = -H - \delta, \tag{3.0.11a}$$

$$u_3(x_1, x_2, H) = H + \delta, \tag{3.0.11b}$$

for all $(x_1, x_2) \in [-L, L]^2$ and every $\ell > 0$ sufficiently small we have

$$E(u) \geq 4L^2 C_1(p) \ell^{\frac{1-p}{2-p}} \delta^{\frac{1}{2-p}}, \tag{3.0.12}$$

independent of H, where, explicitly,

$$C_1(p) = \frac{1}{2}\left(1 - \left(\frac{\sqrt{3}}{2}\right)^p\right)\left((1-p)^{\frac{1}{2-p}} + (1-p)^{\frac{p-1}{2-p}}\right). \tag{3.0.13}$$

proof 3.0.1 *The lower bound follows from one-dimensional considerations in the transverse direction e_3. For fixed $(x_1, x_2) \in [-L, L]^2$, define $f : (-H, H) \to \mathbb{R}$ by*

$$f(x_3) = \left|\frac{\partial u}{\partial x_3}(x_1, x_2, x_3)\right|. \tag{3.0.14}$$

Thus, the function f coincides with the magnitude of the third column of the deformation gradient Du, or transverse deformation. *Its average T is at least as large as the average macroscopic strain, i. e.,*

$$T = \frac{1}{2H}\int_{-H}^{H} f(x_3)dx_3 \geq \frac{1}{2H}\int_{-H}^{H} \frac{\partial u_3}{\partial x_3}\, dx_3 = 1 + \frac{\delta}{H}. \tag{3.0.15}$$

In order to rewrite the energy in terms of f, we consider the minimal energy that can be attained with a transverse deformation of magnitude λ and define $W : (0, \infty) \to \mathbb{R}$ by

$$W(\lambda) = \min\{|F|^p - 3^{p/2},\ \det F = 1,\ |Fe_3| = \lambda\}. \tag{3.0.16}$$

The function W has a minimum at $\lambda = 1$ and has p-growth for large λ (see Lemma 3.0.1.1 and

Figure 3.2). The strain-gradient term can also be easily estimated in terms of f, since

$$|DDu| \geq |D_3 D_3 u| \geq |D_3|D_3 u|| = |Df|. \tag{3.0.17}$$

The inequality holds pointwise if u is twice differentiable and in the appropriate integral sense under the assumption $Du \in BV$. Therefore for almost all $x' = (x_1, x_2) \in [-L, L]^2$ we have

$$\int_{-H}^{H} (|Du|^p - 3^{p/2} + \ell|DDu|)\, dx_3 \geq \int_{-H}^{H} (W(f(x_3)) + \ell|Df(x_3)|)\, dx_3. \tag{3.0.18}$$

Next, we focus on the latter integral, subject to the constraint (3.0.15). The function W has sublinear growth at infinity, hence $\int W(f)$ is minimized by letting f oscillate between a value close to its minimum and a very large value. In particular, if $f = K$ on a $1/K$ fraction of the volume, as $K \to \infty$ the contribution to the average of f is 1, but the contribution to the energy is $W(K)/K \sim K^{p-1} \to 0$. This behavior is regularized by the strain gradient term. To make this precise, we consider the maximum and minimum value of f, namely, $M = \operatorname{ess\,sup} f$ and $N = \operatorname{ess\,inf} f$. Then

$$\int_{-H}^{H} |Df| dx_3 \geq M - N\,. \tag{3.0.19}$$

Moreover, since $N \leq f \leq M$ almost everywhere, it follows that $N \leq T \leq M$. The key energetic balance concerns the competition between the first term, which selects for M large, so that f can be large on a small part of the volume, and the second term, which penalizes oscillations and favors small values of M. In order to make this tradeoff precise, we define the function

$$W_M(s) = \begin{cases} W(s), & \text{if } s \in (0, M], \\ +\infty, & \text{otherwise,} \end{cases} \tag{3.0.20}$$

and consider its convex envelope W_M^{**} (cf. Lemma 3.0.1.2 and Figure 3.2). By Jensen's inequality

we have

$$\frac{1}{2H}\int_{-H}^{H} W(f(x_3))\,dx_3 \geq W_M^{**}(T)\,, \tag{3.0.21}$$

where T was defined in (3.0.15). Therefore it suffices to find a lower bound for the quantity

$$G(T) = HW_M^{**}(T) + \ell(M-N), \tag{3.0.22}$$

subject to $N \leq T \leq M$ and $T \geq 1 + \frac{\delta}{H} > 1$.

In order to proceed further, we distinguish several cases and use the estimates on the convex envelope given by Lemma 3.0.1.2.

If $T \leq a_p^M$, then from Lemma 3.0.1.2(ii) we obtain

$$G(T) \geq HW_M^{**}(T) \geq c_p H(T-1)^2\,. \tag{3.0.23}$$

The function W is monotonically increasing on $[1,\infty)$, a property which is inherited by W_M^{**}. Therefore we can extend this estimate to the values of T which are moderately larger than a_p^M. More precisely, if $a_p^M \leq T$ and $(T-1) \leq 2(a_p^M - 1)$, then

$$G(T) \geq HW_M^{**}(T) \geq HW_M^{**}(a_p^M) \geq c_p H(a_p^M - 1)^2 \geq \frac{1}{4}c_p H(T-1)^2\,. \tag{3.0.24}$$

In the remaining case, $T - 1 > 2(a_p^M - 1)$, from Lemma 3.0.1.2 (i) we obtain

$$G(T) \geq c_p' H\frac{T - a_p^M}{M^{1-p}} + \ell(M-T) \geq \frac{1}{2}c_p' H\frac{T-1}{M^{1-p}} + \ell(M-T)\,, \tag{3.0.25}$$

where the constant c_p' is explicitly given by (3.0.42). If $M \geq 2T$, then

$$G(T) \geq \frac{1}{2}c_p' H\frac{T-1}{M^{1-p}} + \frac{1}{2}\ell M \geq \frac{1}{2}\min\{c_p', 1\}\left(\frac{(T-1)H}{M^{1-p}} + \ell M\right) \tag{3.0.26}$$

and, since $c_p' < 1$, explicit minimization with respect to M of the right-hand side gives

$$G(T) \geq \frac{1}{2} c_p' \gamma(p) \ell^{\frac{1-p}{2-p}} ((T-1)H)^{\frac{1}{2-p}}, \tag{3.0.27}$$

with

$$\gamma(p) = [(1-p)^{\frac{1}{2-p}} + (1-p)^{\frac{p-1}{2-p}}]. \tag{3.0.28}$$

If instead $M < 2T$, then (3.0.25) gives

$$G(T) \geq \frac{1}{2^{2-p}} H c_p' \frac{T-1}{T^{1-p}}\,. \tag{3.0.29}$$

In summary, we have shown that

$$\begin{aligned} &G(T) \geq \\ &\min\left\{ \frac{1}{2} c_p' \gamma(p) \ell^{\frac{1-p}{2-p}} (H(T-1))^{\frac{1}{2-p}},\ \frac{1}{4} c_p H (T-1)^2,\ \frac{1}{2^{2-p}} H c_p' \frac{T-1}{T^{1-p}},\ c_p H (T-1)^2 \right\}. \end{aligned} \tag{3.0.30}$$

Integrating in the tangential directions, using $T \geq 1 + \frac{\delta}{H}$ and the fact that each of the four expressions is nondecreasing as a function of $T-1$, we obtain

$$\begin{aligned} &E(u) \geq \\ &4L^2 \frac{1}{2} \min\left\{ \frac{1}{2} c_p' \gamma(p) \ell^{\frac{1-p}{2-p}} \delta^{\frac{1}{2-p}},\ \frac{1}{4} c_p H (\frac{\delta}{H})^2,\ \frac{1}{2^{2-p}} c_p' H \frac{\frac{\delta}{H}}{(1+\frac{\delta}{H})^{1-p}},\ c_p H (\frac{\delta}{H})^2 \right\}. \end{aligned} \tag{3.0.31}$$

For sufficiently small ℓ the first term is smallest, which concludes the proof of the lower bound. □

We now derive the requisite estimates for W and W_M^{**}.

Lemma 3.0.1.1 *Let $p \in (0,1)$, and for $\lambda > 0$ define*

$$W(\lambda) = \min\{|F|^p - 3^{p/2} :\ F \in \mathbb{R}^{3\times 3},\ \det F = 1,\ |Fe_3| = \lambda\}\,. \tag{3.0.32}$$

Then the following holds:

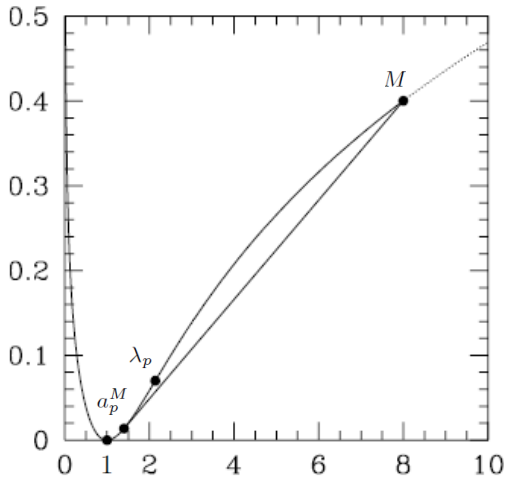

Figure 3.2: Sketch of the functions W and W_M^{**} for $p = 0.2$ and $M = 8$. The marked points correspond to $\lambda = 1, a_p^M, \lambda_p, M$. The upper curve is W, the lower one W_M^{**}.

(i) The function W can be written as

$$W(\lambda) = \left(\lambda^2 + \frac{2}{\lambda}\right)^{p/2} - 3^{p/2}\,. \tag{3.0.33}$$

(ii) $W \geq 0$ everywhere, $W(\lambda) = 0$ only for $\lambda = 1$.

(iii) The function W is convex on $(0, \lambda_p)$ and concave on (λ_p, ∞), where

$$\lambda_p = \left(\frac{4 - p + 3\sqrt{2 - p}}{1 - p}\right)^{1/3} \in [2, \infty)\,. \tag{3.0.34}$$

(iv) There is $c_p > 0$ such that

$$W(\lambda) \geq c_p(\lambda - 1)^2, \quad \text{for all } \lambda \in (0, \lambda_p]\,. \tag{3.0.35}$$

proof 3.0.2 *In order to prove (i), we note that the set over which we minimize in (3.0.32) is closed and nonempty and any minimizing sequence is bounded. Hence the minimum exists. Let F be a minimizer. For any $Q \in SO(3)$ the matrix $\tilde{F} = QF$ is also a minimizer, since* $\det(QF) = \det F$

and $|QF| = |F|$. We choose Q so that $\tilde{F}$ is lower triangular,

$$\tilde{F} = \begin{pmatrix} a_{11} & 0 & 0 \\ a_{21} & a_{22} & 0 \\ a_{31} & a_{32} & \lambda \end{pmatrix} . \tag{3.0.36}$$

All matrices with $a_{11}a_{22}\lambda = 1$ are admissible, and we wish to minimize the norm. Therefore all off-diagonal entries vanish. Further, the minimum of $a_{11}^2 + a_{22}^2$ subject to $a_{11}a_{22}\lambda = 1$ is achieved when $a_{11} = a_{22} = \pm\frac{1}{\sqrt{\lambda}}$. Therefore a minimizer is

$$\tilde{F} = \begin{pmatrix} \lambda^{-1/2} & 0 & 0 \\ 0 & \lambda^{-1/2} & 0 \\ 0 & 0 & \lambda \end{pmatrix} \tag{3.0.37}$$

which yields $W(\lambda) = (\lambda^2 + \frac{2}{\lambda})^{p/2} - 3^{p/2}$. Claim (ii) follows easily from the definition or from the formula just derived. Claim (iii) follows by differentiating twice, and observing that the sign of the second derivative is determined by the sign of a quadratic expression on λ^3, which has the given expression as a root and is positive at $\lambda = 2$. In order to proof (iv) we define $h : (0, \lambda_p] \to \mathbb{R}$ as

$$h(\lambda) = \begin{cases} \frac{W(\lambda)}{(\lambda-1)^2}, & \text{if } \lambda \neq 1, \\ \frac{1}{2}W''(1), & \text{if } \lambda = 1\,. \end{cases} \tag{3.0.38}$$

The function h is continuous, since W is twice differentiable at 1, and strictly positive by (ii) and $W''(1) > 0$. We set

$$c_p = \min\{h(\lambda) : \lambda \in (0, \lambda_p]\}\,. \tag{3.0.39}$$

The minimum exists, since h is continuous and $\lim_{\lambda\to 0} h(\lambda) = \infty$. Since h is strictly positive we obtain $c_p > 0$. □

Lemma 3.0.1.2 *For $M > 1$, let W_M be the restriction of W to $(0, M]$. The convex envelope W_M^{**}*

of W_M has the following properties:

(i) If $a_p^M < \lambda \le M$, then

$$W_M^{**}(\lambda) \ge c_p' \frac{\lambda - a_p^M}{M^{1-p}} \,. \tag{3.0.40}$$

(ii) If $\lambda \le \min\{M, a_p^M\}$, then

$$W_M^{**}(\lambda) = W(\lambda) \ge c_p(\lambda - 1)^2 \,. \tag{3.0.41}$$

Here,

$$c_p' = 1 - \left(\frac{\sqrt{3}}{2}\right)^p \,, \tag{3.0.42}$$

$c_p > 0$ depends only on p, and $a_p^M > 1$ may depend on p and M.

proof 3.0.3 *From Lemma 3.0.1.1(iii) and Carathéodory's theorem it follows that there is $a_p^M \in (1, M]$ such that*

$$W_M^{**}(\lambda) = \begin{cases} W(\lambda), & \text{for } \lambda \in (0, a_p^M] \cap (0, M], \\ W(a_p^M)\dfrac{M-\lambda}{M-a_p^M} + W(M)\dfrac{\lambda - a_p^M}{M - a_p^M}, & \text{for } \lambda \in (a_p^M, M] \,. \end{cases} \tag{3.0.43}$$

The point a_p^M cannot lie in the set where W is concave, therefore $a_p^M \le \lambda_p$. For $\lambda \le \min\{M, a_p^M\}$ we conclude that $W_M^{**}(\lambda) = W(\lambda)$ and hence, from Lemma 3.0.1.1(iv), claim (ii) follows.

Next we turn to part (i). Since in this case $a_p^M < M$, the function W_M cannot be convex everywhere and we only need to consider the case $M \ge \lambda_p$. By Lemma 3.0.1.1(iii) we have $\lambda_p \ge 2$, hence $M \ge 2$ in particular. From (3.0.43) we estimate, using the formula in Lemma 3.0.1.1(i),

$$W_M^{**}(\lambda) \ge W(M)\frac{\lambda - a_p^M}{M - a_p^M} \ge (M^p - 3^{p/2})\frac{\lambda - a_p^M}{M} \,. \tag{3.0.44}$$

From $M \geq 2$ we obtain

$$M^p - 3^{p/2} \geq c'_p M^p \text{ where } c'_p = 1 - \left(\frac{\sqrt{3}}{2}\right)^p > 0\,, \tag{3.0.45}$$

and the claim follows. □

3.0.9 Upper bound

Theorem 3.0.2 *Let $\Omega = [-L, L]^2 \times (-H, H)$, $H > 1$, $\ell \in (0, 1)$, $p \in (0, 1)$, and*

$$E(u) = \int_\Omega (|Du|^p - 3^{p/2})dx + \ell \int_\Omega |DDu|dx\,. \tag{3.0.46}$$

Fix $\delta > 0$. For every ℓ such that $0 < \ell < (1-p)\min\{\delta, \delta^{p-1}L^{2-p}\}$ there is a map $u : \Omega \to \mathbb{R}^3$ such that

$$u_3(x_1, x_2, -H) = -H - \delta, \tag{3.0.47a}$$

$$u_3(x_1, x_2, H) = H + \delta, \tag{3.0.47b}$$

for all $(x_1, x_2) \in [-L, L]^2$, and

$$E(u) \leq 4L^2 C_2(p) \ell^{\frac{1-p}{2-p}} \delta^{\frac{1}{2-p}}\,. \tag{3.0.48}$$

independent of H, where, explicitly,

$$C_2(p) = c\left((1-p)^{\frac{1}{2-p}} + (1-p)^{\frac{p-1}{2-p}}\right) \tag{3.0.49}$$

and $c > 0$ is a universal constant.

proof 3.0.4 *The outline of the proof is as follows. In Part 1 of the proof, we begin by constructing a map u depending on a parameter $a \in (0, H)$, with $2a$ measuring the size of the layer (in the undeformed configuration) in which voids are nucleated, to be chosen subsequently. In Part 2, we estimate the energy contribution from the local term, and in Part 2 from the non-local term. In Part*

4, we finally combine the partial estimates and optimize a.

Part 1. Construction of the deformation u.

We proceed to construct a map u that opens voids in the layer $\omega = [-L, L]^2 \times (-a, a) \subset \Omega$, with $a < H$ to be chosen subsequently, and defines a transverse translation elsewhere. Specifically, we set

$$u(x) = x + \delta e_3, \quad \text{for } x_3 \geq a, \text{ and } u(x) = x - \delta e_3, \quad \text{for } x_3 \leq -a\,. \tag{3.0.50}$$

The layer ω is subdivided into $(L/a)^2$ cubes of side length $2a$ (in Part 4 we choose $a \in (0, H)$ such that L/a is an integer). Each of the cubes is subject to a deformation that opens a cavity at its center, the boundary undergoing an affine deformation with gradient $\operatorname{diag}(1, 1, \lambda)$, *$\lambda = 1 + \delta/a \geq 1$. In particular the cube $(-a, a)^3$ is mapped onto $(-a, a)^2 \times (-\lambda a, \lambda a) = (-a, a)^2 \times (-a - \delta, a + \delta)$, Figure 3.1.*

Next, we focus on a single cube $C = (-a, a)^3$, the others being identical up to translations. The cube can be decomposed into 6 pyramids: two pyramids at the top and bottom of the cube, transversely, and four lateral pyramids. By symmetry, it is enough to study the top pyramid

$$T = \{x : \max\{|x_1|, |x_2|\} < x_3 < a\} \tag{3.0.51}$$

and one side pyramid

$$S = \{x : \max\{|x_1|, |x_3|\} < x_2 < a\}\,. \tag{3.0.52}$$

We begin by analyzing the top pyramid. The key idea is that T is mapped to a part of the stretched pyramid

$$T_\lambda = \{x : \max\{|x_1|, |x_2|\} < \lambda x_3 < \lambda a\}\,, \tag{3.0.53}$$

so that planes parallel to the base, i. e., orthogonal to e_3, are mapped affinely onto planes with the same orientation. The pyramid T_λ has a volume larger than T. We map T to a part of T_λ close to the base at $x_3 = \lambda a$, thus opening a void close to the vertex, which lies on the center of the cube C. In order to construct the map $u^T : T \to T_\lambda$ in detail, we choose a function $h : (0, a) \to (0, \lambda a)$ and

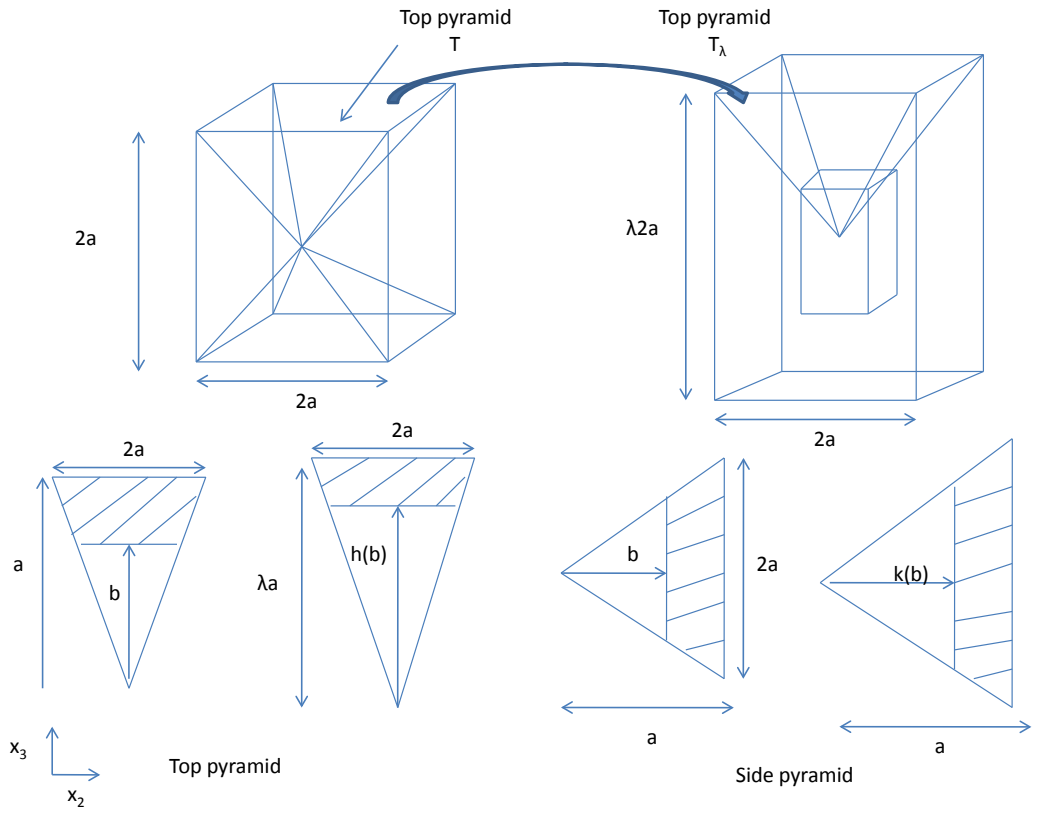

Figure 3.3: Void growth within a cube of size $2a$. Conservation of volume of the hatched areas is used to determine the functions h and k, see 3.0.56, 3.0.61.

set

$$u_3^T(x) = h(x_3)\,, \tag{3.0.54}$$

the other two components are defined so that for any $x_3 \in (0,a)$ *the square* $(-x_3,x_3)^2 \times \{x_3\}$ *is mapped affinely to the square* $(-h(x_3)/\lambda, h(x_3)/\lambda)^2 \times \{h(x_3)\}$. *In particular, we set*

$$u_1^T(x) = x_1 \frac{h(x_3)}{\lambda x_3}\,, \qquad \textit{and} \qquad u_2^T(x) = x_2 \frac{h(x_3)}{\lambda x_3}\,. \tag{3.0.55}$$

Finally, we choose the function h *so that* $h(a) = \lambda a$ *and volume is conserved. To this end, we simply equate the volume of* $T \cap \{b < x_3 < a\}$ *to the volume of its image, which immediately gives, Figure*

3.3,

$$\frac{1}{3}(4a^3 - 4b^3) = \frac{1}{3}\left[4a^2\lambda a - 4\left(\frac{h(b)}{\lambda}\right)^2 h(b)\right] \tag{3.0.56}$$

for all $b \in (0, a)$. *Therefore*

$$a^3\left(1 - \frac{b^3}{a^3}\right) = \lambda a^3\left[1 - \frac{h(b)^3}{a^3\lambda^3}\right] \tag{3.0.57}$$

and

$$h(x_3) = \lambda a\left(1 - \frac{1}{\lambda} + \frac{x_3^3}{\lambda a^3}\right)^{1/3}. \tag{3.0.58}$$

Summarizing, the deformation in the top pyramid is given by

$$u^T(x) = \begin{pmatrix} x_1 h(x_3)/(\lambda x_3) \\ x_2 h(x_3)/(\lambda x_3) \\ h(x_3) \end{pmatrix}. \tag{3.0.59}$$

The side pyramid is similar, but not identical, since the stretching is now in a tangential direction. In particular, we seek a function $k : (0, a) \to (0, a)$ *such that*

$$u_2(x) = k(x_2) \tag{3.0.60}$$

and has similar properties as above. In particular, we map $(-b, b) \times \{b\} \times (-b, b)$ *to* $(-k(b), k(b)) \times \{k(b)\} \times (-\lambda\, k(b), \lambda\, k(b))$. *The same argument based on conservation of volume, Figure 3.3, now yields*

$$\frac{1}{3}(4a^3 - 4b^3) = \frac{1}{3}\left[4\lambda a^3 - 4\lambda k(b)^3\right] \tag{3.0.61}$$

i.e.,

$$1 - \frac{b^3}{a^3} = \lambda\left[1 - \frac{k(b)^3}{a^3}\right]. \tag{3.0.62}$$

Therefore,

$$k(x_2) = a\left(1 - \frac{1}{\lambda} + \frac{x_2^3}{\lambda a^3}\right)^{1/3}. \tag{3.0.63}$$

and the deformation in the side pyramid is given by

$$u^S(x) = \begin{pmatrix} x_1 k(x_2)/x_2 \\ k(x_2) \\ \lambda x_3 k(x_2)/x_2 \end{pmatrix}. \tag{3.0.64}$$

It is easy to see that $u^S = u^T$ *at the common boundary,* $x_2 = x_3$*, and the same holds for the remaining symmetry-related pyramids.*

In order to estimate the energy, we proceed to compute the deformation gradients. Since $h'(x_3)h^2(x_3) = \lambda^2 x_3^2$*,*

$$Du^T = \begin{pmatrix} \frac{h(x_3)}{\lambda x_3} & 0 & \frac{x_1}{\lambda}\partial_3(\frac{h(x_3)}{x_3}) \\ 0 & \frac{h(x_3)}{\lambda x_3} & \frac{x_2}{\lambda}\partial_3(\frac{h(x_3)}{x_3}) \\ 0 & 0 & \lambda^2 \frac{x_3^2}{h(x_3)^2} \end{pmatrix} \tag{3.0.65}$$

and, similarly, using $k'(x_2)k^2(x_2) = x_2^2/\lambda$ *we obtain*

$$Du^S = \begin{pmatrix} \frac{k(x_2)}{x_2} & x_1\partial_2\frac{k(x_2)}{x_2} & 0 \\ 0 & \frac{x_2^2}{\lambda k(x_2)^2} & 0 \\ 0 & \lambda x_3\partial_2(\frac{k(x_2)}{x_2}) & \lambda\frac{k(x_2)}{x_2} \end{pmatrix}. \tag{3.0.66}$$

Part 2. Estimate for the gradient term.

Step 2.1: Top pyramid.

We begin by estimating the quantity $\int_T |Du^T|^p\,dx$*. We treat each of the remaining* 5 *non-zero components of the energy separately.*

For the Du_{11}^T *component we observe that* $h(x_3) \le \lambda a$ *and therefore*

$$|Du_{11}^T| = \frac{h(x_3)}{\lambda x_3} \le \frac{a}{x_3}. \tag{3.0.67}$$

This implies that

$$\int_T |(Du^T)_{11}|^p \leq \int_T (\frac{a}{x_3})^p \, dx = \int_0^a 4x_3^2 \frac{a^p}{x_3^p} dx_3 = \frac{4}{3-p} a^3 \,. \tag{3.0.68}$$

The Du_{22}^T component is identical.

For the Du_{33}^T component we observe that, by (3.0.58),

$$(\frac{h(x_3)}{\lambda x_3})^3 = \left(1 - \frac{1}{\lambda}\right) \frac{a^3}{x_3^3} + \frac{1}{\lambda} \,. \tag{3.0.69}$$

This is a decreasing function of x_3, which equals 1 at $x_3 = a$. Therefore $h(x_3) \geq \lambda x_3$ everywhere. In particular,

$$|Du_{33}^T| = \frac{\lambda^2 x_3^2}{h(x_3)^2} \leq 1 \tag{3.0.70}$$

and hence

$$\int_T |Du_{33}^T|^p \leq |T| = \frac{4}{3} a^3 \,. \tag{3.0.71}$$

We now turn to the Du_{13}^T component and compute

$$\frac{x_1}{\lambda} \frac{\partial}{\partial x_3} (\frac{h(x_3)}{x_3}) = \frac{x_1}{\lambda} \frac{h'(x_3)}{x_3} - \frac{x_1}{\lambda} \frac{h(x_3)}{x_3^2} \,. \tag{3.0.72}$$

Since $|x_1| \leq x_3$ and $\lambda \geq 1$ we have

$$\left| \frac{x_1}{\lambda} \frac{h'(x_3)}{x_3} \right| \leq |h'(x_3)| = |Du_{33}^T|, \tag{3.0.73}$$

which has already been treated. Simultaneously,

$$\left| \frac{x_1}{\lambda} \frac{h(x_3)}{x_3^2} \right| \leq \frac{h(x_3)}{\lambda x_3} = |Du_{11}^T|, \tag{3.0.74}$$

which has also been treated. Therefore, we have

$$\int_T |Du_{13}^T|^p \leq \int_T |Du_{11}^T|^p + \int_T |Du_{33}^T|^p \leq \frac{4}{3-p}a^3 + \frac{4}{3}a^3\,. \tag{3.0.75}$$

The term Du_{23}^T is identical after exchanging x_1 and x_2.

Finally, from the preceding estimates we conclude that

$$\int_T |Du^T|^p \leq (4 + \frac{16}{3-p})a^3 \tag{3.0.76}$$

Step 2.2: Side pyramid.

We now turn to the side pyramid. Since $k(x_2) \leq a$, we have

$$\frac{k(x_2)}{x_2} \leq \frac{a}{x_2}\,. \tag{3.0.77}$$

Therefore the Du_{11}^S term can be treated as Du_{11}^T, and we obtain

$$\int_S |Du_{11}^S|^p \leq \frac{4}{3-p}a^3\,. \tag{3.0.78}$$

Since $Du_{33}^S = \lambda Du_{11}^S$, we also obtain

$$\int_S |Du_{33}^S|^p \leq \lambda^p \frac{4}{3-p}a^3\,. \tag{3.0.79}$$

In order to treat the Du_{22}^S term we observe that

$$(\frac{k(x_2)}{x_2})^3 = \left(1 - \frac{1}{\lambda}\right)\frac{a^3}{x_2^2} + \frac{1}{\lambda} \tag{3.0.80}$$

is decreasing in x_2 and equals 1 at $x_2 = a$. Therefore $k(x_2) \geq x_2$, and

$$|Du_{22}^S| = \frac{x_2^2}{\lambda k(x_2)^2} \leq \frac{1}{\lambda} \ \leq 1\,. \tag{3.0.81}$$

Thus, we conclude that

$$\int_S |Du_{22}^S|^p \leq |S| = \frac{4}{3}a^3\,. \tag{3.0.82}$$

The terms Du_{12}^S and Du_{32}^S are similar to the Du_{13}^T treated earlier. We start with Du_{32}^S and compute

$$\lambda x_3 \frac{\partial}{\partial x_2}(\frac{k(x_2)}{x_2}) = \lambda x_3 \frac{k'(x_2)}{x_2} - \lambda x_3 \frac{k(x_2)}{x_2^2}\,. \tag{3.0.83}$$

Using $|x_3| \leq x_2$ and (3.0.81) we obtain

$$|\lambda x_3 \frac{k'(x_2)}{x_2}| \leq |\lambda k'(x_2)| = \frac{x_2^2}{k(x_2)^2} \leq 1\,. \tag{3.0.84}$$

Simultaneously,

$$\left|\lambda x_3 \frac{k(x_2)}{x_2^2}\right| \leq \left|\lambda \frac{k(x_2)}{x_2}\right| = |Du_{33}^S|\,. \tag{3.0.85}$$

Recalling (3.0.79) and (3.0.82), we obtain

$$\int_S |Du_{32}^S|^p \leq \frac{4}{3}a^3 + \lambda^p \frac{4}{3-p}a^3\,. \tag{3.0.86}$$

The Du_{12}^S term is similar but yields a smaller contribution, since it misses the factor λ. Therefore,

$$\int_S |Du_{12}^S|^p \leq \frac{4}{3}a^3 + \frac{4}{3-p}a^3\,. \tag{3.0.87}$$

Collecting terms we finally obtain

$$\int_S |Du^S|^p \leq (4 + \frac{16}{3-p})\lambda^p a^3 \tag{3.0.88}$$

Step 2.3: Summary.

Summing over the six pyramids we obtain

$$\int_C |Du|^p \leq 2(4 + \frac{16}{3-p})a^3 + 4(4 + \frac{16}{3-p})\lambda^p a^3 \leq 72\lambda^p a^3,\,. \tag{3.0.89}$$

Since there are $(\frac{L}{a})^2$ *distinct cubes, we get*

$$\int_\omega |Dy|^p dx \leq c_1 L^2 a \lambda^p, \tag{3.0.90}$$

with $c_1 = 72$*. This immediately gives*

$$\int_\Omega |Du|^p - 3^{p/2} = \int_\omega |Du|^p - 3^{p/2} \leq c_1 L^2 a \lambda^p, \tag{3.0.91}$$

since on $\Omega \setminus \omega$ *the deformation gradient* Du *is the identity matrix.*

Part 3. Estimate for the strain gradient term.

Step 3.1: Preliminaries.

We begin by making the following observation. Let Ω *be decomposed, up to a null set, into finitely many polyhedra* $\omega_1, \ldots, \omega_N$ *(they will be the* $6(L/a)^2$ *pyramids and the two sets where* u *is affine) and assume that* $u = u^{(n)}$ *on* ω_n*. Then, we can separate the contributions of the different sets as*

$$\begin{aligned} \int_\Omega |DDu| &= \sum_{n=1}^N \int_{\omega_n} |DDu^{(n)}| + \sum_{n \neq m} \int_{\partial\omega_n \cap \partial\omega_m} |Du^{(n)} - Du^{(m)}| d\mathcal{H}^2 \\ &\leq \sum_{n=1}^N \int_{\omega_n} |DDu^{(n)}| + \int_{\partial\omega_n} |Du^{(n)}| d\mathcal{H}^2 \,. \end{aligned} \tag{3.0.92}$$

Physically, this decomposition means that the deformation gradient term measures both the smooth variation of Du *inside the sets and the jumps across the boundaries. Since the deformation* u *is continuous but the deformation gradient is discontinuous across the boundaries, we need to estimate both contributions.*

Assume that, for some index n *and for some choice of* $i, j, k \in \{1, 2, 3\}$*, we can show that* $D_i D_j u_k^{(n)} \geq 0$ *everywhere in* $\omega^{(n)}$*. Then, by the Gauss-Green theorem we obtain*

$$\begin{aligned} \int_{\omega^{(n)}} |D_i D_j u_k^{(n)}| &= \int_\omega D_i D_j u_k^{(n)} \\ &= \int_{\partial\omega^{(n)}} n_i D_j u_k^{(n)} d\mathcal{H}^2 \leq \int_{\partial\omega^{(n)}} |D_j u_k^{(n)}| d\mathcal{H}^2 \,. \end{aligned} \tag{3.0.93}$$

Evidently, the same conclusion holds if $D_iD_j u_k^{(n)} \le 0$ everywhere. Therefore, for the components which have this monotonicity property we only need to estimate the boundary integral. By symmetry, we only need to consider the top and side pyramid.

Step 3.2: Top pyramid.

As already noted in (3.0.69) that $h(x_3)/x_3$ is monotonic in x_3 and does not depend on the other two variables. Hence the $D(Du_{11}^T)$ and $D(Du_{22}^T)$ terms reduce to boundary integrals. Furthermore, $|Du_{11}^T| \le a/x_3$. We compute, by separating the base and the four lateral faces of T,

$$\begin{aligned}\int_{\partial T} |Du_{11}^T| \le \int_{\partial T} \frac{a}{x_3} &= 4a^2 + 4\int_0^a \int_{-x_3}^{x_3} \frac{a}{x_3}\sqrt{2}dx_2dx_3 \\ &= 4a^2 + 8a^2\sqrt{2}\,.\end{aligned} \tag{3.0.94}$$

The Du_{22}^T follows likewise. Similarly, Du_{33}^T is monotonic in x_3, and does not depend on the other two variables. From (3.0.70) we find that

$$\int_{\partial T} |Du_{33}^T| \le |\partial T| = (4+4\sqrt{2})a^2\,. \tag{3.0.95}$$

Next, we turn to the off-diagonal terms. We start with 13, and observe that $\partial_1(\frac{x_1}{\lambda}\partial_3(\frac{h(x_3)}{x_3})) = \frac{1}{\lambda}\partial_3(\frac{h(x_3)}{x_3}) \le 0$, hence this term only needs to be considered on the boundary. Finally, we compute

$$\begin{aligned}\frac{\partial (Du^T)_{13}}{\partial x_3} = \frac{x_1}{\lambda}\frac{\partial^2}{\partial x_3^2}\frac{h(x_3)}{x_3} &= \frac{x_1}{\lambda}\frac{\partial}{\partial x_3}\left[\frac{\lambda^2 x_3}{h(x_3)^2} - \frac{h(x_3)}{x_3^2}\right] \\ &= \frac{x_1}{\lambda}\left[-2\lambda^4\frac{x_3^3}{h(x_3)^5} + \frac{\lambda^2}{h(x_3)^2} + 2\frac{h(x_3)}{x_3^3} - \frac{\lambda^2}{h(x_3)^2}\right] \\ &= \frac{x_1}{\lambda}\left[-2\lambda^4\frac{x_3^3}{h(x_3)^5} + 2\frac{h(x_3)}{x_3^3}\right] \ge 0,\end{aligned} \tag{3.0.96}$$

since $h(x_3) \ge \lambda x_3$ and $\lambda \ge 1$. Therefore, the remaining derivative also has a sign. Recalling that $|Du_{13}^T| \le |Du_{11}^T| + |Du_{33}^T|$ by (3.0.72–3.0.74)), we conclude that

$$\begin{aligned}\int_T |D(Du^T)_{13}| &\le 2\int_{\partial T} |(Du^T)_{13}| d\mathcal{H}^2 \\ &\le 2\int_{\partial T} |(Du^T)_{11}| + |(Du^T)_{33}| d\mathcal{H}^2 \le (16+24\sqrt{2})a^2\,.\end{aligned} \tag{3.0.97}$$

The $D(Du^T)_{23}$ term follows likewise.

In summary, we conclude that

$$\int_T |DDu^T| + \int_{\partial T} |Du^T| d\mathcal{H}^2 \leq (72 + 112\sqrt{2})a^2 \,. \tag{3.0.98}$$

Step 3.3: Side pyramid.

All monotonicities may be checked as before and we do not repeat the calculations here. One can also observe that Du^S can be obtained from Du^T by composing it on both sides with affine maps, an operation that does not change the sign of the second derivatives. The integrals over the surfaces are also estimated as above. In particular, Du^S_{11} behaves as Du^T_{11}, whereas Du^S_{33} differs by a factor of λ and gives

$$\int_{\partial S} |Du^S_{33}| \leq (4 + 8\sqrt{2})\lambda a^2 \,. \tag{3.0.99}$$

The Du^S_{22} term is again estimated by (3.0.81), and for the Du^S_{32} term we use $|Du^S_{32}| \leq 1 + |Du^S_{33}|$, cf. (3.0.83–3.0.85)), which implies

$$\int_S |DDu^S_{32}| \leq 2 \int_{\partial S} |Du^S_{32}| \leq 2((4 + 4\sqrt{2}) + \lambda(4 + 8\sqrt{2}))a^2 \,. \tag{3.0.100}$$

In addition, the Du^S_{12} term obeys $|Du^S_{31}| \leq 1 + |Du^S_{11}|$ and thus one has also

$$\int_S |DDu^S_{12}| \leq 2 \int_{\partial S} |Du^S_{12}| \leq 2((4 + 4\sqrt{2}) + \lambda(4 + 8\sqrt{2}))a^2 \,. \tag{3.0.101}$$

In summary,

$$\int_S |DDu^S| + \int_{\partial S} |Du^S| d\mathcal{H}^2 \leq (72 + 112\sqrt{2})\lambda a^2 \,. \tag{3.0.102}$$

Step 3.4: Summary.

Adding all terms (6 pyramides per cube) and accounting for the number of cubes $\frac{L^2}{a^2}$ we obtain

$$\int_\Omega |DDy| dx \leq c_2 \lambda L^2, \,. \tag{3.0.103}$$

with

$$c_2 = 6(72 + 112\sqrt{2}) \simeq 1382.4. \tag{3.0.104}$$

Part 4. Choice of a and conclusion of the proof.

We may now proceed to add the local contribution from (3.0.91) and the non-local contribution from (3.0.103) to obtain

$$E(u) = \int_\Omega (|Du|^p - 3^{p/2})dx + \ell \int_\Omega |DDu|\, dx \le cL^2 a\lambda^p + cL^2\ell\lambda\,. \tag{3.0.105}$$

Here, c is a universal constant, and $\lambda = 1 + \delta/a$, where δ is the prescribed displacement. More precisely

$$c = max\{c_1, c_2\} \simeq 1382.4 \tag{3.0.106}$$

We thus obtain

$$E(u) \le cL^2 a\left(1 + \frac{\delta}{a}\right)^p + cL^2\ell\left(1 + \frac{\delta}{a}\right) \le caL^2 + ca^{1-p}\delta^p L^2 + c\ell L^2 + c\ell\frac{\delta}{a}L^2\,. \tag{3.0.107}$$

For small ℓ and δ large enough, the second and the last terms are dominant. We choose a so that their sum is minimal. This is achieved for $a^{2-p} = \frac{\delta^{1-p}\ell}{1-p}$. However, since we need L/a to be an integer, we define

$$a_* = (\frac{\delta^{(1-p)}\ell}{1-p})^{1/(2-p)} \tag{3.0.108}$$

and $a = L/\lceil L/a_*\rceil$. For $\ell \le (1-p)\delta^{p-1}L^{2-p}$, it follows that $a_*/2 \le a \le a_* \le L$. Since $\delta/a_* = ((1-p)\delta/\ell)^{1/(2-p)}$, for $\ell \le (1-p)\delta$ the first term in (3.0.107) is smaller than the second, and the third is smaller than the fourth. We thus conclude that, for all $\ell \le \min\{(1-p)\delta, (1-p)\delta^{p-1}L^{2-p}\}$,

$$\begin{aligned} E(u) &\le 4cL^2(a_*^{1-p}\delta^p + \ell\frac{\delta}{a_*}) \\ &= 4cL^2[(1-p)^{\frac{1}{2-p}} + (1-p)^{\frac{p-1}{2-p}}]\,\ell^{(1-p)/(2-p)}\delta^{1/(2-p)}\,. \end{aligned} \tag{3.0.109}$$

This concludes the proof. □

Chapter 4

Physical Interpretation and Experimental Validation

4.1 Physical interpretation

Ductile fracture emerges as the net result of two competing effects: whereas the sublinear growth of the energy in the large-body limit promotes localization of deformation in large samples to failure planes, the size-dependence of metal plasticity stabilizes this process of localization in its advanced stages, thus resulting in an orderly progression towards failure and a well-defined specific fracture energy. The optimal scaling laws confirm that ductile fracture results from the localization of damage to a plane (void sheet) and that it requires a well- defined fracture energy.

The essential role of the intrinsic length ℓ in determining the optimal scaling behavior is particularly noteworthy. Thus, if $\ell = 0$, i. e., if the material is *local*, then we see from (theorem 3.0.1 and theorem 3.0.2) that the energy is bounded above and below by zero, since $\frac{1-p}{2-p} > 0$, which would correspond to a void spacing $a = 0$. The energy then relaxes to zero as a result of localization of deformations to a negligibly thin band. Thus, in the absence of an internal length scale the fracture energy degenerates to zero, as expected from the sublinear growth of the energy, and the solid can fracture spontaneously at no energy cost. This in particular confirms the prediction of 2.1. The upper bound theorem by itself provides an alternate proof that the energy relaxes to zero when $\ell = 0$.

The fracture properties of materials are characterized by means of standardized tests designed

to measure specific fracture parameters such as fracture toughness, critical energy-release rate and specific fracture energy ([61]). Therefore, in order to make contact with test data we proceed to reinterpret the preceding results in terms of standard fracture concepts.

4.1.1 Cohesive-energy interpretation

We note that the upper and lower energy bounds theorem 3.0.1 and theorem 3.0.2 scale with the in-plane area $4L^2$ and are independent of the thickness $2H$ of the slab. This type of scaling is characteristic of *fracture processes*, in which the deformation is concentrated in the neighborhood of a fracture surface and the energy scales with the area of the surface. In particular, the specific energy per unit area

$$\Phi = \frac{E_{\min}}{4L^2} \tag{4.1.1}$$

is well-defined and independent of the thickness $2H$ of the slab. We note that, as a corollary, *fractal* modes of fracture, characterized by energy scaling intermediate between area and volume scaling, are ruled out under the assumptions of the analysis.

The bounds (theorem 3.0.1 and theorem 3.0.1) can be recast in terms of this specific energy per unit area as

$$C_1(p)\frac{K}{p}\ell^{\frac{1-p}{2-p}}\delta^{\frac{1}{2-p}} \leq \Phi \leq C_2(p)\frac{K}{p}\ell^{\frac{1-p}{2-p}}\delta^{\frac{1}{2-p}}. \tag{4.1.2}$$

where

$$C_1(p) = \frac{1}{2}\left(1-\left(\frac{\sqrt{3}}{2}\right)^p\right)\left((1-p)^{\frac{1}{2-p}} + (1-p)^{\frac{p-1}{2-p}}\right). \tag{4.1.3}$$

and

$$C_2(p) = 1382.4\left((1-p)^{\frac{1}{2-p}} + (1-p)^{\frac{p-1}{2-p}}\right) \tag{4.1.4}$$

Fix now ℓ and regard the specific energy per unit area as a function $\Phi(\delta)$ of the opening displacement. By the work-energy theorem the corresponding applied normal traction then follows as

$$\sigma = \frac{\partial \Phi}{\partial \delta} = \sigma(\delta). \tag{4.1.5}$$

This relation may be regarded as a cohesive law that relates opening displacement δ and traction σ. The optimal scaling laws (4.1.2) thus imply that ductile fracture is cohesive in nature, i.e., it obeys a well-defined relation between tractions and opening displacements. This is in contrast to Griffith models of brittle fracture, which posit a sudden loss of bearing capacity across incipient fracture planes. It is also interesting to note that the optimal scaling laws (4.1.2) are of the *power-law* type and thus consistent with power-law cohesive behavior. Since $0 < p < 1$, such power-law cohesive behavior then expresses a monotonically decreasing relation between applied normal traction and opening displacement.

4.1.2 Relation to J_c

We recall that the attainment of a critical value J_c of Rice's J-integral [95] provides a standard and widely used non-linear fracture criterion with several attractive properties (cf., e.g., [59, 61] for reviews): i) For linear elastic materials J coincides with G, the elastic energy-release rate; ii) for power-law small-strain plastic behavior, J determines the strength of the HRR singular field [57, 97] at the crack tip; and iii) it can be evaluated experimentally in a convenient manner. For a material obeying a cohesive fracture law, an application of Rice's J-integral [95] gives the plane-strain value of J at crack-growth initiation as

$$J_c = \int_0^{+\infty} \sigma(\delta)\, d\delta = \Phi(+\infty) - \Phi(0). \tag{4.1.6}$$

The stress follows as $\sigma \sim \delta^{\frac{p-1}{2-p}}$ but the function $\delta \mapsto \delta^{\frac{p-1}{2-p}}$ is not integrable on $[0, \infty)$. Therefore we find that the integral necessarily diverges at infinity, i.e., it predicts an infinite J_c. In order to eliminate this divergence we may introduce a cut-off δ_c, representing a critical opening displacement at crack-growth initiation, and write

$$J_c = \int_0^{\delta_c} \sigma(\delta)\, d\delta = \Phi(\delta_c) - \Phi(0). \tag{4.1.7}$$

Evidently, a mechanistic model for δ_c requires consideration of additional physics, not accounted for by either the local or non-local models considered so far, at the point of final separation of the fracture surface. For instance, the final stages of separation may entail the formation of thin *ligaments* which eventually neck to a point, or slough off in shear, or cleave by brittle fracture, or fail by some other mechanism.

Inserting the bounds (4.1.2) into (4.1.7) we obtain

$$C_1(p)\frac{K}{p}\ell^{\frac{1-p}{2-p}}\delta_c^{\frac{1}{2-p}} \leq J_c \leq C_2(p)\frac{K}{p}\ell^{\frac{1-p}{2-p}}\delta_c^{\frac{1}{2-p}}, \tag{4.1.8}$$

which supplies bounds for J_c as a function of the internal length ℓ, the critical opening displacement δ_c and the hardening constant $A = K/n$, and the hardening exponent $n = p$. Moreover, the bounds can be recast in terms of the surface energy $B = \ell A$ in the form

$$C_1(p)\frac{K}{p}\left(\frac{B}{A}\right)^{\frac{1-p}{2-p}}\delta_c^{\frac{1}{2-p}} \leq J_c \leq C_2(p)\frac{K}{p}\left(\frac{B}{A}\right)^{\frac{1-p}{2-p}}\delta_c^{\frac{1}{2-p}}, \tag{4.1.9}$$

The bounds (4.1.8,4.1.9) therefore supply a link between micromechanical properties (such as length scale, surface energies, etc.) and macroscopic fracture properties (fracture energy), and reveal the relative roles that surface energy and microplasticity play as contributors to the specific fracture energy of the material. Moreover, the optimal scaling laws implicitly predict a temperature dependence of the specific fracture energy J_c, as it relates to material parameters such as K and n (which enter the model through the parameter A), which in turn, may vary as function of temperature. Hence the scaling laws supply a relation between independently measurable material and fracture properties, and thus open the theory to experimental validation or invalidation. This experimental validation is attempted next.

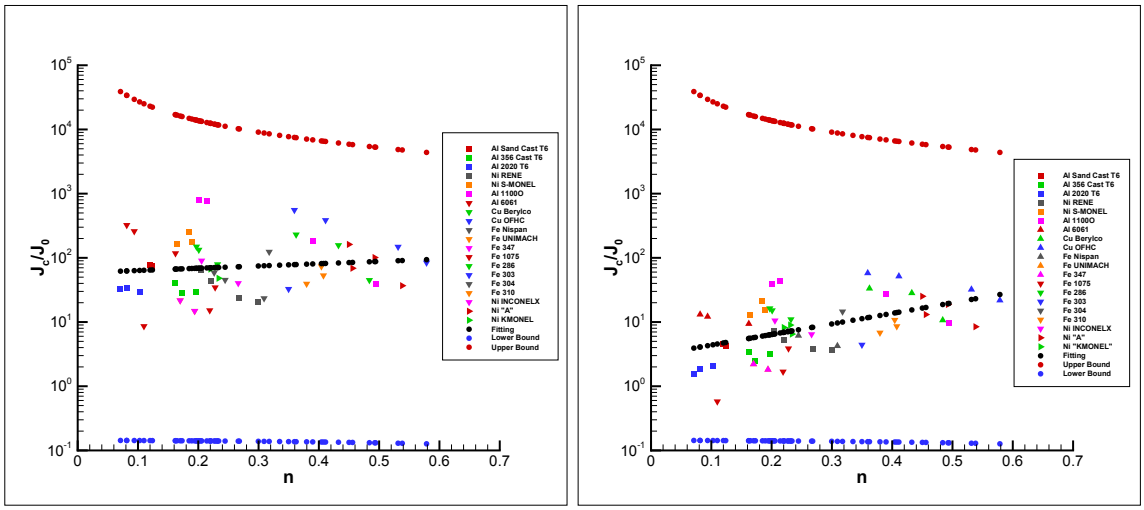

(a) (b)

Figure 4.1: Renormalized specific fracture energy J_c/J_0 and bounds shown as a function of the hardening exponent n for nickel, iron, copper and aluminium alloys at temperature of 300K, 195K, and 76K (data from [131]). a) Dislocation wall model of ℓ. b) Nix-Gao [90] model of ℓ.

4.2 Comparison with experiment

We now proceed to assess the validity of the optimal bounds (4.1.8) through quantitative comparisons with experimental data. To this end, we employ an assortment of experimental data from the monograph of Warren and Reed [131]. The data are derived from tensile tests and impact Charpy tests and pertain to nickel, iron, copper and aluminium alloys at temperature of 300K, 195K, and 76K. These test data conveniently supply the material parameters required to evaluate (4.1.8), namely the strength coefficient K, the hardening exponent n, which we take to equal the growth exponent p, J_c and the critical opening displacement δ_c. The parameters K and n are obtained by fitting to the stress-strain curves reported in [131]. The value of J_c is identified with the Charpy energy per unit fracture area. The critical opening displacement δ_c is obtained from the reported tensile strain to failure and the gage length of the specimen. The data set used as a basis for validation is collected in Table 4.1.

For purposes of comparison to experimental data, suppose that the energy density of the material is well approximated by

$$W(F, DF) = A(|F|^p - 3^{p/2} + \ell|DF|), \tag{4.2.1}$$

in which case the energy of the material corresponds exactly to the energy functional (3.0.1) considered in this analysis. Then, with the identification $p = n$, we can define a reference J as

$$J_0 = K\ell^{\frac{1-n}{2-n}}\delta_c^{\frac{1}{2-n}}, \tag{4.2.2}$$

whereupon the optimal scaling law (4.1.8) reduces to

$$C_L(n) \leq \frac{J_c}{J_0} \leq C_U(n), \tag{4.2.3}$$

where

$$C_L(n) = \frac{1}{2n}\left(1 - \left(\frac{\sqrt{3}}{2}\right)^n\right)\left((1-n)^{\frac{1}{2-n}} + (1-n)^{\frac{n-1}{2-n}}\right), \tag{4.2.4}$$

and

$$C_U(n) = \frac{1382.4}{n}\left((1-n)^{\frac{1}{2-n}} + (1-n)^{\frac{n-1}{2-n}}\right) \tag{4.2.5}$$

are functions of the hardening exponent n only.

For purposes of comparison, we present results for two length scale models: the dislocation walls model for ℓ presented in section 2.2.6, and the length scale model of Nix and Gao ([90]) derived from their nanoindentation experiments. The renormalized specific fracture energy J_c/J_0 and the bounds $C_L(n)$ and $C_U(n)$ are shown in Figure 4.1 for the dislocation wall model (2.2.54) of ℓ, Figure 4.1a, and the Nix and Gao [90] model $\ell \sim b(\mu/K)^2$, Figure 4.1b. As expected, J_c/J_0 falls within the bounds $C_L(n)$ and $C_U(n)$ in both cases. The plots also suggest that the ratio J_c/J_0 is well-approximated by a universal, or material-independent, function of n, i. e.,

$$J_c \approx C(n)J_0 = C(n)K\ell^{\frac{1-n}{2-n}}\delta_c^{\frac{1}{2-n}}. \tag{4.2.6}$$

It should be noted that the reduced data exhibits variation commensurate with the level of experimental scatter. However, given the heterogeneity of the experimental data, corresponding to several disparate materials, the degree of consolidation of the data achieved through renormalization is

remarkable. A polynomial fit to the reduced data in Figure 4.1a gives

$$C(n) = exp(0.8142n + 4.0695), \tag{4.2.7}$$

whereas a polynomial fit to the reduced data in Figure 4.1b gives

$$C(n) = exp(3.7878n + 1.0986). \tag{4.2.8}$$

Relation (4.2.6) can be used to estimate the value of J_c for metals on the basis of its hardening characteristics K and n, its critical opening displacement δ_c and and it intrinsic length ℓ.

Material	$K(MPa)$	n	$2\delta_c(m)$	$J_c(J/m^2)$	$E(MPA)$	ν	$b(m)$
Al Sand Cast T6(RT)	436.0417	0.1239	0.0007788	42369	65008	0.33	2.86E-10
Al Sand Cast T6(195K)	470.8574	0.12	0.000708	42369	65008	0.33	2.86-E10
Al 356 Cast T6(RT)	430.657	0.1731	0.0023	33895	42950	0.33	2.86E-10
Al 356 Cast T6(195K)	428.5973	0.1618	0.0021	42369	42950	0.33	2.86E-10
Al 356 Cast T6(76K)	562.303	0.1969	0.0019	42369	42950	0.33	2.86E-10
Al 2020 T6(RT)	730.0321	0.071	0.0018	25421	74507	0.33	2.86E-10
Al 2020 T6(195K)	803.8159	0.0812	0.0012	25421	74507	0.33	2.86E-10
Al 2020 T6(76K)	970.9448	0.1027	0.0009204	25421	74507	0.33	2.86E-10
Ni RENE(RT)	2131.6	0.2044	0.0038	508430	160610	0.31	2.49E-10
Ni RENE(195K)	2294.5	0.2209	0.0043	423690	160610	0.31	2.49E-10
Ni RENE(76K)	2926.3	0.2681	0.0041	355900	160610	0.31	2.49E-10
Ni RENE(20K)	3253.2	0.2996	0.0038	372845	160610	0.31	2.49E-10
Ni S-MONEL(RT)	1307.1	0.1848	0.0012	694850	157320	0.31	2.49E-10
Ni S-MONEL(195K)	1371.5	0.1893	0.0023	737220	157320	0.31	2.49E-10
Ni S-MONEL(76K)	1387.7	0.1647	0.0028	660950	157320	0.31	2.49E-10
Al 1100O(RT)	150.2777	0.2012	0.0081	1559170	68900	0.33	2.86E-10
Al1100O(195K)	181.6292	0.2142	0.0089	1898120	68900	0.33	2.86E-10
Al1100O(76K)	451.2561	0.3898	0.01	2372650	68900	0.33	2.86E-10
Al1100O(20K)	792.6967	0.4942	0.0096	1423590	68900	0.33	2.86E-10
Al6061(RT)	400.5347	0.0814	0.0032	271160	69739	0.33	2.86E-10
Al6061(195K)	448.0616	0.0938	0.0035	271160	69739	0.33	2.86E-10
Al6061(76K)	634.0282	0.1622	0.0043	279630	69739	0.33	2.86E-10
Cu Berylco25Annealed(RT)	958.698	0.4325	0.0111	5558780	127550	0.36	2.55E-10
Cu Berylco25Annealed(195K)	909.375	0.3623	0.0122	5341900	127550	0.36	2.55E-10
Cu Berylco25Annealed(76K)	1434.3	0.4838	0.0124	3127400	127550	0.36	2.55E-10
Cu OFHC(RT)	432.4807	0.3594	0.0095	7117950	137900	0.36	2.55E-10
Cu OFHC(195K)	545.3506	0.4111	0.0094	7728060	137900	0.36	2.55E-10
Cu OFHC(76K)	794.1043	0.5314	0.0106	8880490	137900	0.36	2.55E-10
Cu OFHC(20K)	931.6159	0.5786	0.0122	8609330	137900	0.36	2.55E-10
Fe Nispan(RT)	2071	0.2264	0.0035	488088	149540	0.3	2.48E-10
Fe Nispan(195K)	2286.7	0.2445	0.0039	474530	149540	0.3	2.48E-10
Fe Nispan(76K)	2850.8	0.3091	0.0046	460972	149540	0.3	2.48E-10
Fe UNIMACH(RT)	3692.5	0.17	0.0015	135580	250050	0.3	2.48E-10
Fe UNIMACH(195K)	4479.1	0.194	0.0011	101680	250050	0.3	2.48E-10
Fe 347(RT)	1318.2	0.3349	0.008	1796400	121220	0.3	2.48E-10
Fe 1075(RT)	2122.8	0.228	0.0025	271160	191620	0.3	2.48E-10
Fe 1075(195K)	2231.7	0.219	0.0026	118630	191620	0.3	2.48E-10
Fe 1075(76K)	2169.7	0.1099	0.0018	25421	191620	0.3	2.48E-10
Fe 286(RT)	1823.2	0.197	0.0037	940590	134690	0.3	2.48E-10
Fe 286(195K)	1939.7	0.2009	0.0042	957530	134690	0.3	2.48E-10
Fe 286(76K)	2376.3	0.232	0.0052	881270	134690	0.3	2.48E-10
Fe 303(RT)	1325	0.3498	0.0102	935502	193000	0.3	2.48E-10
Fe 304(RT)	1207.3	0.3176	0.0114	2960200	196500	0.3	2.48E-10
Fe 310(RT)	1103.8	0.4042	0.0085	2389600	200000	0.3	2.48E-10
Fe 310(195K)	1396.9	0.4076	0.0103	2304860	200000	0.3	2.48E-10
Fe 310(76K)	2075	0.3797	0.0097	1762540	200000	0.3	2.48E-10
Ni INCONELX(RT)	2120.6	0.2055	0.0037	677900	146080	0.31	2.49E-10
Ni INCONELX(76K)	2751.3	0.2663	0.0047	593160	146080	0.31	2.49E-10
Ni "A"(RT)	919.5184	0.45	0.0086	6304470	205000	0.31	2.49E-10
Ni "A"(195K)	1070.7	0.4926	0.0089	5829940	205000	0.31	2.49E-10
Ni "A"(76K)	1377.5	0.5383	0.0108	3886600	205000	0.31	2.49E-10
Ni "A"(20K)	1541.9	0.4559	0.0105	4428900	205000	0.31	2.49E-10
Ni KMONEL(RT)	1982	0.231	0.0039	627060	143850	0.31	2.49E-10
Ni KMOMEL(195K)	2082.3	0.2204	0.0041	576215	143850	0.31	2.49E-10
Ni KMONEL(76K)	2322.5	0.2338	0.0048	525370	143850	0.31	2.49E-10

Table 4.1: Table of experimental data for various materials at various temperatures. RT: room temperature. The values of K (strength coefficient) and n (hardening exponent, equal to p) were obtained by fitting the stain strain curves of the corresponding material. Impact toughness is expressed as the Charpy energy per unit of fracture area. Source: K. A. Warren and R. P. Reed, Tensile and Impact Properties of Selected Materials from 20 to 300K, Monograph 63, National Bureau of Standards, June 1963.

Chapter 5

Conclusion and Future Work

5.1 Summary

The present work has been geared toward the development of a multiscale model for ductile fracture. The analysis presented strongly relied on tools from the Calculus of Variations, which was possible by recourse to the deformation theory of plasticity. This indeed allowed to recast plasticity problems into the minimization of energy functionals.

In Chapter 2, we showed that conventional plasticity fails to provide a full description of ductile fracture. This is due to the sublinear growth of the strain energy density, an observation that is experimentally confirmed by standard constitutive tests. Mathematically, such *local* energies relax to zero by developing localization or necking, which in the limit leads to fracture of the specimen. This motivated the addition of a stabilizing energy that is tied to size effects and thus strain gradients. We developed a strain gradient plasticity model within the context of deformation theory which led to formulate a strain energy density that depends on both the deformation gradient and the deformation second gradient through an additive decomposition. Contrary to previous strain gradient models which include the gradient of plastic strain into the constitutive law, the present model introduced strain gradients in the energy density. The present study concerned materials which have a sublinear growth with respect to the deformation gradient and a linear growth with respect to the deformation second gradient. The linear growth in the non-local part of the energy density is characteristic of Γ-limits of microplasticity theories based on dislocation mechanics.

In Chapter 3, we proposed a rigorous analysis of ductile fracture. The problem considered was an infinite slab with a finite thickness subjected to a prescribed imposed displacement to its two surfaces. The goal was to derive optimal bounds on the infimum energy as a function of the imposed displacement and the length scale, as opposed to searching for an exact solution. The upper bound construction consisted of a deformation mapping opening voids inside a layer and affine outside the layer. The optimal size of the layer was found to depend on the length scale ℓ. The lower bound, obtained by means of a direct proof, confirmed that the upper bound was indeed optimal, in the sense of matching the exponents. This mathematical result, which is the cornerstone of this thesis, is referred to as the *optimal scaling laws* in ductile fracture. It revealed that size effects and thus non local-plasticity stabilize the unstable behavior due to the sublinear growth and lead to a specific distribution of damage on the fracture plane and a well- defined fracture energy. The result mainly predicts a power law between the fracture energy and the imposed displacement, which strongly suggests that ductile fracture is cohesive by nature and not Griffith. Additionally, the laws supply a relationship between the fracture energy and microscopic properties such as surface energies and length scale, along with other material parameters such as the hardening exponent and the strength coefficient. The temperature dependence is implicitly predicted in this model because the material parameters also depend on temperature.

In Chapter 4, we presented an experimental validation of the scaling laws. The experimental assessment is based on test data collected from the monograph of Warren and Reed [131] pertaining to nickel, iron, copper and aluminium alloys over a range of temperatures. Conveniently, these test data suffice to identify the material constants characterizing the hardening behavior of the materials, which is ostensibly of the power-law type, and, simultaneously, the elongation at failure and J_c, the specific fracture energy. As expected, the data falls within the upper and lower bounds. More remarkably, when J_c is renormalized in a manner suggested by the optimal scaling laws, the data ostensibly collapses, with allowances made for experimental scatter, on a master curve dependent on the hardening exponent, but otherwise material independent. This collapse is all the more remarkable considering the vast heterogeneity of the experimental data, corresponding to several

different metals.

One possible limitation of the present model is that it requires a rectangular void construction, a geometry that has not been investigated by previous authors or observed experimentally. As a consequence, the proposed construction, which is optimal in terms of matching exponents, may not be optimal with regards to the upper bound constant. However, it should be noted that the shape of voids would in general affect the constants in the optimal scaling laws, rather than the exponents, which are intrinsic to the material.

5.2 Future work

The work presented in this thesis mainly covered a mathematical analysis and an experimental validation of optimal scaling in ductile fracture. A numerical verification of the scaling results would greatly complement this work. The goal would be twofold. On the one hand, verify the scaling relations predicted by the theoretical analysis covered in Chapter 3. On the other hand, estimate the best upper bound constant $C(p)$ in order to solve completely the optimization problem of Chapter 3. The main tool for the numerical implementation would be the finite element method. Within this framework, two particular features make this problem non-standard: the non-local regularization, i.e. the deformation second gradient term and the incompressibility constraint. When solving constrained problems using finite elements, one usually faces the issue of *locking*, which sometimes requires the development of special elements that account for incompressibility. In this case, the use of high order simplicial elements would help address the constraint issue, thereby avoiding the need for specific mean dilatation elements in finite deformation. The non-local regularization requires a specific treatment. This is due to second order spatial derivatives, whereas standard finite elements require only first derivatives. A possible solution strategy, which is briefly described in Appendices A and B, would consist of formulating the primal optimization problem in its dual form and employing a mixed finite element method, in the spirit of Hurtardo and Ortiz [56].

Appendix A

Non-local regularization

In this Appendix, we propose ideas for a possible finite element solution strategy to account for the non-local term in the energy density. We wish to minimize

$$E(u) = \int_\Omega (|Du|^p - 3^{p/2})dx + \ell \int_\Omega |DDu| \tag{A.0.1}$$

subject to

$$detDu = 1 \tag{A.0.2}$$

In order to account for incompressibility, we add a compressible term in the non-local part of the energy density. More precisely,

$$W^{loc} = \lambda f(J) + |F|^p - 3^{p/2} \tag{A.0.3}$$

where λ is a Lagrange multiplier (set to large values to enforce the constraint), $J = detF$ and $F = Du$. f is chosen to be a convex function which vanishes at $J = 1$ and takes infinite values at $J = 0$ and $J = \infty$. This evidently requires the uses of at least quadratic shape functions in order to avoid *locking*. The non-local term of the energy density is simply

$$W^{nonloc} = g(DF) \tag{A.0.4}$$

where

$$g(Q) = |Q| \tag{A.0.5}$$

We integrate the total non-local energy and use the Legendre transform

$$\int_\Omega |DF| dx = \int_\Omega \sup_Q (Q.DF - g^*(Q)) dx \tag{A.0.6}$$

The convex conjugate of the absolute value function is $g^*(Q) = \mathbf{1}_{\{|Q|leq1\}}$. Therefore

$$\int_\Omega |DF| dx = \sup_{|Q|\leq 1} \int_\Omega Q.DF dx \tag{A.0.7}$$

After integrating by parts and assuming zero boundary conditions, it follows that

$$\int_\Omega |DF| dx = -\sup_{|Q|\leq 1} \int_\Omega DivQ.F dx = -\sup_{|Q|\leq 1} \int_\Omega Q_{iJK,K} F_{iJ} dx \tag{A.0.8}$$

In this way, the non-local energy does not depend on the second gradient, albeit at the expense of introducing an additional field Q which is a third order tensor field to be approximated at every node. Suppose that the optimal $Q*$ has been found, then the (pseudo) energy density reads:

$$W(F, Q^*) = \lambda f(J) + |F|^p - 3^{p/2} + \ell DivQ^*.F \tag{A.0.9}$$

At this point, only the first derivatives of u and Q need to be evaluated. We decompose u and Q in the same standard finite element basis, i.e.

$$u_i = \sum_{a=1}^{n} u_i^a N_a(X) \tag{A.0.10}$$

where u_i^a are the nodal displacements and N_a the shape function at node a. Therefore, the deformation gradient reads:

$$Du_{ij} = \sum_{a=1}^{n} u_i^a N_{a,J} \tag{A.0.11}$$

Similarly, the trial tensor Q is decomposed such that

$$Q_{iJK} = \sum_{b=1}^{n} Q_{iJK}^{b} N_b(X) \tag{A.0.12}$$

The corresponding divergence then reads

$$Q_{iJK,K} = \sum_{b=1}^{n} Q_{iJK}^{b} N_{b,K}(X) \tag{A.0.13}$$

The suppremum problem in (A.0.8) turns into a maximization problem for $|Q_{iJK}^{b}| \leq 1$ for any b. Therefore, we are led to the problem

$$-\max_{|Q_{iJK}^{b}|\leq 1} \int_{\Omega} Q_{iJK,K} F_{iJ} dx = -\max_{|Q_{iJK}^{b}|\leq 1} \int_{\Omega} (\sum_{a=1}^{n}\sum_{b=1}^{n} N_{b,K} Q_{iJK}^{b} N_{a,J} u_i^a) dx \tag{A.0.14}$$

which results into

$$max \sum_{b=1}^{n}\sum_{a=1}^{n} \int_{\Omega} N_{b,K} N_{a,J} dx Q_{iJK}^{b} = max \sum_{b=1}^{n} A_{iJK}^{b} A_{iJK}^{b} Q_{iJK}^{b} \tag{A.0.15}$$

where

$$A_{iJK}^{b} = \sum_{a=1}^{n} \int_{\Omega} N_{b,K} N_{a,J} dx \tag{A.0.16}$$

subject to $|Q_{iJK}^{b}| \leq 1$ for any node b. Because the constraints are independent, it is equivalent to solve a set of independent problems for every node b:

$$max A_{iJK}^{b} Q_{iJK}^{b} \ subject\ to\ |Q_{iJK}^{b}| \leq 1 \tag{A.0.17}$$

The solution is obtained from the Kuhn-Tucker optimality conditions and the optimal trial tensor is achieved by

$$Q_{iJK}^{b^*} = \begin{cases} \frac{A_{iJK}^{b}}{|A_{iJK}^{b}|} \text{if} \{s,i\} |A_{iJK}^{b}| \neq 0 \\ 0 \qquad\qquad\qquad\qquad \text{otherwise.} \end{cases} \tag{A.0.18}$$

The optimal tensor field is therefore expressed as:

$$Q^*_{iJK} = \sum_{b=1}^{n} Q^{b^*}_{iJK} N_b \tag{A.0.19}$$

and $Q^{b^*}_{iJK}$ depends on A^b_{iJK} which can be computed by standard numerical quadrature.

At this stage, we can use a staggered scheme for the numerical solution. In this way, we resume to a local problem to which conventional constitutive updates are applicable. The idea is to consider a process of incremental deformations where the solution is to be determined at time $t_0, t_1, .., t_n$. If at time t_n, we know the optimal trial tensor Q^*_n, then the deformation gradient F_{n+1} at time t_{n+1} is obtained by minimizing the incremental energy density

$$W(F_{n+1}, Q^*_n) = \lambda f(J) + |F_{n+1}|^p - 3^{p/2} + \ell Div Q^*_n . F_{n+1} \tag{A.0.20}$$

for a fixed Q^*_n. Then Q^*_{n+1} is updated by the procedure outlined above. Therefore, we solve a local problem first and a non-local problem on top of it. Solving the local problem is a standard procedure which is done via dynamic relaxation for instance, which is well suited for non-convex problems.

Appendix B

Non-local regularization : General case

In this Appendix, we propose a potential generalization of the finite element strategy to convex functions g of the second gradient. In what follows, only the non local term is considered.

Non-local energy:

$$E(u) = \int_\Omega g(DDu)dx \tag{B.0.1}$$

Using duality (Legendre transform as in Appendix A)

$$\int_\Omega |DDu|dx = \int_\Omega \sup_Q (Q.DDu - g^*(Q))dx \tag{B.0.2}$$

By integration by parts and zero boundary conditions, it follows

$$\int_\Omega |DDu|dx = -\sup_Q \int_\Omega [DivQ.Du - g^*(Q)]dx \tag{B.0.3}$$

Now use a finite element discretization with lumping as before to obtain

$$E(u_h) = -\sup_{Q_h} \sum_a \sum_b A_{aJbK} u_i^a Q_{iJK}^b + \sum_b V_b g^*(Q^b) \tag{B.0.4}$$

with

$$A_{aJbK} = \int_\Omega N_{a,J} N_{b,K} dx \tag{B.0.5}$$

and

$$V_b = \int_\Omega N b dx \tag{B.0.6}$$

We can then rewrite $E(u)$ as

$$E(u_h) = \sum_b V_b sup_{Q_h}(-\frac{1}{V_b}(\sum_a A_{aJbK} u_i^a)Q^b - g^*(Q^b)) \tag{B.0.7}$$

i.e.

$$E(u_h) = \sum_b V_b g(-V_b^{-1} \sum_a A_{aJbK} u_i^a) \tag{B.0.8}$$

The expression of the discretized energy (B.0.8) only involves the nodal displacements u_i^a. Therefore, a standard Newton-Raphson procedure is applicable to solve for u_i^a and it would require the first derivatives and the second derivatives of u_h with respect to u_i^a, which are straightforward from B.0.8.

Bibliography

[1] R.A. Adams. *Sobolev Spaces*. Academic Press, New York, 1975.

[2] Fusco N. Ambrosio, L. and D. Pallara. *Functions of bounded variation and free discontinuity problems*. Oxford University Press, Great Clarendon Street, Oxford OX2 6DP, 2000.

[3] R.W. Armstrong and S.M. Walley. High strainrate properties of metals and alloys. *Int. Mat. Reviews*, 53(3), 2008.

[4] S. Aubry and M. Ortiz. The mechanics of deformation-induced subgrain-dislocation structures in metallic crystals at large strains. *Proc. R. Soc. Lond.*, A 459:31313158, 2003.

[5] Y. Bai and B. Dodd. *Adiabatic shear localization : occurrence, theories, and applications*. Pergamon Press, Oxford; New York, 1st edition, 1992.

[6] J. M. Ball. Discontinuous equilibrium solutions and cavitation in nonlinear elasticity. *Philos. Trans. Roy. Soc. London Ser. A*, 306(1496):557–611, 1982.

[7] J.M. Ball. Convexity conditions and existence theorems in non linear elasticity. *Arch.rational Mech. Anal.*, 63:337–403, 1976/77.

[8] J.M. Ball and F. Murat. $W^{1,p}$ quasiconvexity and variational problems for multiple integrals. *J. Func. Anal.*, 58:225–253, 1984.

[9] J. L. Bassani. Incompatibility and a simple gradient theory of plasticity. *Journal of the Mechanics and Physics of Solids*, 49(9):1983–1996, 2001.

[10] Hutchinson J.W. Begley, M.R. The mechanics of size-dependent indentation. *J. Mech. Phys. Solids*, 46:2049–2068, 1998.

[11] J.A. Begley and J.D. Landes. The j-integral as a fracture criterion. *Fracture Toughness, Part II, ASTM STP 514, American Society for Testing and Materials, Philadelphia*, pages 1–20, 1972.

[12] Rice J.R. Shih C.F. Beltz, G.E. and L. Xia. A self consistent model for cleavage in the presence of plastic flow. *Acta Mater.*, 44(10):3943–3954, 1996.

[13] H. Brezis. *Analyse fonctionnelle, theorie et applications.* Masson, Paris, 1983.

[14] L.M. Brown and W.M. stobbs. The work-hardening of copper-silicav. Equilibrium plastic relaxation by secondary dislocations. *Phi. Mag.*, 34(3):351–372, 1976.

[15] R. Choksi, R. V. Kohn, and F. Otto. Domain branching in uniaxial ferromagnets: a scaling law for the minimum energy. *Comm. Math. Phys.*, 201:61–79, 1999.

[16] C. Chu and A. Needleman. Void nucleation effects in biaxially stretched sheets. *Journal of Engineering Materials and Technology*, 102:249–256, 1980.

[17] A. Considère. Mémoire sur l′emploi du fer et de lacier dans les constructions. *Annales des Ponts et Chaussées*, 9:574–775, 1885.

[18] S. Conti and C. DeLellis. Some remarks on the theory of elasticity for compressible neohookean materials. *Ann. Scuola Norm. Sup. Pisa Cl. Sci. (5)*, pages 521–549, 2003.

[19] S. Conti, A. Garroni, and S. Müller. Singular kernels, multiscale decomposition of microstructure, and dislocation models. *Archive for Rational Mechanics and Analysis*, 199(3):779–819, 2011.

[20] S. Conti and M. Ortiz. Dislocation microstructures and the effective behavior of single crystals. *Arch. Rat. Mech. Anal.*, 176:103–147, 2005.

[21] B. Dacorogna. *Introduction au calcul des variations.* Presses Polytechniques Universiatires Romandes, Lausanne, 1992.

[22] B. Dacorogna and P. Marcellini. *Implicit partial differential equations.* Birkhauser, Boston.

[23] Neubauer G. Flinn P. De Guzman, M.S. and W.D. Nix. The role of indentation depth on the measured hardness of materials. *Material Research Symposium Proceedings*, 308:613–618, 1993.

[24] M. Briane J. Casado Diaz and F. Murat. The div-curl lemma trente ans après: an extension and an application to the G-convergence of unbounded monotone operators. *Journal de Mathématiques Pures et Appliquées*, 91(5):476–494, 2009.

[25] I. Ekeland and R. Temam. *Analyse convexe et problemes variationnels*. Dunod, Paris, 1974.

[26] L.C. Evans. *Partial differential equations*. American Mathematical Society, Providence, 1998.

[27] N. A. Fleck and J. W. Hutchinson. A phenomenological theory for strain gradient effects in plasticity. *Journal of the Mechanics and Physics of Solids*, 41(12):1825–1857, 1993.

[28] N. A. Fleck and J. W. Hutchinson. Strain gradient plasticity. *Advances in Applied Mechanics, Vol 33*, 33:295–361, 1997.

[29] N. A. Fleck and J. W. Hutchinson. A reformulation of strain gradient plasticity. *Journal of the Mechanics and Physics of Solids*, 49(10):2245–2271, 2001.

[30] N. A. Fleck, G. M. Muller, M. F. Ashby, and J. W. Hutchinson. Strain gradient plasticity - theory and experiment. *Acta Metallurgica Et Materialia*, 42(2):475–487, 1994.

[31] W. M. Garrison and N. R. Moody. Ductile fracture. *Journal of Physics and Chemistry of Solids*, 48:1035–1074,, 1987.

[32] A. Garroni, G. Leoni, and M. Ponsiglione. Gradient theory for plasticity via homogenization of discrete dislocations. *Journal of the European Mathematical Society*, 12(5):1231–1266, 2010.

[33] A. Garroni and S. Müller. Gamma-limit of a phase-field model of dislocations. *Siam Journal on Mathematical Analysis*, 36(6):1943–1964, 2005.

[34] A. Garroni and S. Müller. A variational model for dislocations in the line tension limit. *Archive for Rational Mechanics and Analysis*, 181(3):535–578, 2006.

[35] D. Gilbard and N.S. Trudinger. *Elliptic partial differential equations of second order*. Springer-Verlag, Berlin, 1977.

[36] E. Giusti. *Direct methods in the calculus of variations*. World Scientific, Singapore, 2003.

[37] Leblond J.-B. Gologanu, M. and J. Devaux. Approximate models for ductile metals containing non-spherical voids case of axisymmetric prolate ellipsoidal cavities. *J. Mech. Phys. Solids*, 41:17231754, 1993.

[38] Leblond J.-B. Gologanu, M. and J. Devaux. Numerical and theoretical study of coalescence of cavities in periodically voided solids. in: Noor, A. K., Needleman, A. (eds.). *Computational Material Modeling.*, AD-42/PVP-294. ASME, New York:223244, 1994.

[39] Leblond J.-B. Devaux J. Gologanu, M. Approximate models for ductile metals containing nonspherical voids case of axisymmetric oblate ellipsoidal cavities. *Journal of Engineering Materials and Technology*, 116:290297, 1994.

[40] Leblond J.-B. Devaux J. Gologanu, M. Theoretical models for void coalescence in porous ductile solids ii: Coalescence in columns. *International Journal of Solids and Structures.*, 38:55955604, 2001.

[41] Leblond J.-B. Perrin J. Devaux J. Gologanu, M. Recent extensions of gursons model for porous ductile metals. in: Suquet, p. (ed.). *Continuum Micromechanics, CISM Lectures Series. Springer, New York*, 38:61–130, 1997.

[42] Leblond J.-B. Perrin J. Devaux J. Gologanu, M. Theoretical models for void coalescence in porous ductile solids i: Coalescence in layers. *International Journal of Solids and Structures.*, 38:55815594, 2001.

[43] M. Gologanu. Etude de quelques problemes de rupture ductile des metaux. *Thesis University Paris 6*, 1997.

[44] S.H. Goods and L.M. Brown. The nucleation of cavities by plastic deformation. *Acta Metallurgica*, 27:1–15, 1979.

[45] A.L. Gurson. Continuum theory of ductile rupture by void nucleation and growth-i. yield criteria and flow rules for porous ductile media. *J. Engng. Materials Technol.*, 99:2–15, 1977.

[46] C. Carstensen K. Hackl and A. Mielke. Nonconvex potentials and microstructures in finites-train plasticity. *Proc. Royal Soc. London, Ser. A*, 458:299317, 2002.

[47] J.W. Hancock and D.K. Brown. On the role of strain and stress state in ductile failure. *J. Mech. Phys. solids*, 31:1–24, 1983.

[48] J.W. Hancock and A.C. Mackenzie. On the mechanisms of ductile failure in high strength steels subjected to multiaxial stress-states. *J. Mech. Phys. solids*, 24:147–169, 1976.

[49] A. Heller. How metals fail. *Science & Technology Review Magazine, Lawrence Livermore National Laboratory*, pages 13–20, July/August 2002.

[50] D. Henao and C. Mora-Corral. Invertibility and weak continuity of the determinant for the modelling of cavitation and fracture in nonlinear elasticity. *Arch. Ration. Mech. Anal.*, 197:619–655, 2010.

[51] K. Higashida, J. Takamura, and N. Narita. The Formation of Deformation Bands in f.c.c. Crystals. *Materials Science and Engineering*, 81:239–258, 1986.

[52] R. Hill. Acceleration waves in solids. *J. Mech. Phys, Solids*, 10:1–16, 1987.

[53] J. P. Hirth and J. Lothe. *Theory of Dislocations*. McGraw-Hill, New York, 1968.

[54] Y. Huang, Z. Xue, H. Gao, W. D. Nix, and Z. C. Xia. A study of microindentation hardness tests by mechanism-based strain gradient plasticity. *Journal of Materials Research*, 15(8):1786–1796, 2000.

[55] Derek Hull and D. J. Bacon. *Introduction to dislocations*. Butterworth-Heinemann, Oxford Oxfordshire; Boston, 4th edition, 2001.

[56] D.E. Hurtardo and M. Ortiz. Finite element analysis of geometrically necessary dislocations in crystal plasticity. *Int. J. Numer. Meth. Eng.*, 93:66–79, 2013.

[57] J. W. Hutchinson. Singular behaviour at end of a tensile crack in a hardening material. *Journal of the Mechanics and Physics of Solids*, 16(1):13–31.

[58] J.W. Hutchinson and V. Tvergaard. Softening due to void nucleation inmetals. *Harvard University, Divison of Appl. Sci.,Mech-99*, 1987.

[59] J. W. Hutchison. A course on nonlinear fracture mechanics. Dept. Solid Mechanics, TU Denmark, 1979.

[60] Srinivas M. Kamat, S.V. and P. Rama Rao. Effect of temperature on the mode i and mixed mode i/iii fracture toughness of sa333 steel. *Mat. Sci. and Engineering A*, 528:4141–4146, 2011.

[61] M. F. Kanninen and C. H. Popelar. *Advanced fracture mechanics*. Oxford engineering science series. Oxford University Press, New York, 1985.

[62] R. V. Kohn and S. Müller. Branching of twins near an austenite-twinned-martensite interface. *Phil. Mag. A*, 66:697–715, 1992.

[63] R. V. Kohn and S. Müller. Surface energy and microstructure in coherent phase transitions. *Comm. Pure Appl. Math.*, 47:405–435, 1994.

[64] E. Kröner, International Union of Theoretical, and Applied Mechanics. *Mechanics of generalized continua; proceedings of the IUTAM-symposium on the Generalized Cosserat Continuum and the Continuum Theory of Dislocations with Applications, Freudenstadt and Stuttgart (Germany) 1967*. Springer-Verlag, Berlin, Heidelberg, New York, 1968.

[65] John O. Kufner, A. and S. Fucik. *Function spaces*. Academia, Prague, 1977.

[66] M. Kuroda and V. Tvergaard. A finite deformation theory of higher-order gradient crystal plasticity. *Journal of the Mechanics and Physics of Solids*, 56(8):2573–2584, 2008.

[67] M. Kuroda and V. Tvergaard. On the formulations of higher-order strain gradient crystal plasticity models. *Journal of the Mechanics and Physics of Solids*, 56(4):1591–1608, 2008.

[68] M. Kuroda and V. Tvergaard. An alternative treatment of phenomenological higher-order strain-gradient plasticity theory. *International Journal of Plasticity*, 26(4):507–515, 2010.

[69] O.A. Ladyzhenskaya and N.N. Uraltseva. *Linear and quasilinear elliptic equations*. Academic Press, New York, 1968.

[70] Perrin-G. Leblond, J.-B. and J. Devaux. An improved gursontype model for hardenable ductile metals. *European Journal of Mechanics*, 14:499527, 1995.

[71] Clarke D.R. Lipkin, D.M. and A.G. Evans. Effect of interfacial segregation on metal/ceramic fracture in the gold/sapphire system. *work in progress, University of California Santa Barbara*, 1996.

[72] J. Lubliner. *Plasticity theory*. Macmillan; Collier Macmillan, New York London, 1990.

[73] G. Modica M. Giaquinta and J. Soucek. Cartesian currents, weak diffeomorphisms and existence theorems in non linear elasticity. *Arch. Rational Mech. Anal.*, 106:97–159, 1989.

[74] C. Miehe M. Lambrecht and J. Dettmar. Energy relaxation of non-convex incremental stress potentials in a strain-softening elastic-plastic bar. *Int. J. Solids Struct.*, 40:1369–1391, 2003.

[75] J. B. Martin. *Plasticity: fundamentals and general results*. MIT Press, Cambridge, Mass., 1975.

[76] F. A. McClintock and Ali S. Argon. *Mechanical behavior of materials*. Addison-Wesley series in metallurgy and materials,. Addison-Wesley Pub. Co., Reading, Mass., 1966.

[77] F.A. McClintock. A criterion for ductile fracture by growth of holes. *J. appl. Mech.*, 35:363–371, 1968.

[78] Vlassak J.J. McElhaney, K.W. and W.D. Nix. Determination of indenter tip geometry and indentation contact area of depth-sensing indentation experiments. *Journal of Materials research*, 13(5):1300–1306, 1998.

[79] M.E. Mear and J.W. Hutchinson. Influence of yield surface curvature on flow localization in dilatant plasticity. *Mechanics of Materials*, 4:395407, 1985.

[80] C. Miehe. Computational micro-to-macro transitions for discretized micro-structures of heterogeneous materials at finite strains based on the minimization of averaged incremental energy. *Comput. Meth. Appl. Mech. Eng.*, 192:559591, 2003.

[81] A. Mielke. Deriving new evolution equations for microstructures via relaxation of variational incremental problems. *Comput. Methods Appl. Mech. Eng*, 193:50955127, 2004.

[82] A. Mielke and S. Muller. Lower semicontinuity and existence of minimizers in incremental finite-strain elastoplasticity. *Z. Angew. Math. Mech.*, 86(3):233–250, 2006.

[83] A. Mielke and M. Ortiz. A class of minimum principles for characterizing the trajectories and the relaxation of dissipative systems. *Esaim-Control Optimisation and Calculus of Variations*, 14(3):494–516, 2008.

[84] C.B. Morrey. *Multiple integrals in the calculus of variations*. Springer-Verlag, Berlin, 1966.

[85] S. Müller and S. J. Spector. An existence theory for nonlinear elasticity that allows for cavitation. *Arch. Rat. Mech. Anal.*, 131:1–66, 1995.

[86] F. Murat. Compacité par compensation. *Ann. Scuola Norm. Sup. Pisa*, Ser. IV5(3):489507, 1978.

[87] F. Murat. Compacité par compensation : condition nécéssaire et suffisante de continuite faible sous une hypothèse de rang constant. *Ann. Scuola Norm. Sup. Pisa*, Ser. IV 8(1):69102, 1981.

[88] A. Needleman and V. Tvergaard. An analysis of ductile rupture in notched bars. *J. Mech. Phys. Solids*, 32:461–490, 1984.

[89] K. L. Nielsen and V. Tvergaard. Failure by void coalescence in metallic materials containing primary and secondary voids subject to intense shearing. *Int. J. Sol. and Structures*, 48:1255–1267, 2011.

[90] W. D. Nix and H. J. Gao. Indentation size effects in crystalline materials: A law for strain gradient plasticity. *Journal of the Mechanics and Physics of Solids*, 46(3):411–425, 1998.

[91] M. Ortiz and E.A. Repetto. Nonconvex energy minimization and dislocation structures in ductile single crystals. *J. Mech. Phys. Solids*, 47(2):397462, 1999.

[92] Repetto E. Ortiz, M. and L. Stainier. A theory of subgrain dislocation structures. *J. Mech. Phys. Solids*, 48:20772114, 2000.

[93] T. Pardoen and J. W. Hutchinson. Micromechanics-based model for trends in toughness of ductile metals. *Acta Materialia*, 51(1):133–148, 2003.

[94] K. E. Puttick. Ductile fracture in metals. *Philosophical Magazine*, 4:964–969, 1959.

[95] J. R. Rice. A path independent integral and approximate analysis of strain concentration by notches and cracks. *Journal of Applied Mechanics*, 35(2):379–386.

[96] J. R. Rice. The localization of plastic deformation. *Theoretical and Appl. Mech.(W.T. Koiter ed.)*, pages 207–220, 1977.

[97] J. R. Rice and G. F. Rosengren. Plane strain deformation near a crack tip in a power-law hardening material. *Journal of the Mechanics and Physics of Solids*, 16(1):1–12, 1968.

[98] J.R. Rice and D.M. Tracey. On the ductile enlargement of voids in triaxial stress fields. *J. Mech. Phys. solids*, 17:201–217, 1969.

[99] Paris P.C. Rice, J.R. and J.G. Merkle. Some further results of J-integral analysis and estimates. *Progress in flaw growth and fracture toughness testing, ASTM STP 536, American Society for Testing and Materials, Philadelphia*, pages 231–245, 1973.

[100] J.W. Rudnicki and J. R. Rice. Conditions for the localization deformation in pressure-sensitive dilatant materials. *J. Mech. Phys. Solids*, 23:371–394, 1975.

[101] K.C. Russel and M.F. Ashby. Slip in aluminum crystals containing strong, plate-like particles. *Acta Metallurgica*, 18(8):891–901, 1970.

[102] Hackl S. Bartels, C. Carstensen K. and U. Hoppe. Effective relaxation for microstructure simulations: algorithms and applications. *Comput. Methods Appl. Mech. Engrg.*, 193:51435175, 2004.

[103] Dolzmann S. Conti G. and S. Muller. The div-curl lemma for sequences whose divergence and curl are compact in $W^{-1,1}$. *C.R.Acad.Sci.Paris*, Ser.I(349):175–178, 2011.

[104] Q. Tang S. Muller and B.S. Yan. On a new class of deformations not allowing for cavitation. *Ann. Inst. H. Poincare Anal. Non Lineaire*, 11:217–243, 1994.

[105] Viswanathan B. Shetty, M.N. and A. Sengupta. Some temperature dependent correlations of fracture toughness, strength, notch toughness and microstructure in an hsla steel. *Z. Metallkd*, 85, 1994.

[106] Hwang B. Kim S. Shin, S.Y. and S. Lee. Fracture toughness analysis in transition temperature region of api x70 pipeline steels. *Mat. Sci. Enginering A*, 429:196–204, 2006.

[107] J. W. Steeds. Dislocation arrangement in copper single crystals as a function of strain. *Proceedings of the Royal Society of London*, A292:343–373, 1966.

[108] Walls M.G. Brown L.M. Stelmashenko, N.A. and Y.V. Milman. Microindentation on w and mo oriented single crystals: an stm study. *Acta Metallurgica et Materiala*, 41:2855–2865, 1993.

[109] Walls M.G. Brown L.M. Stelmashenko, N.A. and Y.V. Milman. Stm study of microindentation on ordered metallic single crystal. in mechanical properties and deformation behavior of materials having ultra-fine microstructures, ed. m. nastasi, d.m. parkin and h. gleiter. *NATO ASI Series*, E 233:605–610, 1993.

[110] Shih C.F. Suo, Z. and A.G. Varias. A theory for cleavage cracking in the presence of plastic flow. *acta metall. mater.*, 41(5):1551–1557, 1993.

[111] V. Sverák. Regularity properties of deformations with finite energy. *Arch. Rat. Mech. Anal.*, 100:105–127, 1988.

[112] Besson J. Tanguy, B. and A. Pineau. Ductile to brittle transition of an A508 steel characterized by charpy impact test. partI:experimental results. *Engineering Fracture Mechanics*, 72:49–72, 2005.

[113] L. Tartar. Une nouvelle méthode de résolution d′́quations aux dérivées partielles non linéaires, in: Journées d′Analyse non linéaire. *Proc.Conf., Besanon, 1977, in: Lecture Notes in Math.*, vol. 665(Springer, Berlin):pp. 228241, 1978.

[114] L. Tartar. Compensated compactness and applications to partial differential equations, in: Nonlinear analysis and mechanics, Heriot Watt Symposium IV,. *Pitman, San Francisco*, page pp. 136212, 1979.

[115] L. Tartar. Oscillations in nonlinear partial differential equations: compensated compactness and homogenization. *in: Nonlinear Systems of Partial Differential Equations in Applied Mathematics, Part 1, Santa Fe, N.M., 1984, in: Lectures in Appl. Math.*, vol. 23 Amer. Math. Soc.:243–266, 1986.

[116] A.S. Tetelman and A.J. McEvily. *Fracture of Structural Materials*. John Wiley Sons, INC, New York London Sydney, 1967.

[117] P. F. Thomason. A threedimensional model for ductile fracture by the growth and coalescence of microvoids. *Acta Metallurgica*, 33:10871095, 1985.

[118] P. F. Thomason. Threedimensional models for the plastic limitloads at incipient failure of the intervoid matrix in ductile porous solids. *Acta Metallurgica*, 33:10871095, 1985.

[119] P.F. Thomason. A theory for ductile fracture by internal necking of cavities. *J. Inst. Metals*, 96:139, 1968.

[120] P.F. Thomason. A theoretical estimate of the surface energy in ductile fracture. *International Journal of Fracture Mechanics*, 6(4):353–356, 1970.

[121] V. Tvergaard. Influence of voids on shear band instabilities under plane strain conditions. *Int. J. Fracture*, 17:389–407, 1981.

[122] V. Tvergaard. Ductile fracture by cavity nucleation between larger voids. *Journal of the Mechanics and Physics of Solids*, 30(4):265–286, 1982.

[123] V. Tvergaard. Ductile fracture by cavity nucleation between larger voids. *J. Mech. Phys. solids*, 30:265–286, 1982.

[124] V. Tvergaard. On the localization in ductile materials containing spherical voids. *Int. J. Fracture*, 18:237–252, 1982.

[125] V. Tvergaard. 3d-analysis of localization failure in a ductile material containing two size-scales of spherical particles. *Technical University of Denmark, DCAMM report No. 365*, 1987.

[126] V. Tvergaard. Effect of anisotropic hardening on ductile failure of a material containing two size-scales of spherical particles. *Technical University of Denmark, DCAMM report No. 354*, 1987.

[127] V. Tvergaard. Material failure by void growth to coalescence. *Advances in Applied Mechanics*, 27:83–151, 1990.

[128] V. Tvergaard and A. Needleman. An analysis of the temperature and rate dependence of charpy v-notch energies for a high nitrogen steel. *Int. J. Fracture*, 37:197–215, 1988.

[129] V. Tvergaard and C. Niordson. Non local plasticity effects on interaction between different size voids. *International Journal of Plasticity*, 20:107–120, 2004.

[130] Kobayashi T. Toda H. Wang, L. and M. Hayakawa. Effect of loading velocity and testing temperature on the fracture toughness of a sicw/6061Al alloy composite. *Mat. Sci. Engineering A*, 280:214–219, 2000.

[131] K.A. Warren and R.P. Reed. Tensile and impact properties of selected materials from 20 to 300K. *U.S. National Bureau of Standards*, Monograph 63, June 1963.

[132] Z. Xue, Y. Huang, F. Gao, and W. D. Nix. The strain gradient effects in micro-indentation hardness experiments. *Multiscale Phenomena in Materials-Experiments and Modeling*, 578:53–58, 2000.